Towards a kinetic model of the Entner-Doudoroff Pathway in *Zymomonas mobilis*

by

Charles Theo Van Staden

Thesis presented in partial fulfilment of the requirements for the degree of Master of Science at the University of Stellenbosch

Department of Biochemistry
University of Stellenbosch
Private Bag X1, 7602 Matieland, South Africa

Supervisor: Prof J. M. Rohwer
Co-supervisor: Prof J. L. Snoep

December 2014

Declaration

By submitting this dissertation electronically, I declare that the entirety of the work contained therein is my own, original work, and that I have not previously in its entirety or in part submitted it for obtaining any qualification.

Date: December 2014 .....

Abstract

Metabolic networks of cellular systems are complex, in that there are numerous components with multiple non-linear interactions. To understand how these networks work they are often split into manageable pieces and studied individually. However, an individual part is unable to account for the complex properties of systems. In order to study these interactions the field of systems biology has developed. Systems biology makes use of computers to construct models as a method to describe aspects of living systems. Using cellular pathways, kinetic models of metabolic pathways can be constructed and used as a tool to study the biological systems and provide a quantitative description. This thesis describes the quantitative analysis of a bacterium using a systems biology approach.

Zymomonas mobilis is a rod shaped, Gram-negative, non-mobile facultative anaerobe and has one of the fastest observed fermentations, yet least energy efficient extractions found in nature. Furthermore it is the only known micro-organism to use the Entner-Doudoroff (2-keto-3-deoxy-6-phosphogluconate) pathway anaerobically. The low energy yield of fermentation in *Z. mobilis* is a result of the usage of the Entner-Doudoroff glycolytic pathway, which has half the energy yield per mol substrate compared to the well known Embden-Meyerhof-Parnas glycolytic pathway.

The work presented in this thesis forms part of a larger project to compare glycolytic regulation in different micro-organisms *Z. mobilis*, *Escherichia coli*, *Saccharomyces cerevisiae* and *Lactococcus lactis*. These organisms were chosen based on their usage of different glycolytic mechanisms. Kinetic models are suitable tools to draw a comparison between these organisms. The emphasis here is on the construction of a kinetic model of the Entner-Doudoroff glycolytic pathway as it occurs in *Z. mobilis*.

The aim of this thesis was to characterise as many of the Entner-Doudoroff pathway enzymes as possible, under standard conditions. This was done using enzyme assays, to obtain the kinetic parameters of each of the enzymes. Microtitre plate assays were used to characterise most of the enzymes of the Entner-Doudoroff pathway. However, not all characterisations could be done using plate assay methods, as some intermediates were not commercially available to perform coupled assays. Nuclear magnetic resonance (NMR) spectroscopy was used to characterise these enzymes.

These experimentally obtained parameters were then incorporated in a mathematical framework. Time simulations on the initial model were unable to reach a steady-state, with a build up of metabolic intermediates. A secondary model was constructed (using calculated maximal activities) which allowed us to identify discrepancies in the initial model. This showed that the experimentally determined maximal activities of three enzymes in lower glycolysis were unrealistically low, which might be due to protein denaturation by sonication.

A final model was constructed which incorporated a correction factor for these three enzymes. The models' predicted output (steady-state concentrations and flux) was compared to that of

either literature or experimentally determined values, as a method to validate the model. The model output compared well to literature values. The constructed and partially validated kinetic model was then used as an analytical tool to identify points of control and regulation of glycolysis in *Z. mobilis*.

The model presented in this work was also compared to published models. Our model relies much less on literature obtained values, and uses kinetic parameters experimentally determined under the same conditions. The parameters of the published models were obtained from the literature and in many instances, the assay conditions for these parameters were set-up to yield the maximum activity under non-physiological conditions. Furthermore, the number of excluded or assumed parameters is much less in our model. However, introduction of a milder, more predictable extraction technique for preparing cell lysates, should be considered for future work, to obtain the parameters that was not determined during this study. The published models do include reactions not included in our model (e.g ATP metabolism), which should be considered for inclusion, as we strive to construct a detailed kinetic model of glycolysis in *Z. mobilis* in the future.

Opsomming

Sellulêre metaboliese netwerke is komplekse stelsels, omdat hulle bestaan uit talle komponente met verskeie nie-lineêre interaksies. Om die funksionering van hierdie netwerke te verstaan, word hulle dikwels in hanteerbare stukke verdeel en individueel bestudeer. 'n Enkele komponent is egter nie in staat om die komplekse eienskappe van sulke stelsels te verklaar nie. Die veld van sisteembiologie het ontwikkel met die doel om sulke stelsels te bestudeer. Sisteembiologie maak gebruik van rekenaarmodelle as 'n metode om aspekte van lewende sisteme te beskryf. Kinetiese modelle van metaboliese paaie word gebou en gebruik as gereedskap om die biologiese stelsels te bestudeer en 'n kwantitatiewe beskrywing te bekom. Hierdie tesis beskryf die kwantitatiewe ontleding van 'n bakterie deur middel van 'n sisteembiologiese benadering.

Zymomonas Mobilis is 'n staafvormige, Gram-negatiewe, nie-mobiele fakultatiewe anaërobe, en het een van die vinnigste waargenome fermentasies, maar met die minste energie-doeltreffende ekstraksie wat in die natuur aangetref word. Verder is dit die enigste bekende mikro-organisme wat die Entner-Doudoroff (2-keto-3-dioksi-6-fosfoglukonaat) pad anaërobies gebruik. Die lae-energie-opbrengs van fermentasie in *Z. mobilis* is 'n gevolg van die gebruik van die Entner-Doudoroff metaboliese pad, wat die helfte van die energie-opbrengs per mol substraat lewer, in vergelyking met die bekende Embden-Meyerhof-Parnas pad.

Die werk wat in hierdie tesis aangebied word, vorm deel van 'n groter projek om glikolitiese regulering in verskillende mikro-organismes te vergelyk, naamlik *Z. mobilis*, *Escherichia coli*, *Saccharomyces* en *Lactococcus lactis*. Hierdie organismes is gekies op grond van hul gebruik van verskillende glikolitiese meganismes. Kinetiese modellering is 'n handige metode om 'n vergelyking tussen hierdie organismes te trek. Hierdie werk fokus op die bou van 'n kinetiese model van die Entner-Doudoroff glikolitiese metaboliese pad soos dit in *Z. mobilis* voorkom.

Die doel van hierdie tesis was om so veel moontlik van die Entner-Doudoroff ensieme onder standaard-toestande te karakteriseer. Die kinetiese parameters van elk van die ensieme is met behulp van ensimatiese essai's bepaal. Vir die meeste essai's is 96-put mikrotiterplate gebruik, maar nie al die karakteriserings kon met behulp van hierdie metode gedoen word nie, omdat sommige intermediate nie kommersieel beskikbaar was om gekoppelde essai's mee uit te voer nie. Kernmagnetiese resonansie (KMR) spektroskopie is gebruik om hierdie ensieme te karakteriseer.

Die eksperimenteel bepaalde parameters is opgeneem in 'n wiskundige raamwerk. Tydsimulasies op die aanvanklike model was nie in staat om 'n bestendige toestand te bereik nie, omdat metaboliete opgebou het. 'n Sekondêre model is gebou (met behulp van berekende maksimale aktiwiteite) wat ons toegelaat om teenstrydighede in die aanvanklike model te identifiseer. Dit het getoon dat die eksperimenteel bepaalde maksimale aktiwiteite van drie ensieme in die laer gedeelte van glikolise te laag was, waarskynlik as gevolg van proteïen denaturering tydens die ultrasoniese disintegrasieproses.

'n Finale model is gebou waarin 'n korreksiefaktor vir hierdie drie ensieme opgeneem is. Die modelle se voorspelde uitset (bestendige toestand konsentrasies en fluksie) is vergelyk met waardes uit die literatuur of wat ons self bepaal het, as 'n metode om die model te valideer. Die model uitset was in goeie ooreenstemming met hierdie waardes. Die gedeeltelik gevalideerde kinetiese model is voorts gebruik as 'n analitiese instrument om beheer en regulering van glikolise in *Z. mobilis* te ondersoek.

Die model wat in hierdie werk ontwikkel is, is ook vergelyk met die vorige gepubliseerde modelle. Ons model berus baie minder op waardes uit die wetenskaplike literatuur, en maak gebruik van parameters wat eksperimenteel bepaal is, onder identiese toestande. Die parameters van die gepubliseerde modelle is meesal verkry uit die literatuur, en in baie gevalle was die eksperimentele kondisies vir hierdie analises opgestel om die maksimale aktiwiteit te lewer onder nie-fisiologiese toestande. Verder bevat ons model minder parameters wat of uitgesluit is of wie se waardes aangeneem moes word. In toekomstige werk sal daar egter klem gelê moet word op 'n minder wisselvallige ekstraksietegniek vir die verkryging van selekstrakte, om sodoende parameters te identifiseer wat nie in hierdie werk bepaal kon word nie.

Die gepubliseerde modelle sluit ook reaksies in wat nie ingesluit is in ons model nie (bv. ATP metabolisme). Hierdie sou in ag geneem moet word vir insluiting in 'n toekomstige uitgebreide model, om daarna te streef om 'n gedetailleerde kinetiese model van glikolise in *Z. mobilis* te bou.

Acknowledgements

I would like to express my gratitude to the following people and organisation:

Firstly, I would like to extend heartfelt thanks to my very patient supervisor **Prof. Johann Rohwer**. I was allowed the freedom to explore, but guided back when I got lost.

My co-supervisor **Prof. Jacky Snoep**, for key suggestions to experimental work, and expert guidance in this respect.

Arrie Arends: A lab manager who makes a large contribution to an enjoyable research experience, and making sure we have what we need.

Dr. Johann Eicher, for the immense amount of help with the NMR-work, and taking me under your wing.

I would also like to thank my family (Antoinette, Johann and Rudolph), and friends (Nina and Pieter) for their patience, care and support.

Francois du Toit and Dawie van Niekerk, for your friendship, support and preparation of figures.

I thank all the members of the Department of Biochemistry at Stellenbosch University, and especially those belonging to the Triple-J research group. Very helpful conversations and fun were shared with Francois du Toit, Carl Christensen, Waldo Adams, C-J Sidego, and many others.

The National Research Foundation for financial support during this research, and for their willingness to accommodate unexpected obstacles. Special thanks must be extended to Sinazo Peter for painstakingly fulfilling all of the administrative requirements.

Dedications

Aan my ouers Charles en Lettie, sonder julle was die nooit moontlik.

&

My ouma, Hannie.

&

Lafras, the giant in whose footsteps I walk.

Contents

List of Figures

List of Tables

Abbreviations

Abbreviations regularly used in this text.

2PG	2-Phosphoglycerate
3PG	3-Phosphoglycerate
6PG	6-Phosphogluconate
6PGL	6-Phosphogluconolactone
ACET	Acetaldehyde
ADH	Alcohol dehydrogenase (EC 1.1.1.1)
ADP	Adenosine diphosphate
ATP	Adenosine triphosphate
bPG	1,3-biphosphoglycerate
BSA	Bovine serum albumin
ED	Entner-Douderoff
EDA	2-Keto-3-deoxy-6-phosphogluconate aldolase (E.C. 4.1.2.12)
EDD	6-Phosphogluconate dehydratase (E.C. 4.2.1.12)
EMP	Embden-Meyerhof-Parnas
ENO	Enolase (EC 4.2.1.11)
F6P	Fructose-6-phosphate
FID	Free induction decay
FRK	Fructokinase (E.C 2.7.1.4)
FRU	Fructose
G6P	Glucose-6-phosphate
G6PDH	Glucose-6-phosphate dehydrogenase (E.C. 1.1.1.49)
GAP	Glyceraldehyde 3-phosphate
GAPDH	Glyceraldehyde-3-Phosphate dehydrogenase (EC 1.2.1.12)

GLC	Glucose
GLK	Glucokinase (E.C 2.7.1.2)
HPLC	High-performance liquid chromatography
KDG	2-Keto-3-deoxygluconate
KDPG	2-Keto-3-deoxy-6-phosphogluconate
LDH	L-Lactate dehydrogenase (E.C. 1.1.1.27)
MCA	Metabolic control analysis
MES	2-(N-morpholino)ethanesulfonic acid
NAD^+	Oxidised nicotinamide adenine dinucleotide
NADH	Reduced nicotinamide adenine dinucleotide
$NADP^+$	Oxidised nicotinamide adenine dinucleotide phosphate
NADPH	Reduced nicotinamide adenine dinucleotide phosphate
NOE	Nuclear Overhauser effect
ODE	Ordinary differential equations
PDC	Pyruvate decarboxylase (EC 4.1.1.1)
PDC	Pyruvate kinase (EC 2.7.1.40)
PEP	Phosphoenolpyruvate
PGI	Phosphoglucose isomerase (E.C. 5.3.1.9)
PGK	3-Phosphoglycerate kinase (EC 2.7.2.3)
PGLS	6-Phosphogluconolactonase (E.C. 3.1.1.31)
PGM	Phosphoglycerate mutase (EC 5.4.2.1)
PK	Pyruvate kinase (E.C. 2.7.1.40)
PTS	Phosphoenolpyruvate phosphotransferase system
PYR	Pyruvate
SDA	Supply-demand analysis
TEP	Triethyl phosphate

Symbols

μ	Micro
V	Maximal rate
v	Rate
V_f	Maximal forward rate
g	Gravitational acceleration
Hz	Hertz
kDa	Kilodalton
kPa	Kilopascal
MHz	Megahertz
mM	Millimolar
OD	Optical density
U	Enzyme unit

Chapter 1

General Introduction

Metabolic networks of cellular systems are complex, and to understand how these networks work they are often split into manageable pieces and studied individually. However, an individual part is unable to account for the complex properties of a system. This reductionistic view which has identified most of the components and many interactions, fails to account for characteristics of biological networks and system properties. These pieces form part of a larger network and one must consider that there might be interactions between the separate parts [1]. Cellular metabolism cannot be fully understood from reductionist characterisation of the individual components alone, but has to include the interaction of these components in a "systems" framework. In order to describe complex relationships between the separate parts, of the cellular environment and make sense of these data there is a need for a descriptive mathematical framework [2, 3]. Using metabolic pathways, enzymatic reactions and metabolite concentrations, metabolic models can be constructed within a mathematical framework, and experimentally validated [4, 1].

In order to study these interactions of the separate parts the field of systems biology has developed. Systems biology makes use of computers to construct models as a method to describe aspects of living systems, joining the separate parts. Four properties of a biological system can be used to provide insight at system level. These include the system structure and dynamics, where structure relates to the biochemical pathways and their interactions, and dynamics a description of how the system behaves over time. Additionally one must consider control and design methods. Control methods include strategies to change dynamic behaviour and are incorporated into the design method to obtain a certain behaviour from the cell environment [4, 5].

Using cellular pathways (for instance glycolysis), kinetic models of these pathways can be constructed and used as a tool to study the biological systems and provide a quantitative description of the system.

Metabolic control analysis (MCA) is a mathematical framework that has been developed for the quantitative analysis of these systems [6, 7, 8]. MCA is a method for analysing how the control of fluxes and intermediate concentrations in a metabolic pathway depends on network parameters (e.g the enzymes that constitute the pathway). In particular it is able to describe the sensitivity of metabolic variables to local reaction rates (for instance enzyme activity), in terms of so called control coefficients (Chapter 3).

Metabolism in cellular systems can be viewed as a molecular economy. This cellular economy can be organised into a supply block, and a demand block. These blocks are linked either by metabolic intermediates or co-factor cycles. The supply block is formed by the reactions responsi-

ble for the production of an intermediate, and a demand block being the reactions that consume the intermediate. Supply-demand analysis (SDA), developed by Hofmeyr and Cornish-Bowden [9], provides a method for analysing the control and regulation of cellular systems. SDA provides a quantitative, experimentally measurable framework to understand metabolism in terms of the elasticities of supply and demand blocks. Furthermore it allows us to distinguish between the kinetic and thermodynamic aspects of regulation, and shows that if one block has control of flux, then the other block has control over the homoeostatic maintenance of the linking metabolite [9].

This study is part of a larger project, with the aim to compare glycolytic regulation in several different micro-organisms, these include *Zymomonas mobilis* [10], *Escherichia coli* [11], *Saccharomyces cerevisiae* [12] and *Lactococcus lactis* [13].

The structure of the glycolitic pathways differs for each of these micro-organisms. In *E. coli*, the primary route for glucose uptake is the PTS system. *Z. mobilis* utilises a facilitated diffusion system and glucose is intracellularly phosphorylated by glucokinase (GLK) to produce glucose 6-phosphate, futhermore *S. cerevisiae* also utilises a facilitated diffusion system and glucose is phosphorylated by hexokinase.

In *S. cerevisiae* anaerobic fermentation of glucose occurs by means of the Embden-Meyerhof-Parnas pathway. The overall stoichiometry of the catabolism of a single glucose molecule to pyruvate is as follows:

$$1\ glucose + 2\ NAD^+ + 2\ ADP + 2\ P_i = 2\ pyruvate + 2\ NADH + 2\ ATP + 2\ H_2O + 2\ H^+ \tag{1.1}$$

The overall reaction for the glycolytic conversion of glucose to ethanol is:

$$1\ glucose + 2\ ADP\ + 2\ P_i\ = 2\ ethanol + 2\ CO_2 + 2\ ATP \tag{1.2}$$

In *L. lactis* anaerobic fermentation of glucose also occurs by means of the Embden-Meyerhof-Parnas (EMP) pathway, as described in a review [14]. *L. lactis* has a phosphoenolpyruvate-dependent sugar phosphotransferase system (PTS), which catalyses the phosphorylation of a variety of carbohydrates, concomitantly with their translocation across the cell membrane with phosphoenolpyruvate being the phosphoryl donor. This system is involved in lactose transport across the membrane (PTS, reviewed in [15, 16, 17]). The net result of single glucose molecule catabolism is the generation of two molecules of ATP.

The overall stoichiometry of the catabolism of a single glucose molecule to pyruvate is in this case also given by Equation 1.1.

Pyruvate can then enter a number of enzymatically catalysed pathways to yield a variety of products. *L. lactis* follows homolactic- or mixed acid- fermentation.

$$1\ glucose + 2\ ADP\ + 2\ P_i\ = 2\ lactic\ acid + 2\ ATP \tag{1.3}$$

for homolatic fermentation, and

$$1\ glucose + 3\ ADP\ + 3\ P_i\ = 1\ ethanol + 1\ acetate + 2\ formate + 3\ ATP \tag{1.4}$$

for mixed acid fermentation.

E. coli employs mixed acid fermentation, which makes alternative end products and in variable concentrations, in contrast to other fermentation pathways which give fewer products and in fixed concentrations. Fermentation of glucose occurs by means of the EMP-pathway, however, the micro-organism can utilise the carbon from gluconate, and this is metabolised through the use of enzymes from the Entner-Doudoroff pathway. Futhermore the glucose transporter of *E. coli* couples translocation with phosphorylation of glucose mediated by the bacterial PTS [15, 18]. The overall stoichiometry from glucose to pyruvate is the same as in Equation 1.1.

Pyruvate is subsequently converted into variable amounts of the end products (lactate, acetate, ethanol, succinate, formate and CO_2). The variation in end products affects the ATP yield per glucose consumed.

Z. mobilis employs the Entner-Doudoroff pathway as strictly fermentative. The overall stoichiometry of the catabolism of a single glucose molecule to pyruvate is as follows:

$$1\ glucose + 2\ NAD^+ + 1\ ADP + 1\ P_i = 2\ pyruvate + 2\ NADH + 2\ H^+ + 1\ ATP. \tag{1.5}$$

The Entner-Doudoroff pathway yields the same amount of pyruvic acid from glucose as the EMP-pathway, however, oxidation occurs before the cleavage, and the net energy yield is only one mole of ATP per mole of glucose utilized.

$$1\ glucose + 1\ ADP\ + 1\ P_i = 2\ ethanol + 2\ CO_2 + 1\ ATP. \tag{1.6}$$

In order to compare glycolytic regulation in these organisms there is a need to integrate experimental aspects with theoretical aspects. In this study both the experimental and theoretical components are combined to construct a mathematical model of glycolysis in *Z. mobilis*. Model construction requires the following to be identified: pathway stoichiometry, kinetic parameters and steady-state intermediate concentrations.

The detailed glycolytic pathway as it occurs in *Z. mobilis* has already been described [19, 20] and kinetic models of the pathway have been constructed [21, 22]. However, the kinetic parameters for these models have not been experimentally determined for the enzymes using the same strain and experimental conditions. Parameter sets for published models often make use of optimal conditions of each enzyme (from several organisms). In many instances, assay conditions for enzyme-kinetic parameters are set-up to yield the maximum activity of each enzyme, with various pH values, buffer compositions, and temperatures, conditions which are not representative of *in vivo* conditions. These published models [21, 22], also depend on model generated optimised parameter sets for the final model. Following are some of the optimisation assumptions made for one of these published models [22].

- Maximum velocities of all reactions were optimised according to experimentally obtained steady-state intermediate concentrations.
- Initial values of the maximum velocities were derived from the data of the 18th hour of batch fermentation, to ensure that the intermediate concentrations and maximum velocities used correspond roughly to the same physiological condition of the cells, using glycolytic flux for parameter optimisation.

- Maximum velocities for each reaction during parameter optimisation were between a factor of 5 above and below the initial values.
- K_m values, which have been assumed or obtained from other databases attributable to other micro-organisms, were optimized within a factor of 3 above and below the initial values.

1.1 Project outline

The aim of this study was to construct and validate a detailed kinetic model of the Entner-Doudoroff glycolytic pathway in *Zymomonas mobilis*.

The project consists of two components: first an experimental component, which included the following:

i Establish cultures of *Z. mobilis*growing under anaerobic conditions.

ii Optimise the extraction procedure, to obtain cell lysates for kinetic characterisation of the enzymes.

iii Obtain kinetic parameters for the glycolytic enzymes experimentally (under the same experimental conditions) or from literature if they could not be experimentally determined.

iv Measure glucose uptake flux, for model validation.

Second: a theoretical component. The criteria for the theoretical aspects of the project included:

i The construction of a kinetic model using the experimentally determined kinetic parameters.

ii The partial validation of the model using steady state flux data obtained in this study. Furthermore comparing the model output to steady-state metabolite concentration and flux from the literature.

iii Brief model analysis to identify control and regulation of the cellular system.

The remainder of this thesis is organised as follows:

Chapter 2 gives a brief review of pertinent literature of the Entner-Doudoroff glycolytic pathway and the enzymes of this pathway. Furthermore the results of the experimental characterisation of the enzymes are also presented. Chapter 3 covers an overview of kinetic modelling, and summarises the rate equations and parameters for the construction of the model. The chapter also shows model analysis. Chapter 4 gives a general discussion and critique of the work presented in this study. The thesis is concluded in Chapter 5 with an outline of the materials and methods used for both the experimental and theoretical components of this study.

Chapter 2

Characterising the Entner-Doudoroff pathway enzymes

2.1 The Entner-Doudoroff pathway - an alternative way

The Entner-Doudoroff (2-keto-3-deoxy-6-phosphogluconate) pathway can be viewed as an alternative glycolytic pathway, and is active in many Gram-negative bacteria. This pathway for glucose metabolism was first discovered in 1952 in *Pseudomonas saccharophila* in a paper published by Entner and Doudoroff [23]. The ED-pathway is present in all three of the phylogenetic domains. The prevalence is indicative of the pathway's importance, and it has been suggested that it might pre-date the commonly known Embden-Meyerhof-Parnas pathway (EMP) in evolutionary terms [24].

The overall schemes of these two pathways are alike in that priming of 6-carbon sugars takes place by phosphorylation, and two 3-carbon intermediates are obtained by C_3-C_3 aldol cleavage. However, it is the 6-carbon intermediates that serve as substrates for aldolase enzymes that distinguish the two glycolytic pathways from one another.

The Entner-Doudoroff glycolytic pathway cleaves 2-keto-3-deoxy-6-phosphogluconate (KDPG) via 2-keto-3-deoxy-6-phosphogluconate aldolase (EDA), forming one molecule each of 3-phosphoglycerate (3PG) and pyruvate, compared to the EMP-glycolytic pathway which cleaves fructose-1,6-bisphosphate via fructose bisphosphate aldolase to yield glyceraldehyde 3-phosphate (GAP) and dihydrooxyacetone phosphate [19, 25]. Pyruvate decarboxylase action yields CO_2 and ethanol, correspondingly the same products are formed when 3PG is metabolised via the triose phosphate portion of the EMP pathway. The net yield of 1 mol glucose metabolism via the ED pathway is 2 mol ethanol, 2 mol CO_2 and 1 mol ATP (see Figure 2.1).

The ED-pathway is known to operate in different modes:

Cyclic In *Pseudomonas aeruginosa* for carbohydrate metabolism (Figure 2.2), mannitol is catabolised with glucose-6-phosphate dehydrogenase (G6PDH) activity, by production of the intermediate glucose-6-phosphate (G6P). Fructose is produced by mannitol dehydrogenase from mannitol. Phosphorylation of fructose, produces fructose-6-phosphate (F6P), which undergoes isomeration to produce G6P, which the ED-pathway can utilise to produce GAP and pyruvate. The cycling is induced when GAP is recycled to fructose-1,6-bisphosphate and F6P, via fructose diphosphate aldolase and fructose diphosphatase respectively [26, 27, 28, 29].

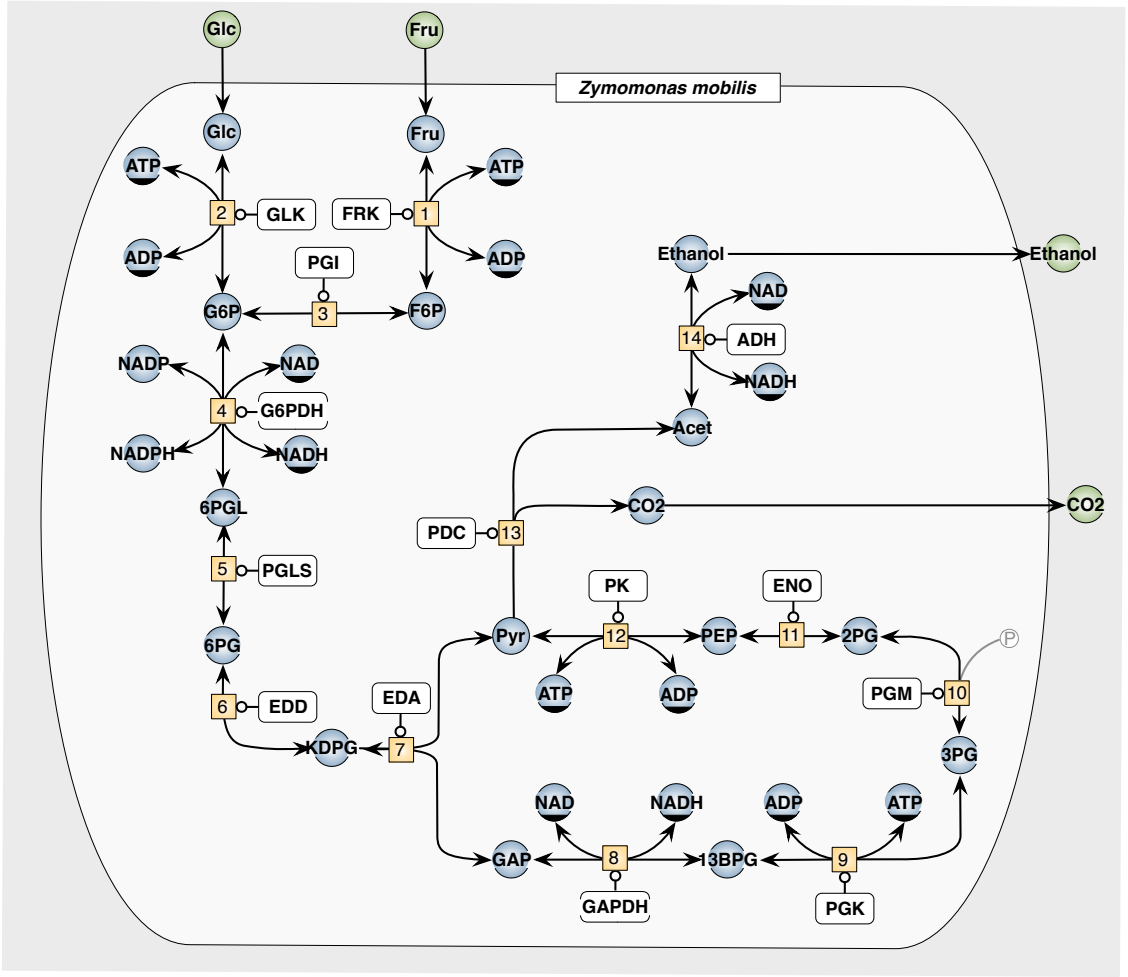

Figure 2.1: Overview of the Entner-Doudoroff pathway in *Z. mobilis*. ***Abbreviations of enzymes***: fructokinase (FRK), glucokinase (GLK), phosphoglucose isomerase (PGI), glucose-6-phosphate dehydrogenase (G6PDH), 6-phosphogluconolactonase (PGLS), 6-phosphogluconate dehydratase (EDD), 2-keto,3-deoxy-6-phosphogluconate aldolase (EDA), glyceraldehyde-3-phosphate dehydrogenase (GAP), 3-phosphoglycerate kinase (PGK), phospoglycerate mutase (PGM), enolase (ENO), pyruvate kinase (PK), pyruvate decarboxylase (PDC) and alcohol dehydrogenase (ADH). ***Abbreviation of substrates***: glucose (GLC) adenosine diphopshate (ADP), adenosine triphosphate (ATP), fructose-6-phosphate (F6P), glucose-6-phosphate (G6P), oxidised nicotinamide adenine dinucleotide (NAD^+), reduced nicotinamide adenine dinucleotide (NADH), oxidised nicotinamide adenine dinucleotide phosphate ($NADP^+$), reduced nicotinamide adenine dinucleotide phosphate (NADPH), 6-phosphogluconolactone (6PGL), 6-phosphogluconate (6PG), 2-keto-3-deoxy-6-phosphogluconate (KDPG), glyceraldehyde 3-phosphate (GAP), 1,3-biphosphoglycerate (1,3BPG), 3-phosphoglycerate (3PG), 2-phosphoglycerate (2PG), phosphoenolpyruvate (PEP), pyruvate (Pyr), and acetaldehyde (Acet)

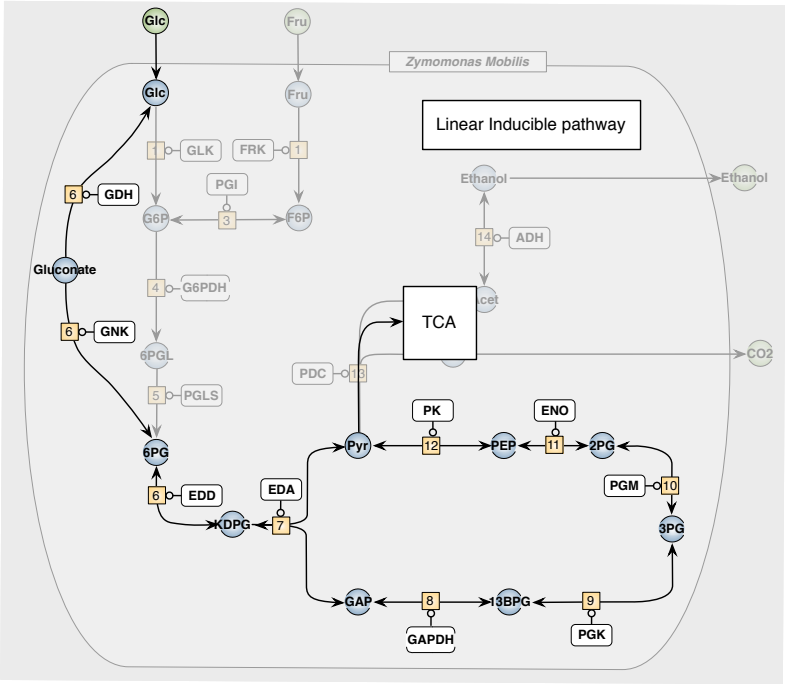

(a) Inducible linear Entner-Doudoroff pathway. The pathway has a secondary role to central metabolism in organisms, and is only utilised for the metabolism of specific substrates

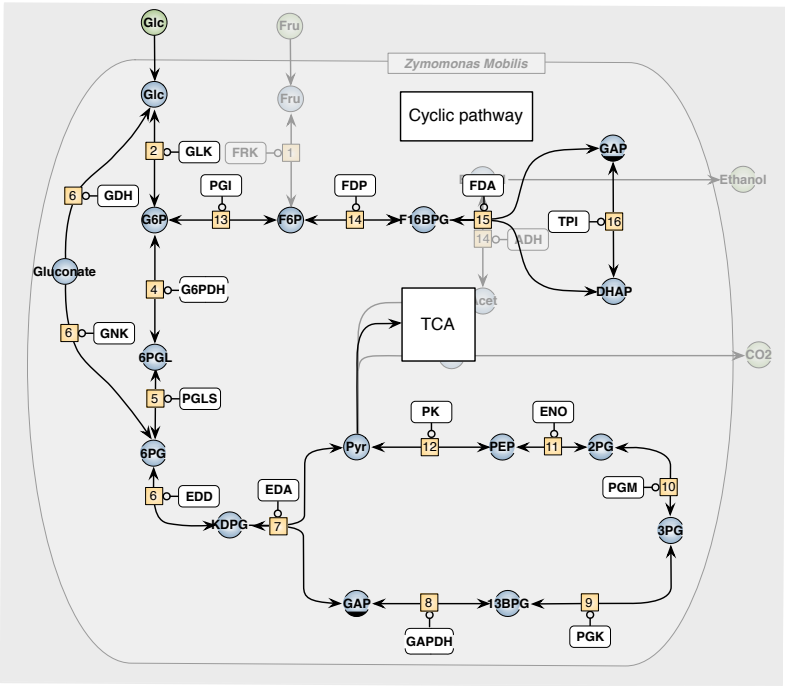

(b) Cyclic Entner-Doudoroff pathway. The cycling is induced when GAP is recycled to fructose-1,6-bisphosphate and F6P, via fructose diphosphate aldolase and fructose diphosphatase respectively

Figure 2.2: Inducible & cyclic linear Entner-Doudoroff pathway. The pathways are superimposed on the constitutive linear pathway of *Z. mobilis* for comparison (Figure 2.1). Abbreviations as in legend of Figure 2.1 and: glucose dehydrogenase (GDH), gluconokinase (GNK), triose phosphate isomerase (TPI), fructose diphosphate aldolase (FDA), fructose diphosphatase (FDP), fructose-1,6-bisphosphate (F16BPG), dihydroxyacetone phosphate (DHAP) and tricarboxylic acid cycle (TCA).

Modified pathways Several examples of micro-organisms that use a modified ED-pathway exist, of which there are two modifications. The first involves non-phosphorylated intermediates, found in thermophiles *Sulfolobus, Thermoplasma* and *Thermoproteus*, where activation via phosphorylation occurs only at the level of glycerate, formed by glyceraldehyde dehydrogenase from glyceraldehyde [30, 31, 32].

The second involves the semi-phoshorylative ED-pathway, where gluconokinase and 6-phosphogluconate dehydratase (EDD) are absent. 2-Keto-3-deoxygluconate (KDG) is formed via gluconate dehydratase from gluconate. Phosphorylation occurs at this level with KDG phosphorylated to 2-keto-3-deoxy-6-phosphogluconate (KDPG) by 2-keto-3-deoxygluconate kinase [33, 34].

Inducible, linear pathway in numerous bacteria, as a secondary role to central metabolism (Figure 2.2). The pathway is only induced for the metabolism of specific substrates. When these substrates are available the enzymes of the ED-pathway are synthesised. In conjunction with playing a secondary role the pathway can be used anaerobically or aerobically [35, 36, 37]. *E. coli* can grow on gluconate by transport and phosphorylation of the substrate to form 6-phosphogluconate (6PG), a substrate of the ED-pathway [38, 39]. In the absence of gluconate, when cells are grown on glucose, gluconate dehydratase activity is absent, however, the ED-pathway can be induced by gluconate availability [40].

Constitutive, linear pathway, found in *Neisseria gonorrhoeae* where glucose is catabolised, by combining the ED-pathway with the pentose phosphate pathway under aerobic conditions [41]. *Z. mobilis* uses the ED-pathway in a linear fashion, however, it employs the pathway under anaerobic conditions. Considering that *Z. mobilis* is used in this study, a more detailed review of the enzymes follows in the next section.

2.2 *Zymomonas mobilis* has a unique ED-pathway

Zymomonas mobilis is a rod shaped, Gram-negative, non-mobile facultative anaerobe bacterium. The bacterium is part of the Sphingomonadaceae family, Group 4 of the alpha-subclass of the Proteobacteria class [42, 43]. The micro-organism was discovered in warm, tropical climates, fermenting in sugar-rich plant saps for instance African palm wine, ripening honey and traditional palque drink from Mexico [44, 45]. The organism degrades sucrose, glucose and fructose via an anaerobic version of the Entner-Doudoroff pathway, to an equimolar mixture of ethanol and carbon dioxide. *Z. mobilis* is the only known organism to use this pathway anaerobically, notable in view of the inefficiency of the pathway for energy metabolism. The pathway operates in a linear way and is constitutively expressed, forming the core of central metabolism in *Z. mobilis* (Figure 2.1). Glucose metabolism can only take place via the ED-pathway, due to the absence of 6-phosphofructokinase, which converts fructose-6-phosphate into fructose-1,6-bisphosphate in *Z. mobilis* [46, 47, 44].

The next section will broadly review the *Z. mobilis* glycolytic enzymes - fructokinase (FRK), glucokinase (GLK), phosphoglucose isomerase (PGI), glucose-6-phosphate dehydrogenase (G6PDH), 6-phosphogluconolactonase (PGLS), 6-phosphogluconate dehydratase (EDD), 2-keto,3-deoxy-6-phosphogluconate aldolase (EDA), glyceraldehyde-3-phosphate dehydrogenase (GAP), 3-phospho-

glycerate kinase (PGK), phospoglycerate mutase (PGM), enolase (ENO), pyruvate kinase (PK), pyruvate decarboxylase (PDC) and alcohol dehydrogenase (ADH).

2.3 Glycolytic enzymes of the Entner-Doudoroff pathway

Glucokinase (EC 2.7.1.2) GK is a dimeric isozyme of hexokinase, with a molecular weight of 65kDa. The enzyme catalyses the first reaction in the ED-pathway and phosphorylates glucose in an ATP dependent reaction, yielding glucose-6-phosphate (G6P) and ADP, thereby preventing transport of sugar out of the cell. K_{m} values of 0.22 mM for glucose and 0.8 mM for ATP have been reported. Furthermore G6P acts as a weak competitive inhibitor with ATP, with a reported K_{i} of 15 mM. Glucokinase is activated by Mg^{2+} or Mn^{2+} cations, with little or no activity other than with these cations [48].

Fructokinase (EC 2.7.1.4) FK is dimeric, with a molecular mass of 56kDa, and is encoded by the *frk* gene. In comparison to the amino acid sequence of the glucokinase enzyme there is little homology, notwithstanding that fructokinase can bind and is also strongly inhibited by glucose, with reported K_{i} of 0.14 mM [49, 48]. The enzyme phosphorylates fructose in an ATP dependent reaction, yielding F6P and ADP [50].

Phosphoglucose Isomerase (EC 5.3.1.9) PGI catalyses the interconversion of F6P to G6P, with a K_{m} of 0.2 mM for F6P. The enzyme is dimeric, with 60 to 65 kDa size subunits and is 43% homologous to the *E.coli* enzyme [51]. Together with FRK this forms a peripheral link which allows *Z. mobilis* to utilise fructose as a substrate, linking it to *Z. mobilis* central metabolism [52]. The role of PGI is reversed in the ED-pathway when compared to the EMP-pathway. There, G6P is isomerised to form F6P, which is phosphorylated to form fructose-1,6-bisphospate, a key intermediate of the EMP-pathway.

Glucose-6-Phosphate Dehydrogenase (EC 1.1.1.49) The conversion of G6P and NAD^+ and/or $NADP^+$, to 6PG and NADH and/or NADPH is catalysed by the G6PDH. Although the enzyme can operate effectively with NAD^+ ($K_{\mathrm{m}} \approx 0.21$ mM) and $NADP^+$ ($K_{\mathrm{m}} \approx 0.04$ mM), the affinity for $NADP^+$ is greater, however, the V_{max} is lower when compared to NAD^+. The enzyme is weakly inhibited by ATP ($K_{\mathrm{i}} \approx 1.4$ mM) which is competitive with NAD^+. The *zwf* gene encodes a tetrameric protein with 52 kDa subunit [48, 53]. Snoep *et al.* showed that the control of the glycolytic flux in *Z. mobilis* lies with G6PDH [53]. There is no available data for the reverse reactions affinities.

6-Phosphogluconolactonase (EC 3.1.1.31) This 26kDa monomeric enzyme catalyses the reaction that converts 6-phosphogluconolactone to 6-phosphogluconate. The oxidation of G6P produces unstable 6-phosphoglucono-δ-lactone, which spontaneously hydrolyses to an open-chain 6-phosphogluconate, this rate is not sufficient to compensate for lactone accumulation within the cell, and therefore the enzyme is utilised to hydrolyse the excess lactone [54]. Reported K_{m} values for 6PG vary between 0.02-0.29 mM, with G6P acting as a competitive inhibitor, with a K_{i} of 0.3 mM [54, 21].

6-Phosphogluconate Dehydratase (EC 4.2.1.12) 6-Phosphogluconate dehydratase, known as the Entner-Doudoroff dehydratase (EDD) is one of the enzymes unique to the ED-pathway, and encoded by the *edd* gene. The enzyme is dimeric with two 63kDa subunits [55]. The enzyme catalyses dehydration of 6PG to form 2-keto-3-deoxy-6-phosphogluconate (KDPG), and requires ferrous ions for activation [19]. Evidence of spontaneous rearrangement of the enol to keto form in an irreversible sequence was shown to exist [56, 57]. The reported K_{m} for 6PG is 0.04 mM, with G3P ($K_{\mathrm{i}} \approx 2$ mM) acting as a competitive inhibitor [55].

2-Keto-3-Deoxy-6-Phosphogluconate Aldolase (EC 4.1.2.14) The conversion of KDPG to 3PG and pyruvate is catalysed by this enzyme in *Z. mobilis*. 2-Keto-3-deoxy-6-phosphogluconate aldolase, known as Entner-Doudoroff aldolase (EDA), is the second key enzyme in the ED-pathway; however, it is not unique to the EDD pathway for it acts as a multifunctional enzyme in many organisms. The multi functionality comes from EDA, which can take both KDPG and 2-keto-4-hydroxyglutarate (KHG) as substrates, producing 3PG and pyruvate as well as pyruvate and glyoxylate respectively. The protein is encoded by the *eda* gene and forms a trimer with two 23kDa subunits. The reported K_{m} for KDPG varies between 0.25 - 0.29 mM [55, 52].

Glyceraldehyde-3-Phosphate Dehydrogenase (EC 1.2.1.12) GAPDH, an oxidoreductase, catalyses the reaction of glyceraldehyde-3-phosphate (aldehyde), P_i and NAD to 1,3-biphosphoglycerate (acyl phosphate) and NADH. This reaction together with PGK produces high-energy phosphate bonds, by the ester bond that attached the phosphate to the acyl carbon. The bond facilitates the transfer of P_i to ADP, producing ATP during glycolysis [21, 58, 59]. This enzyme system together with PK forms the primary ATP synthesis routes in this organism. There is currently no information on binding affinities for this enzyme.

3-Phosphoglycerate Kinase (EC 2.7.2.3) This enzyme catalyses the conversion of 1,3-biphosphoglycerate to 3PG, generating ATP in the process (one of two ATP regeneration reactions, the other being the reaction of pyruvate kinase). This monomeric 44kDa subunit protein appears similar to other PGK of plants and bacteria, however, the kinetic properties differ in that there is less prominent substrate activation, compared to that of the yeast PGK [60, 59, 61, 62]. The K_{m} varies significantly for 3PG with reported values between 0.8 mM [63] and 1.5 mM [62], and between 1.0 and 1.1 mM for ATP.

Phosphoglycerate Mutase (EC 5.4.2.1) The interconversion of 3PG and 2PG is catalysed by PGM in a reversible reaction. The enzyme is a dimer with 26kDa subunits, encoded by the *pgm* gene. The enzyme is not allosterically controlled but requires low levels of 2,3-bisphosphoglycerate to maintain phosporylation [64, 63]. The K_{m} for 3PG was determined to be 1.1 mM, with no reported K_{m} for 2PG [63].

Enolase (EC 4.2.1.11) ENO catalyses the uninhibited one substrate inter-conversion of 2-phosphoglycerate ($K_{\mathrm{m}} \approx 0.08$ mM) and phosphoenolpyruvate, with the reaction running close to V_{max}. The gene *eno* is present in a single copy in the genome and encodes for a protein subunit with a predicted molecular weight of 45 kDa [63, 65]. *Z. mobilis* enolase is octomeric, which is unusual as it is mostly in the dimeric form in other organisms. *Z. mobilis* enolase closely resembles the *E.coli* enolase, with a 72% homology for the first 132 amino acids [65].

Pyruvate Kinase (EC 2.7.1.40) PK catalyses substrate level phosphorylytion, by transferring a phosphate group from PEP to an ADP, yielding pyruvate and ATP, in a physiologically irreversible reaction. The ATP produced represents the net yield from anaerobic hydrolysis. The protein is encoded by the *pyk* gene, and it appears as a 51 kDa homodimer. The K_m values are 0.08 mM and 0.17 mM for PEP and ADP respectivley [63]. *Z. mobilis* PK is unique among the characterised pyruvate kinases of prokaryotes, which are controlled by allosteric activators, due to its high activity in the absence of any allosteric activator [63, 66]. The allosteric effectors of PK such as 6PG, G6P, fructose 1,6-bisphosphate and AMP have no effect on the K_m of *Z. mobilis* PK [67, 68].

Pyruvate Decarboxylase (EC 4.1.1.1) PDC catalyses the penultimate step in alcohol fermentation. The enzyme catalyses the non-oxidative decarboxylation of pyruvate to acetaldehyde with the formation of carbon dioxide, in a thiamine diphosphate dependent reaction [69, 70]. The protein is tetrameric with an approximate molecular mass of 240kDa, and an apparent K_m of 0.4 mM for pyruvate [71, 72, 73].

Alcohol Dehydrogenase (EC 1.1.1.1) The final step in alcohol fermentation in *Z. mobilis* is catalysed by ADH, where NADH reduces acetaldehyde to ethanol and NAD^+. A potential key to the organism's efficient ethanol production might be due to the regeneration of NAD^+ by this reaction in the pathway.

Z. mobilis possesses two well characterised isozymes of ADH, ZADH-1 and ZADH-2, where ZADH-1 is a homotetramer with 40kDa subunits, and ZADH-2 dimeric with 37kDa subunit mass [74, 75]. ZADH-2 requires ferrous ions for activation. ZADH-1 functions as the major ADH, and has a higher specific activity for substrate compared to ZADH-2.

K_m values for ZADH-1 are 0.086 mM, 4.8 mM, 0.027 mM and 0.073 mM for acetaldehyde, ethanol, NADH and NAD respectively. ZADH-2 K_m values are 1.3 mM, 27 mM, 0.012 mM and 0.11 mM for acetaldehyde, ethanol, NADH and NAD^+ respectively [76, 75].

The next section gives an overview of the equations used for fitting data and the rate equations used in model construction.

2.4 Generic enzyme kinetic rate equations

Modelling of biological systems has polarised into two different approaches: "top-down" where systemic properties are used to give insight through deduction by using statistical models, and "bottom-up" where molecular properties are used to construct models to predict systemic properties, using kinetic models [77].

Key requirements for the"bottom-up" approach are a set of mathematical enzyme kinetic equations, and kinetic data to populate these equations [78]. In order to do so, an enzyme catalysed reaction has to be kinetically characterised.

It was in the latter part of the nineteenth century that rates of enzyme-catalysed reactions where first studied, however, at the time methods for enzyme assays where primitive and the first model that accurately described an enzyme-catalysed reaction was published in a paper by Michaelis and Menten [79].

For the reaction of invertase;

$$E + S \underset{k_{-1}}{\overset{k_1}{\rightleftharpoons}} ES \underset{k_{-2}}{\overset{k_2}{\rightleftharpoons}} E + P, \tag{2.1}$$

where E and S, are the enzyme and substrate respectively, ES the enzyme-substrate complex and P the product. The association rate constants for enzyme-substrate complex formation are represented by k_1 and k_{-2}, k_2 and k_{-1} are the dissociation rate constants that regenerate free enzyme and product or substrate respectively.

For this they developed a mathematical kinetic rate equation that accurately describes this reaction, generally known as the Michaelis-Menten equation:

$$v = \frac{Vs}{K_m + s}, \tag{2.2}$$

$$v = \frac{Vs}{\frac{k_{-1}+k_2}{k_1} + s} \tag{2.3}$$

where v is the reaction rate, s the free substrate concentration, K_{m} the Michaelis constant (substrate concentration at which the reaction rate is at 0.5 V) and V the limiting velocity. It is often defined as V_{max}, this is discouraged by the International Union of Biochemistry and Molecular Biology as it represents a limit, and not a mathematical maximum [80, 81].

For this rate equation some assumptions are made:

1. $[S] >> [E]$; substrate concentration much greater than enzyme concentration
2. k_1[E][S] = $(k_{-1} + k_2)$[ES]; Steady-state assumption
3. $k_2 >> k_{-2}$; negligible amount of substrate is formed thus making the reaction irreversible

However, these assumptions make the rate equation somewhat artificial in that they do not factor in traits that are important to consider when modelling detailed mechanisms of enzyme-catalysed reactions. These include reversibility, multiple substrates, product-inhibition and cooperativity.

Equations incorporating some of these traits have been derived, but most exclude at least one trait and are inconvenient to use due to a large number of parameters without clear operational definitions, resulting in complex kinetic equations with numerous parameters [78].

The Generic Reversible Hill equations (GRH), provides a method to overcome this, by representing reversibility, cooperativity and allosteric behaviour using simple experimentally determinable operationally-defined kinetic parameters [82].

$$v = \frac{V_f \sigma \left(1 - \dfrac{\Gamma}{K_{eq}}\right)(\sigma + \pi)^{h-1}}{\prod_j^{n_m} \left[\dfrac{(1 + \mu_j^h)}{(1 + \alpha_j^{2h}\mu_j^h)}\right] + (\sigma + \pi)^h}, \tag{2.4}$$

for Uni-Uni reactions, and

$$v = \frac{V_f \sigma_1 \sigma_2 \left(1 - \frac{\Gamma}{K_{eq}}\right) (\sigma_1 + \pi_1)^{h-1} (\sigma_2 + \pi_2)^{h-1}}{\left(\prod_j^{n_m} \left[\frac{(1+\mu_j^h)}{(1+\alpha_j^{2h}\mu_j^h)}\right] + (\sigma_1 + \pi_1)^h\right)\left(\prod_j^{n_m} \left[\frac{(1+\mu_j^h)}{(1+\alpha_j^{2h}\mu_j^h)}\right] + (\sigma_2 + \pi_2)^h\right)}, \tag{2.5}$$

for Bi-Bi reactions,

where K_s, K_p and K_i are the substrate, product and allosteric modifier -concentrations respectively, at which the reaction performs at half the maximal rate. $\sigma = [S]/K_s$ (substrate concentrations scaled by their respective half-saturation constants), $\pi = [P]/K_p$ (product concentrations scaled by their respective half-saturation constants), $\mu = [X_i]/K_i$ (allosteric modifier concentrations scaled by their respective half-saturation constants). h is the Hill coefficient for cooperative binding, where $h > 1 \implies$ positive cooperativity, $h < 1 \implies$ negative cooperativity. The equation also includes a term for the modifier α, ($\alpha > 1 \implies$ activator, $\alpha < 1 \implies$ inhibitor and $\alpha = 1$ no effect).

2.5 Results

This section presents the experimental results of enzyme characterisations under standard conditions. The results are then used to construct a kinetic model of glycolysis in *Z. mobilis*, which is presented in Chapter 3.

Kinetic Characterisation

Glycolytic enzymes were kinetically characterised using *Z. mobilis* lysates. In this section the results of the experimentally determined maximal activity (V) and K_{m} values are presented.

It should be noted that characterisation was done under physiological conditions and not optimal conditions for each enzyme. Using standardised experimental conditions is essential. In many instances, assay conditions for enzyme-kinetic parameters are set-up to yield the maximum activity of each enzyme. Furthermore these are measured in different buffers, various pH values and ionic strengths. Optimal conditions for each reaction would not represent the cellular environment under which these reactions occur, and not be a true model representation of the Enter-Doudoroff pathway in *Z. mobilis* [83, 84]. Equilibrium constants of the enzymatic reactions determined under similar conditions to this study were obtained or calculated from the Goldberg database [85].

Glucokinase GLK catalyses the ATP-dependent phosphorylation of glucose to form G6P and ADP. The enzyme was characterised in terms of both its substrates (glucose and ATP) and products (G6P and ADP) as shown in Figure 2.3.

The saturation curve for glucose followed classical Michaelis-Menten kinetics. Product inhibition by G6P and ADP are also shown, however, GLK seems to be insensitive to low concentrations of G6P as an inhibitor as shown in Figure 2.3 (c) ●. This agrees with reported literature values [48]. The experimental data were fitted to Equation (2.6) which is incorporated into the model (see Chapter 4).

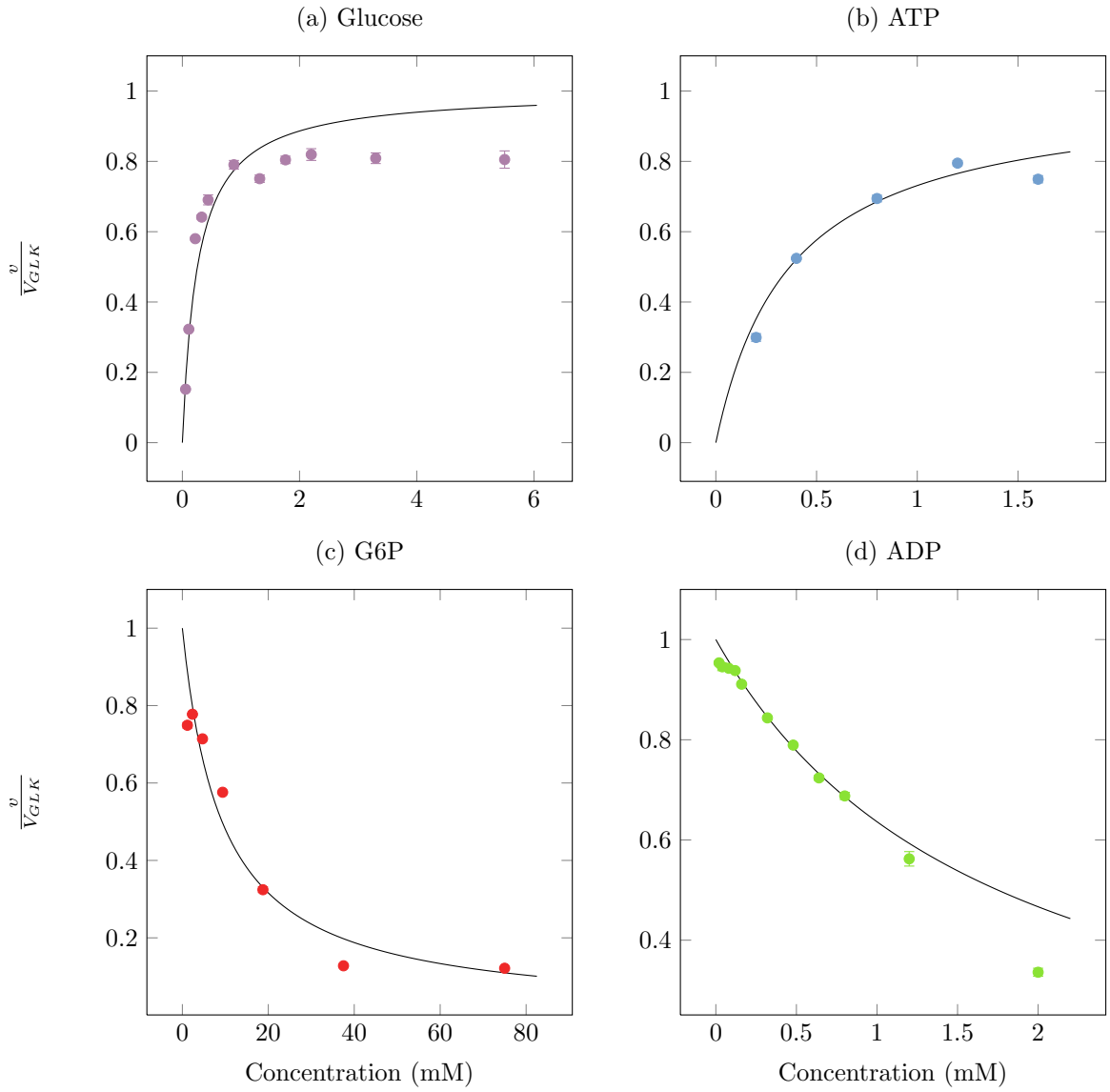

Figure 2.3: The biochemical characterisation of *Z. mobilis* glucokinase. *Top left*(●): Saturation of the enzyme with glucose was achieved by varying the glucose concentration between $0 - 5.5$ mM and semi-saturating with ATP (1 mM). *Top right* (●): The ATP concentration was varied between $0 - 1.6$ mM and semi-saturating with glucose (1 mM). *Bottom left* (●): Inhibition by G6P and, *bottom right* (●), ADP is also shown. Data are scaled to the maximal activity to eliminate day-to-day variations in extraction efficiency (See section 5.9). The lines show Equation 2.6 parameterised with the values of Table 2.1 and the respective substrate, product and inhibitor concentrations used in the assay. Error bars represent SEM (n=6).

$$v_{GLK} = V_{fGLK} \cdot \left(1 - \frac{G6P \cdot ADP}{Glucose \cdot ATP}{K_{eq}}\right) \cdot \frac{\frac{Glucose}{K_{glucose}} \cdot \frac{ATP}{K_{ATP}}}{\left(1 + \frac{Glucose}{K_{glucose}} + \frac{G6P}{K_{G6P}}\right)\left(1 + \frac{ATP}{K_{ATP}} + \frac{ADP}{K_{ADP}}\right)} \tag{2.6}$$

Table 2.1: Summary of the kinetic parameters for *Z. mobilis* glucokinase. The weighted kinetic data were fitted with the Michaelis-Menten equation (Chapter 5) and the fitted curves are shown in Figure 2.3.

Parameter	Fitted Value	Literature Value	Reference
V_{fGLK} (μmol.min^{-1}.mg^{-1})	1.41 ± 0.02	1.54	53
$K_{Glucose}$ (mM)	0.26 ± 0.045	0.22	48
K_{ATP} (mM)	0.41 ± 0.067	0.8	48
K_{G6P} (mM)	9.25 ± 2.32	15	48
K_{ADP} (mM)	1.75 ± 0.139	—	—
K_{eq}		2.26×10^3	85

Glucose-6-Phosphate Dehydrogenase G6PDH catalyses the conversion of G6P and NAD^+ and/or $NADP^+$, to 6PG and NADH and/or NADPH. The reaction was characterised in terms of it substrates G6P (Figure 2.4 (a), ●), NAD^+ (Figure 2.4 (b), ●) and $NADP^+$ (Figure 2.4 (c), ●).

It has been shown that ATP is a competitive inhibitor for G6PDH [86], and our data confirms this as shown in (Figure 2.4 (d), ●). The experimental data were fitted to Equations (2.7) and (2.8) respectively with regards to the substrate, and incorporated as such into the model.

It has also been shown that PEP acts as an allosteric inhibitor [86]. However, it could not be reproducibly measured experimentally, under saturation concentrations of the substrates. Due to the large errors in this parameter, the kinetic parameter were taken from literature.

$$v_{G6PDH} = \frac{V_{fG6PDH} \cdot \left(1 - \frac{6PGL \cdot NADH}{\frac{G6P \cdot NAD}{K_{eq}}}\right) \cdot \frac{G6P}{K_{G6P}} \cdot \frac{NAD}{K_{NAD}}}{\left(\left[\frac{1 + \frac{PEP}{K_{PEP}}}{1 + \alpha \cdot \frac{PEP}{K_{PEP}}}\right] + \frac{G6P}{K_{G6P}} + \frac{6PGL}{K_{6PGL}}\right)\left(\left[\frac{1 + \frac{PEP}{K_{PEP}}}{1 + \alpha \cdot \frac{PEP}{K_{PEP}}}\right] + \frac{NAD}{K_{NAD}} + \frac{NADH}{K_{NADH}} + \frac{ATP}{K_{ATP}}\right)} \tag{2.7}$$

$$v_{G6PDH} = \frac{V_{fG6PDH} \cdot \left(1 - \frac{6PGL \cdot NADPH}{\frac{G6P \cdot NADP}{K_{eq}}}\right) \cdot \left(\frac{G6P}{K_{G6P}} \cdot \frac{NADP}{K_{NADP}}\right)^{h-1}}{\left(\left[\frac{1 + \left(\frac{PEP}{K_{PEP}}\right)^h}{1 + \alpha^{2h} \cdot \left(\frac{PEP}{K_{PEP}}\right)^h}\right] + \left(\frac{G6P}{K_{G6P}} + \frac{6PGL}{K_{6PGL}}\right)^h\right)\left(\left[\frac{1 + \left(\frac{PEP}{K_{PEP}}\right)^h}{1 + \alpha^{2h} \cdot \left(\frac{PEP}{K_{PEP}}\right)^h}\right] + \left(\frac{NADP}{K_{NADP}} + \frac{NADPH}{K_{NADH}} + \frac{ATP}{K_{ATP}}\right)^h\right)} \tag{2.8}$$

6-Phosphogluconolactonase, 6-Phosphogluconate Dehydratase and 2-Keto-3-Deoxy-6-Phosphogluconate Aldolase PGLS catalyses the reaction that converts 6PGL to 6PG, which is converted by EDD to produce 2-keto-3-deoxy-6-phosphogluconate (KDPG), in turn EDA catalyses KDPG conversion to 3PG and pyruvate. The intermediates for this reaction are not commercially available and for this study NMR (Figure 2.5) was used to characterise the kinetics of these enzymes

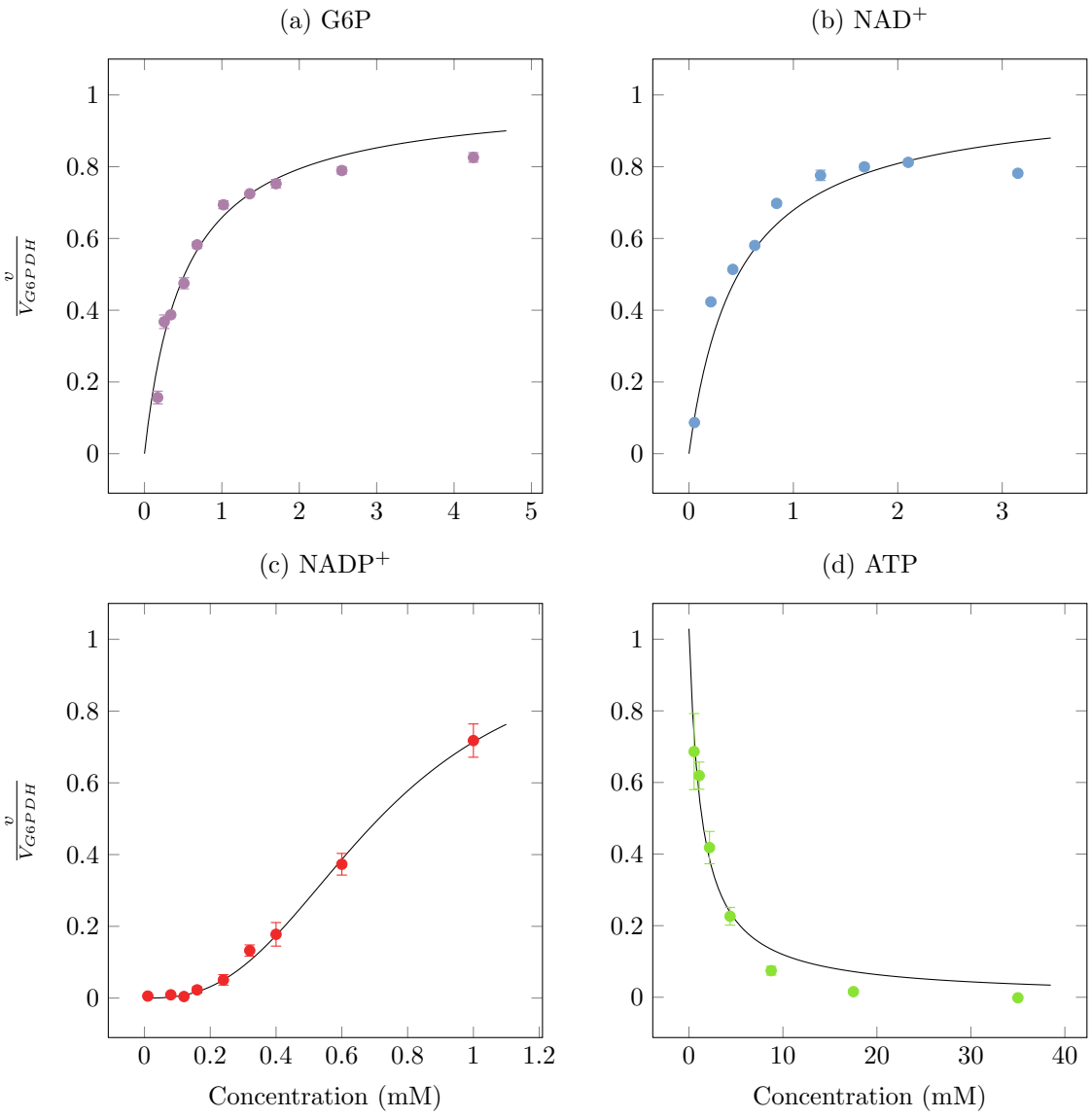

Figure 2.4: The biochemical characterisation of *Z. mobilis* glucose-6-phosphate dehydrogenase. *Z. mobilis* G6PDH was characterised in terms of its substrates. *Top left*(●) and *top right*(●): G6P and NAD^+. The data for the substrates were fitted to Equation 2.7, to obtain Michaelis constants for the substrates (Chapter 5). *Bottom left*(●): $NADP^+$, the data for the substrates were fitted to the GRH-equation (Equation 2.5). *Bottom right*(●): Shows the inhibition by ATP. Data are scaled to the maximal activity to eliminate day-to-day variations in extraction efficiency (See section 5.9). The lines show Equation 2.7 and 2.8, respectively and parameterised with the values of Table 2.5 and the respective substrate, product and inhibitor concentrations used in the assay. Error bars represent weighted mean, SEM (n=3).

Table 2.2: Summary of the kinetic parameters for *Z. mobilis* glucose-6-phosphate dehydrogenase.

Parameter	Fitted Value	Literature Value	Reference
V_{fG6PDH} (μmol.min^{-1}.mg^{-1})	1.54 ± 0.22	2.1	53
K_{G6P} (mM)	0.52 ± 0.04	0.17	48
K_{NAD^+} (mM)	0.47 ± 0.073	0.21	48
K_{NADP^+} (mM)	0.71 ± 0.34	0.04	48
K_{ATP} (mM)	0.42 ± 0.14	1.4	48
K_{PEP} (mM)	—	14.1	86
K_{eq}		450	85
h [a]	2.70	—	
α	—	0.5	22

[a] see Equation (2.8)

(Figure 2.6). 6PG was used as a starting metabolite, and monitoring reaction progress using ^{31}P NMR (see Chapter 5), the experimental data were fitted to Equation (2.9) and (2.10) to obtain kinetic parameters. The reactions catalysed by EDD and EDA are fitted to a single rate equation (Equation 2.10). KDPG could not be identified in NMR spectra, or commercially purchased to perform a standard assay.

$$v_{PGLS} = V_{fPGLS} \cdot \left(1 - \frac{\frac{6PG}{6PGL}}{K_{eq}}\right) \cdot \frac{\frac{6PGL}{K_{6PGL}}}{\left(1 + \frac{6PGL}{K_{6PGL}} + \frac{6PG}{K_{6PG}}\right)} \tag{2.9}$$

$$v_{ED} = V_{fED} \cdot \frac{\frac{6PG}{K_{6PG}} \cdot \left[1 - \frac{GAP \cdot PYR}{\frac{6PG}{K_{eq1} \cdot K_{eq2}}}\right]}{\left(1 + \frac{GAP}{K_{GAP}} + \frac{PYR}{K_{PYR}}\right) + \left(\frac{6PG}{K_{6PG}} + \left(\frac{6PG}{K_{6PG}} \cdot \frac{PYR}{K_{PYR}}\right)\right)} \tag{2.10}$$

Glyceraldehyde-3-Phosphate Dehydrogenase GAPDH catalyses the reaction of GAP, P_i and NAD^+ to 1,3-biphosphoglycerate and NADH. The characterisation of the enzyme was done in the forward direction by varying substrate concentrations. The fitted curve for GAP and NAD^+ is shown in Figure 2.7. The data are fitted to a generic reversible bi-bi substrate equation (2.11). P_i is accounted for by recalculating the K_{eq}, with phosphate at 0.5 mM (fixed concentration in model) [87].

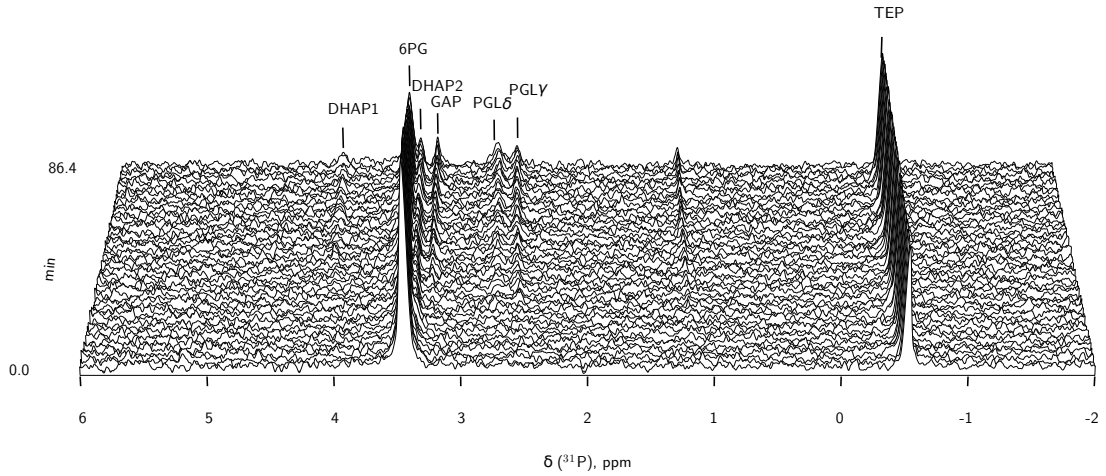

Figure 2.5: Time course of full 1-D NMR spectra for the reactions of 6PGL, 6PG, KDPG and TPI in *Z. mobilis*. ^{31}P NMR was performed at 30 °C, with probe spinning at 10 Hz, pulse angle 90°, repetition time 1.5 s (1.0 s acquisition, 0.5 s relaxation) to collect transients. An initial concentration of 10 mM 6PG was used. 10 mM triethyl phosphate (TEP) was included as an internal standard. The metabolites are assigned to peaks, determined from experimental standards, or literature values for chemical shifts.

Table 2.3: Summary of the kinetic parameters for *Z. mobilis* 6-phosphogluconolactonase.

Parameter	Fitted Value	Literature Value	Reference
V_{fPGLS} (μmol.min^{-1}.mg^{-1})	5.09 ± 0.045		
K_{6PGL} (mM)	—	0.059	21
K_{6PG} (mM)	0.0179 ± 0.0002	0.025	21
K_{eq}		6357	85

Table 2.4: Summary of the kinetic parameters for *Z. mobilis* 6-phosphogluconate dehydratase and 2-keto-3-deoxy-6-phosphogluconate aldolase.

Parameter	Fitted Value	Literature Value	Reference
V_{fED} (μmol.min^{-1}.mg^{-1})	1.465	—	
K_{6PG} (mM)	0.0088 ± 0.002	0.04	55
K_{GAP} (mM)	0.03 ± 0.002	2	55
K_{PYR} (mM)	15.42 ± 0.056	—	—
K_{eq1}[a]		5.7×10^{6}	85
K_{eq2}[b]		1.6×10^{-3}	85

[a] Equilibrium constant for 6PG in Equation (2.10)
[b] Equilibrium constant for KDPG in Equation (2.10)

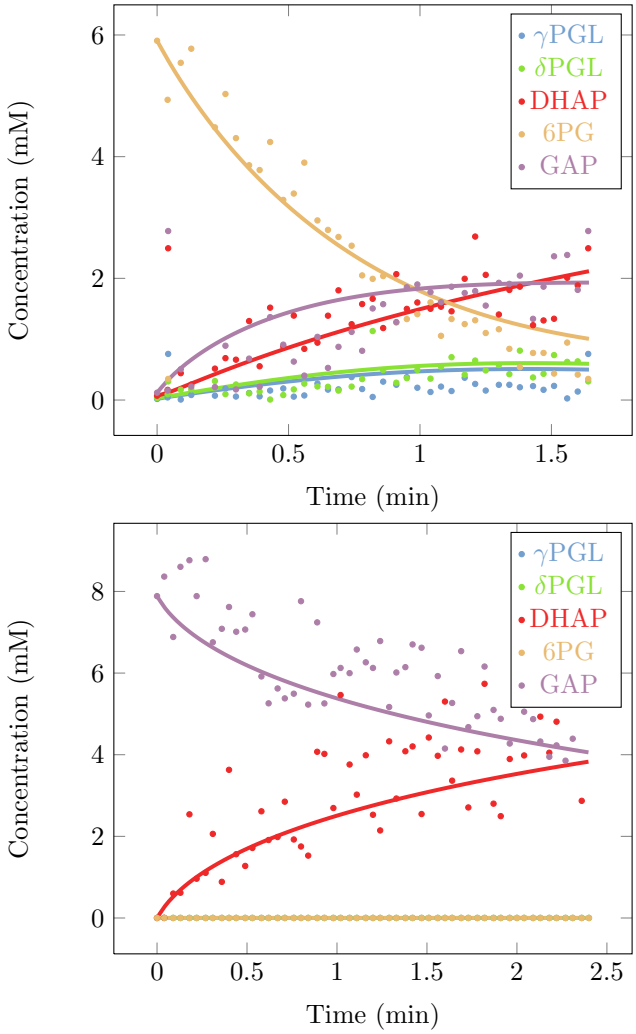

Figure 2.6: The biochemical characterisation of *Z. mobilis* 6PGLS, EDD, EDA and TPI. Time series of enzymatic reactions were acquired using ^{31}P NMR (represented by the data points). *Top*: Reactions where initiated with 6PG (10 mM) as starting metabolite. *Bottom*: Reactions where initiated with GAP (10 mM) as starting metabolite. NMR reaction time courses were fitted with a sub-model representing the reactions (represented by the lines), to characterise the enzymes. To collate reaction time series during model fitting, NMR peak areas were normalised by protein concentration determined by Bradford assay.

Table 2.5: Summary of the kinetic parameters for *Z. mobilis* glyceraldehyde-3-phosphate dehydrogenase. The weighted kinetic data were fitted with the Michaelis-Menten equation and the fitted curves are shown in Figure 2.7.

Parameter	Fitted Value	Literature Value	Reference
V_{fGAPDH} (μmol.min^{-1}.mg^{-1})	0.55 ± 0.0049	2.1	53
K_{GAP} (mM)	0.78 ± 0.28	1.0	21
		0.21	88
K_{NAD^+} (mM)	0.042 ± 0.02	0.09	21, 88
K_{BPG} (mM)	—	1.0	21
	—	0.01	88
K_{NADH} (mM)	—	0.02	21
	—	0.06	88
K_{eq}		0.004	85

$$v_{GAPDH} = V_{fGAPDH} \cdot \left(1 - \frac{\frac{bPG \cdot NADH}{GAP \cdot NAD}}{K_{eq}}\right) \cdot \frac{\frac{GAP}{K_{GAP}} \cdot \frac{NAD}{K_{NAD}}}{\left(1 + \frac{GAP}{K_{GAP}} + \frac{bPG}{K_{bPG}}\right)\left(1 + \frac{NAD}{K_{NAD}} + \frac{NADH}{K_{NADH}}\right)} \tag{2.11}$$

3-Phosphoglycerate Kinase As 3PG was not experimentally measured in this study, kinetic parameters were obtained from the literature (Table 2.6). The parameters are incorporated into the model with a generic reversible bi-bi equation (Equation 2.12).

$$v_{PGK} = V_{fPGK} \cdot \left(1 - \frac{\frac{3PG \cdot ATP}{bPG \cdot ADP}}{K_{eq}}\right) \cdot \frac{\frac{bPG}{K_{bPG}} \cdot \frac{ADP}{K_{ADP}}}{\left(1 + \frac{bPG}{K_{bPG}} + \frac{3PG}{K_{3PG}}\right)\left(1 + \frac{ADP}{K_{ADP}} + \frac{ATP}{K_{ATP}}\right)} \tag{2.12}$$

Phospoglycerate Mutase PGM catalyses the conversion of 3PG to 2PG. The characterisation was done with 3PG as substrate by varying the concentration between $0 - 27.5$ mM as shown in Figure 2.8.

The K_{3PG} determined in previous studies [63], is comparable to the one determined for PGM in yeast [88] and agrees with our data (Table 2.7). Furthermore because the K_{2PG} could not be determined in this study, the literature value was assumed for the rate equation in the model.

The data obtained from experimental work is fitted to a generic reversible uni-uni substrate equation (Equation 2.13).

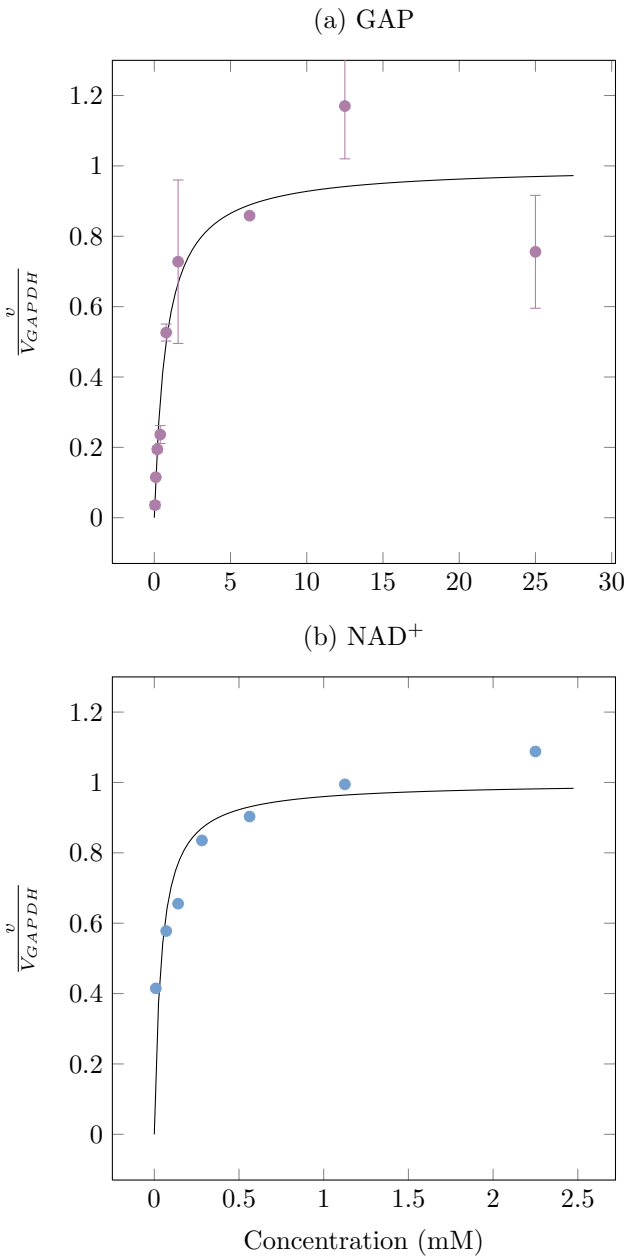

Figure 2.7: *Z. mobilis* glyceraldehyde-3-phosphate dehydrogenase biochemical characterisation. The enzyme was characterised in the forward direction with regard to substrates GAP and NAD^+. *Top*(●): GAP concentration was varied between $0 - 25$ mM at semi-saturating concentrations of NAD^+ (1 mM). *Bottom*(●): The NAD^+ concentration was varied between $0 - 2.25$ mM at semi-saturating concentrations of GAP (1.5 mM). Data are scaled to the maximal activity to eliminate day-to-day variations in extraction efficiency (See section 5.9). The lines show Equation 2.11, parameterised with the values of Table 2.5 and the respective substrate concentrations used in the assay. Error bars represent weighted mean SEM (n=6).

Table 2.6: Summary of the kinetic parameters for *Z. mobilis* 3-phosphoglycerate kinase obtained from literature.

Parameter	Literature Value	Reference
V_{fGAPDH} (μmol.min^{-1}.mg^{-1})	14.3	53
K_{bPG} (mM)	3×10^{-3}	88
K_{ADP} (mM)	0.8	88
K_{3PG} (mM)	1.5	63
K_{ATP} (mM)	1.1	63
K_{eq}	4×10^{3}	89

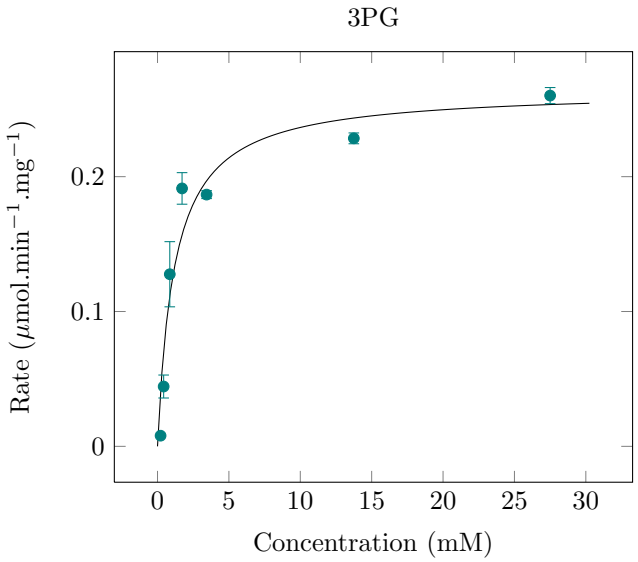

Figure 2.8: The biochemical characterisation of *Z. mobilis* phospoglycerate mutase. The enzyme was characterised in terms of its substrate 3PG in the forward direction. The data for the substrates were fitted to the Michaelis-Menten equation, to obtain Michaelis constants for the substrate. Error bars represent weighted SEM (n=4)

$$v_{PGM} = V_{fPGM} \cdot \left(1 - \frac{\frac{2PG}{3PG}}{K_{eq}}\right) \cdot \frac{\frac{3PG}{K_{3PG}}}{\left(1 + \frac{3PG}{K_{3PG}} + \frac{2PG}{K_{2PG}}\right)} \tag{2.13}$$

Enolase The conversion of 2PG to PEP is catalysed by this enzyme. The characterisation was done with 2PG as substrate in the forward direction and follows classical Michaelis-Menten kinetics.

The characterisation with regards to 2PG was achieved by varying the concentration between $0 - 2.0$ mM. The weighted kinetic data were fitted with the Michaelis-Menten equation and the

Table 2.7: Summary of the kinetic parameters for *Z. mobilis* phospoglycerate mutase.

Parameter	Fitted Value	Literature Value	Reference
V_{fPGM} (μmol.min^{-1}.mg^{-1})	0.26 ± 0.0022	—	
K_{m3PG} (mM)	1.18 ± 0.36	1.1	63, 88
K_{m2PG} (mM)	—	0.08	88
K_{eq}		0.2	85

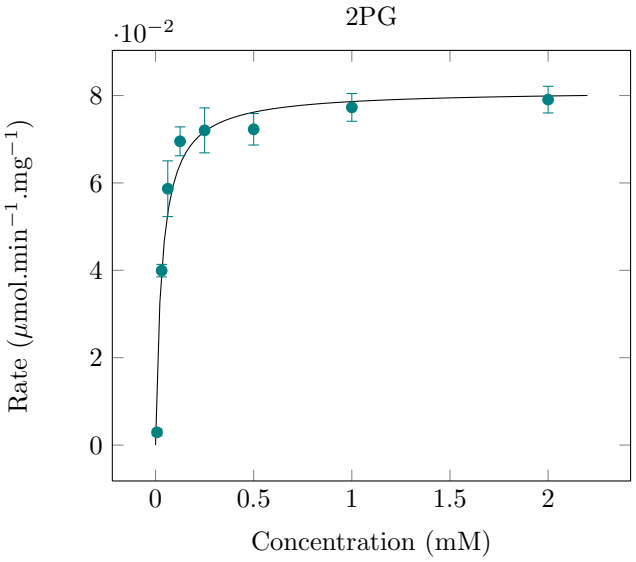

Figure 2.9: The biochemical characterisation of *Z. mobilis* enolase. The characterisation of the enzyme was done in the forward direction by varying the substrate concentration, 2PG. V and K_{m} was determined by fitting to the Michaelis-Menten equation. Error bars represent weighted SEM (n=3).

fitted curves are shown in Figure 2.9. The experimental data were fitted to a Michaelis-Menten equation to obtain kinetic parameters for Equation (2.14) which is incorporated into the model.

$$v_{ENO} = V_{fENO} \cdot \left(1 - \frac{\frac{PEP}{2PG}}{K_{eq}}\right) \cdot \frac{\frac{2PG}{K_{2PG}}}{\left(1 + \frac{PEP}{K_{PEP}} + \frac{2PG}{K_{2PG}}\right)} \tag{2.14}$$

Pyruvate Kinase The reaction catalyses the second ATP generation reaction of the glycolytic pathway, using PEP and substrate level phosphorylation of ADP, to produce pyruvate and ATP. PK was characterised in the forward direction with PEP and ADP as substrates, and product inhibition by ATP. The data for the substrates were fitted to the Michaelis-Menten equation, to obtain Michaelis constants for the substrates. Furthermore it also shows the inhibition by ATP (Figure 2.10). The K_{ATP} was obtained by fitting of the data to Equation (2.15).

Table 2.8: Summary of the kinetic parameters for *Z. mobilis* enolase.

Parameter	Fitted Value	Literature Value	Reference
V_{fENO} (μmol.min^{-1}.mg^{-1})	0.08 ± 0.0038	—	
K_{m2PG} (mM)	0.033 ± 0.008	0.08	63
K_{mPEP} (mM)	—	0.5	88
K_{eq}		4	85

Table 2.9: Summary of the kinetic parameters for *Z. mobilis* pyruvate kinase. The enzyme was assayed in the forward direction and shows inhibition by its product ATP.

Parameter	Fitted Value	Literature Value	Reference
V_{fPK} (μmol.min^{-1}.mg^{-1})	4.3 ± 0.4	—	
K_{PYR} (mM)	—	0.21	63
K_{PEP} (mM)	0.25 ± 0.04	0.08	63
K_{ADP} (mM)	0.08 ± 0.01	0.17	63
K_{ATP} (mM)	0.58 ± 0.10	—	
K_{eq}		3.89×10^{4}	

$$v_{PK} = V_{fPK} \cdot \left(1 - \frac{\frac{Pyruvate \cdot ATP}{PEP \cdot ADP}}{K_{eq}}\right) \cdot \frac{\frac{PEP}{K_{PEP}} \cdot \frac{ADP}{K_{ADP}}}{\left(1 + \frac{PEP}{K_{PEP}} + \frac{Pyruvate}{K_{Pyruvate}}\right)\left(1 + \frac{ADP}{K_{ADP}} + \frac{ATP}{K_{ATP}}\right)} \tag{2.15}$$

Pyruvate Decarboxylase The enzyme catalyses the decarboxylation of pyruvate to acetaldehyde with the formation of carbon dioxide. Since the reaction is thiamine diphosphate dependent it was added to buffer for characterisation of the enzyme (see Chapter 5).

$$v_{PDC} = \frac{V_{fPDC} \cdot \frac{Pyruvate}{K_{pyruvate}}}{1 + \frac{Pyruvate}{K_{Pyruvate}}} \tag{2.16}$$

Alcohol Dehyrogenase ADH catalyses the conversion of acetaldehyde and NADH, to Ethanol and NAD^{+}. The reaction was characterised in terms of these substrates in both the forward and reverse direction. *Z. mobilis* possesses two well characterised isozymes of ADH. It should be noted that most characterisations of these two isozymes are done separately in literature, however since

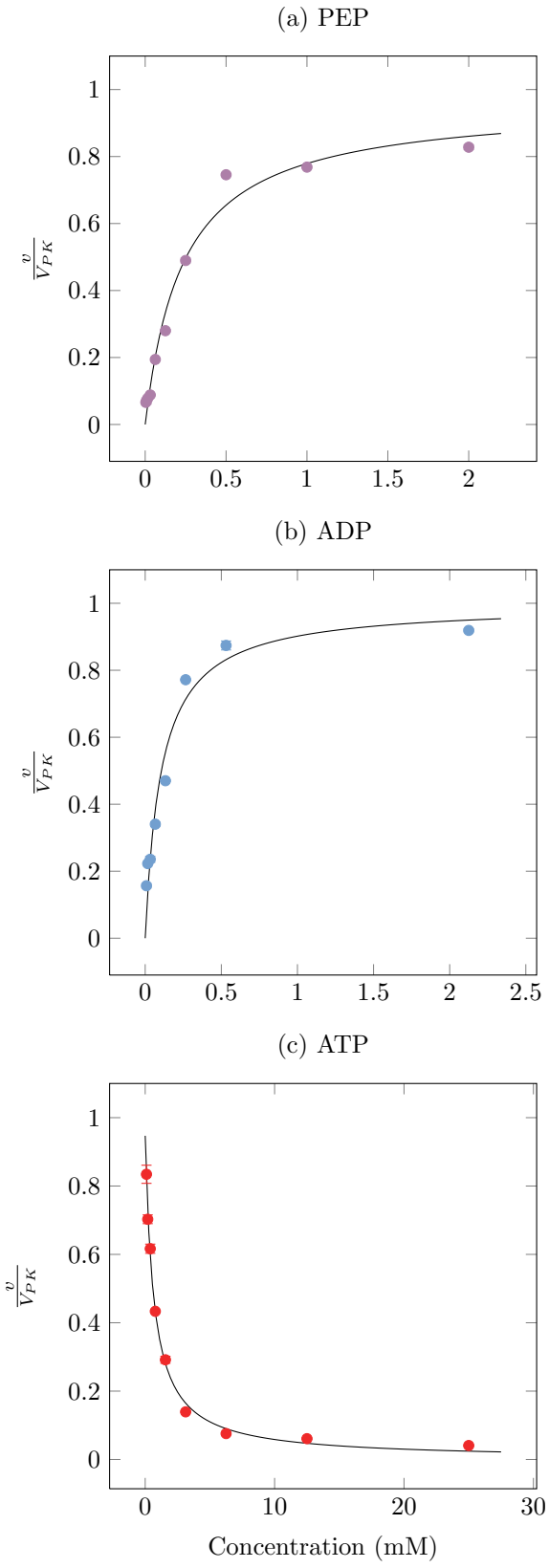

Figure 2.10: *Z. mobilis* pyruvate kinase biochemical characterisation. *Top*(●) & *middle*(●): The reaction was characterised in the forward direction with PEP and ADP as substrates. Saturation of the enzyme with PEP and ADP was achieved by varying the concentration of each respectively, while keeping the other constant at 1 mM. *Bottom*(●): Shows inhibition by the product ATP. Data are scaled to the maximal activity to eliminate day-to-day variations in extraction efficiency (See section 5.9). The lines show Equation 2.15, parameterised with the values of Table 2.9 and the respective substrate and inhibitor concentrations used in the assay.

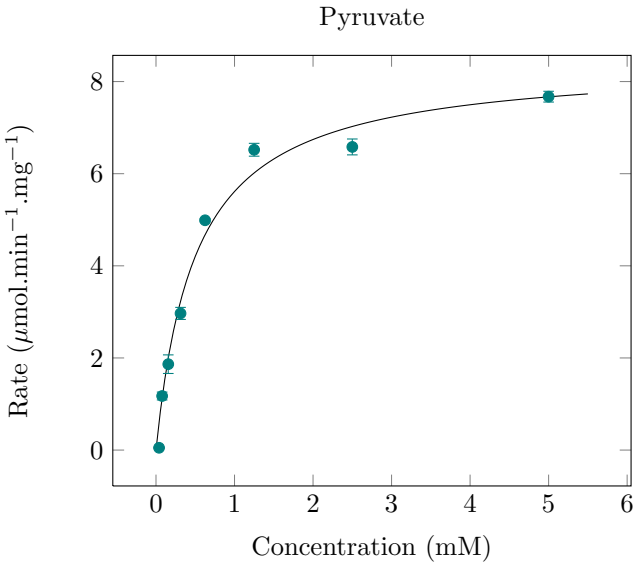

Figure 2.11: The biochemical characterisation of *Z. mobilis* pyruvate decarboxylase. The enzyme was assayed and characterised in the forward direction towards ethanol formation, with regards to substrate pyruvate.

Table 2.10: Summary of the kinetic parameters for *Z. mobilis* pyruvate decarboxylase.

Parameter	Fitted Value	Literature Value	Reference
V_{fPDC} (μmol.min^{-1}.mg^{-1})	8.44 ±0.4	3.2	53
K_{mPYR} (mM)	0.50 ±0.08	0.4	90
K_{eq}	0.5		85

this study was done using cell lysates it was not possible to separate the isozymes of ADH. The cell lysates would contain both isozymes. Furthermore for modelling of the cellular environment the two isozymes separately are not required, since the characterisation would represent the combined behaviour of kinetics for ADH (Equation (2.17)). However, for data interpretation it should be considered that ADH-1 functions as the major ADH, and has a higher specific activity for substrate compared to ADH-2.

$$v_{ADH} = V_{fADH} \cdot \left(1 - \frac{Ethanol \cdot NAD}{ACET \cdot NADH} \frac{1}{K_{eq}}\right) \cdot \frac{\frac{ACET}{K_{ACET}} \cdot \frac{NADH}{K_{NADH}}}{\left(1 + \frac{ACET}{K_{ACET}} + \frac{Ethanol}{K_{Ethanol}}\right)\left(1 + \frac{NADH}{K_{NADH}} + \frac{NAD}{K_{NAD}}\right)} \tag{2.17}$$

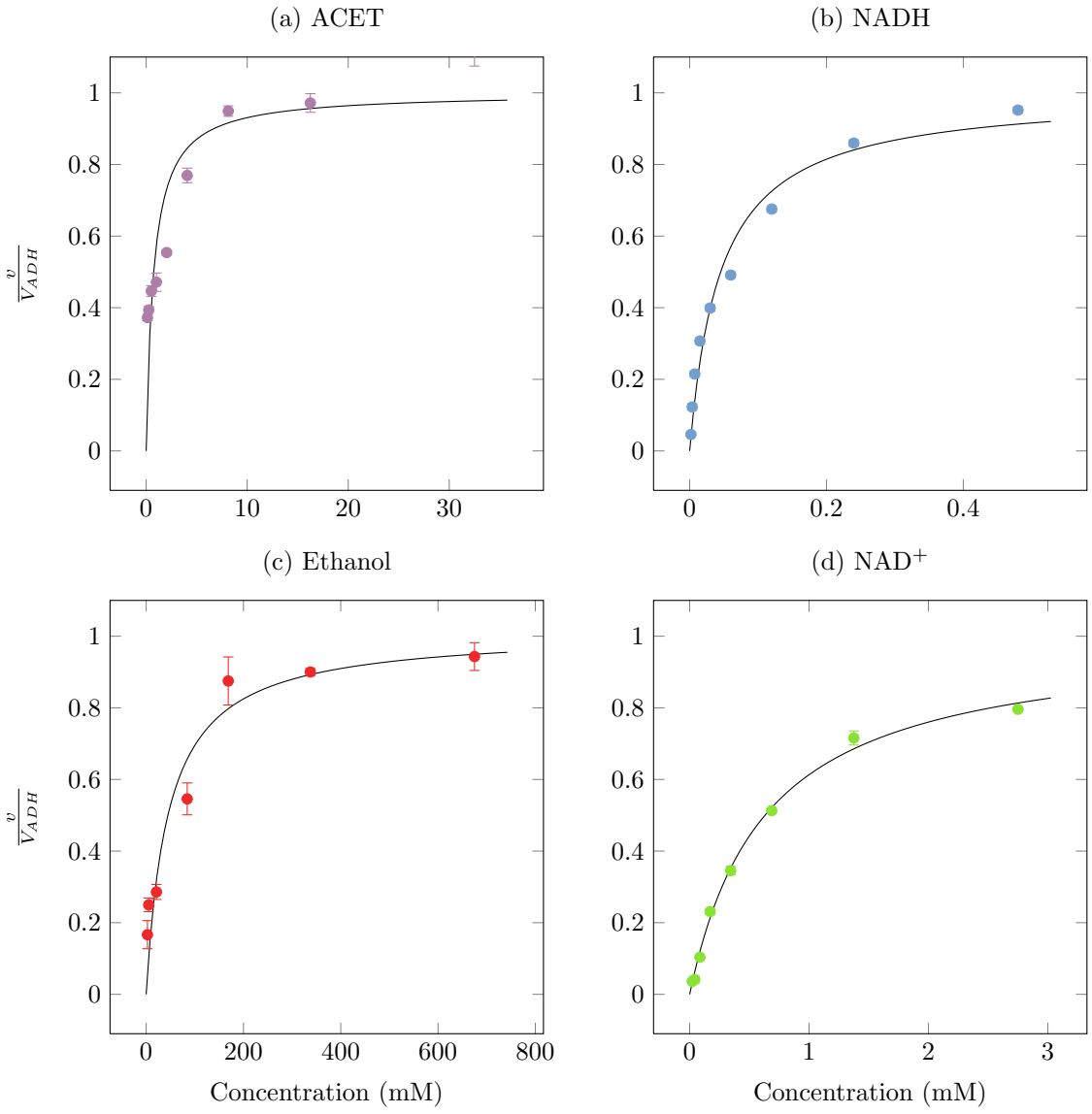

Figure 2.12: The biochemical characterisation of *Z. mobilis* alcohol dehydrogenase. *Top left*(●) & *top right*(●): The enzyme was assayed and characterised in the forward direction in terms of substrates acetaldehyde and NADH. *Bottom left*(●) & *bottom right*(●): Characterisation in the reverse direction with regards to it products ethanol and NAD^+. Data are scaled to the maximal activity to eliminate day-to-day variations in extraction efficiency (See section 5.9). The lines show Equation 2.17, parameterised with the values of Table 2.11 and the respective substrate and product concentrations used in the assay. Error bars represent weighted mean SEM (n=3).

Table 2.11: Summary of the kinetic parameters for *Z. mobilis* alcohol dehydrogenase.

Parameter	Fitted Value	Literature Value	Reference
V_{fADH} (μmol.min^{-1}.mg^{-1})	2.07 ± 0.12	2.9	53
V_{rADH} (μmol.min^{-1}.mg^{-1})	2.67 ± 0.016	—	
K_{mACET} (mM)	0.744 ± 0.29	0.086 (ADH I) 1.3 (ADH II)	91 91, 92
K_{mNADH} (mM)	0.0455 ± 0.00012	0.027 (ADH I) 0.012(ADH II)	91 91
K_{mETOH} (mM)	39.29 ± 1.4	4.8(ADH I) 27(ADH II)	91 91
K_{mNAD^+} (mM)	0.631 ± 0.0579	0.073(ADH I) 0.11(ADH II)	91 91
K_{iNADH} (mM)	—	0.0076 (ADH I) 0.018 (ADH II)	91 91
K_{iNAD^+} (mM)	—	0.024 (ADH I) 0.14 (ADH II)	91 91
K_{eq}		1.0×10^4	85

Chapter 3

Model Construction and Analysis

This chapter gives a short overview on kinetic modelling in general, and describes the construction of a kinetic model of glycolysis in *Z. mobilis*. Furthermore we show how a partially validated model is obtained, and perform model analysis.

3.1 Kinetic modelling - an overview

Computational systems biology can be viewed as a method to mathematically describe aspects of a living system, and is the integration between experimental and computational research. Consider the following pathway;

$$X_1 \xleftrightarrow{E_1} S_2 \underset{E_3}{\overset{E_2}{\rightleftharpoons}} S_3 \xleftrightarrow{E_4} X_4$$

where X_1 and X_4 are external metabolite concentrations and treated as constant (source and sink respectively). S_2 and S_3 are variable metabolite concentrations. E_1 to E_4 are the enzymes catalysing each step [93]. The rate of catalysis of each step can be expressed in terms of an appropriate rate equation, with rate of catalysis v_j, time (t), metabolite concentration vectors (S) and parameter vector p as follows,

$$v_j = v(\mathbf{S}, \mathbf{p}, t), \tag{3.1}$$

where $j \in (1, 2, 3, 4)$, and for steady-state where metabolite concentrations do not explicitly depend on time,

$$v_j = v(\mathbf{S}(t), \mathbf{p}). \tag{3.2}$$

An essential attribute of metabolic reactions is their stoichiometry, which is the relationship between number of substrate and product molecules that enter a reaction, with assigned sign of the stoichiometric coefficients showing product or reactant of the reaction. The set of stoichiometric coefficients can be considered a vector, and it is useful to express this in matrix format, when analysing a system of several reactions. The matrix for the above schema is given by

$$\mathbf{N} = \begin{array}{c} \\ X_1 \\ S_1 \\ S_2 \\ X_2 \end{array} \begin{array}{c} \begin{array}{cccc} E_1 & E_2 & E_3 & E_4 \end{array} \\ \begin{pmatrix} -1 & 0 & 0 & 0 \\ 1 & -1 & 1 & 0 \\ 0 & 1 & -1 & -1 \\ 0 & 0 & 0 & 1 \end{pmatrix} \end{array}$$

Changes in the metabolite concentration are given by

$$\frac{d\mathbf{s}}{dt} = \mathbf{N}\mathbf{v}. \tag{3.3}$$

Where $\mathbf{v}$ and $\mathbf{s}$ denote the vectors of reaction rates and concentrations, respectively. Integrating Equation (3.3) will yield the time dependent dynamics for a system.

3.2 Analyses of kinetic models

Steady state analyses assume that the concentrations of metabolites in the metabolic system do not change. Solving Equation (3.4) will determine the steady-state concentrations and fluxes.

$$\mathbf{N}\mathbf{v} = \mathbf{0} \tag{3.4}$$

Metabolic control analysis (MCA) provides a mathematical framework to quantify the behaviour of metabolic systems at steady-state. It allows us to study the control and regulation of metabolism, or subsystems of metabolism, by relating the various reactions' effect on determining fluxes and metabolite concentrations [6, 93, 5]. It was independently developed by Kascer & Burns [6] and Heinrich & Rapoport [94, 95]. Some of the basic concepts of MCA will be discussed in this section.

Elasticity coefficients allow us to quantify the relative change in local rate, due to a parameter or metabolite perturbation for that reaction. For an enzyme reaction rate with reaction rate v, and a substrate, product or effector x we can express the elasticity as

$$\epsilon_x^v = \frac{\partial \ln v}{\partial \ln x}. \tag{3.5}$$

Control coefficients quantify behaviour around a steady state, due to a change in a local reaction rate. Perturbations of reaction rate v, in relation to steady-state variable y, can be expressed as follows;

$$C_v^y = \frac{\partial \ln y}{\partial \ln v}, \tag{3.6}$$

where y is flux (J), or concentration (s).

Response coefficients describe the relative change in steady-state variable y, due to a perturbation of parameter or external metabolite x, and are expressed as follows;

$$R_x^y = \frac{\partial \ln y}{\partial \ln x}, \tag{3.7}$$

where y is as in Equation (3.6). Response coefficients can be defined operationally as % change in y when x is perturbed by 1 %. These can be further described as the product of there elasticity and control coefficient with respect to steady state variable y and effector x as follows [6];

$$R_x^y = \epsilon_x^v . C_v^y, \tag{3.8}$$

where the parameter x acts directly on step v.

The next sections summarises the kinetic characterisation (Chapter 2), and provides a detail on all model parameters.

3.3 Model Description

Rate Equations, parameter values and moieties

The model consists of 12 reaction steps as shown in Figure 2.1. The model describes the glycolytic conversion of glucose to its end product, ethanol. Chapter 2 has detailed the kinetic characterisation of each reaction step, fitted to a kinetic rate equation (Summarised in Appendix A). The kinetic parameters of the uncharacterised reaction step (PGK), were obtained from literature. Furthermore for reactions that were characterised but where a parameter could not be experimentally determined, this was also obtained from literature. A summary of parameter values is shown in Table 3.1, these were used to populate the rate equations.

The model has three conserved moieties, where the concentration of ATP & ADP, NAD^+ & NADH and $NADP^+$ & NADPH remain constant (Equations (3.9), (3.10) and (3.11)). The concentrations were obtained from literature and are fixed in the model [96].

$$ATP + ADP = [Total\ ATP\ moiety\ ] \tag{3.9}$$

$$NAD^+ + NADH = [Total\ NAD\ moiety\ ] \tag{3.10}$$

$$NADP^+ + NADPH = [Total\ NADPH\ moiety\ ] \tag{3.11}$$

Maximal enzyme rates

The maximal rates of each glycolytic enzyme were all determined from a homogenate of cell lysates, to counter variation in protein expression levels between batches. Since all of the maximal rates are determined from a single homogenate, under saturation or semi-saturating concentrations as determined by experimental characterisation, for many of the enzymes the measured maximal enzyme activities were different than when determined from saturating curves (Chapter 2). There were constraints which influence the maximum concentration of NADH/NADPH we could add to an assay. Absorbance linearity does not allow us to use high concentrations. Furthermore the maximum amounts of ATP/ADP that could be added to an assay require high magnesium concentration to ensure that ATP is in the active MgATP form. To exclude Mg^{2+} interference, we set a limit on the concentration that could be used.

Ordinary Differential Equations of the model

ODEs decribe the change in concentration for each of the metabolites in the model (see Section 3.1 and Equation (3.3)). The ODEs are summarised in Equations (3.12 -3.24).

$$\frac{d}{dt} Glucose_{exsternal} = v_{Glucose_{external}} - v_{GK} \tag{3.12}$$

$$\frac{d}{dt} G6P = v_{GK} - v_{G6PDH} \tag{3.13}$$

$$\frac{d}{dt} PGL = v_{G6PDH} - v_{PGL} \tag{3.14}$$

$$\frac{d}{dt} PG = v_{PGL} - v_{ED} \tag{3.15}$$

$$\frac{d}{dt} GAP = v_{ED} - v_{GAPDH} \tag{3.16}$$

$$\frac{d}{dt} PYR = v_{ED} + v_{PK} - v_{PDC} \tag{3.17}$$

$$\frac{d}{dt} bPG = v_{GAPDH} - v_{PGK} \tag{3.18}$$

$$\frac{d}{dt} 3PG = v_{PGK} - v_{PGM} \tag{3.19}$$

$$\frac{d}{dt} 2PG = v_{PGM} - v_{ENO} \tag{3.20}$$

$$\frac{d}{dt} PEP = v_{ENO} - v_{PK} \tag{3.21}$$

$$\frac{d}{dt} ACET = v_{PDC} - v_{ADH} \tag{3.22}$$

$$\frac{d}{dt} Ethanol = v_{ADH} - v_{Ethanol_{external}} \tag{3.23}$$

Starting conditions

In the model external metabolites, and concentrations of moieties were clamped and initial internal metabolite concentrations were set as shown in Table 3.2. The extracellular ethanol concentration was set at 50 mM based on data reported in [18].

3.4 Towards model validation; in search of a steady state.

Model A - using our determined kinetics

Upon construction of an initial model using the rate equations and parameters listed in Section 3.3, running a time simulation did not yield a valid steady-state. The model could calculate metabolite concentrations during the time simulation, but was unable to reach steady-state. The metabolite concentrations gave insight into possible experimental errors. Model predicted metabolite concentrations showed a continuous build up of specific metabolites. Furthermore the flow of metabolites through lower glycolysis (reactions from GAP to PK), was negligible, causing a build up of glycolytic metabolites, and no flow to end products shown in Figure 3.1. However, steady-states are an experimentally measurable criterion for model validation, given the quasi-steady state assumption. This implied that the constructed model contained errors.

In order to identify the problem we considered the two separate parts of this work, the experimental (kinetic characterisation) and theoretical (modelling). Re-evaluation of the rate equations,

Table 3.1: Summary of the kinetic parameters for *Z. mobilis*.

Enzyme	E.C number	Parameter	Experimental	Literature Value
GLK	2.7.1.2	$K_{Glucose}$	0.26 ± 0.045	0.22 [48]
		K_{ATP}	0.41 ± 0.067	0.8 [48]
		K_{G6P}	9.25 ± 2.32	15 [48]
		K_{ADP}	1.75 ± 0.139	—
		K_{eq}		2.26×10^3 [85]
		V_{fGLK}	1.41 ± 0.02	
G6PDH	1.1.1.49	K_{GAPDH}	0.52 ± 0.04	0.17 [48]
		K_{NAD^+}	0.47 ± 0.073	0.21 [48]
		K_{ATP}	0.42 ± 0.14	1.4 [48]
		K_{NADP^+}	0.71 ± 0.34	0.04 [86]
		K_{PEP}	—	14.1 [86]
		$K_{NADH/NADPH}$	—	1.0 assumed
		h	2.70	—
		K_{eq}		450 [85]
		V_{fG6PDH}	1.54 ± 0.22	
PGLS	3.1.1.31	K_{6PGL}	—	0.059 [21]
		K_{6PG}	0.0179 ± 0.0002	0.025 [21]
		K_{eq}		6357 [85]
		V_{fPGLS}	5.09 ± 0.045	
EDD[a]	4.2.1.12	K_{6PG}	0.0088 ± 0.002	0.04 [55]
EDA[a]	4.1.2.14	K_{GAP}	0.03 ± 0.002	2 [55]
		K_{PYR}	15.42 ± 0.056	—
		K_{eq1}		5.7×10^6 [85]
		K_{eq2}		1.6×10^{-3} [85]
		V_{fED}	1.465	
GAPDH	1.2.1.12	K_{GAP}	0.78 ± 0.28	1.0 [21]
		K_{NAD^+}	0.42 ± 0.002	0.01 [88]
		K_{BPG}	—	0.02 [21]
		K_{NADH}	—	0.06 [88]
		K_{eq}		0.004 [85]
		V_{fGAPDH}	0.55 ± 0.0049	
PGK	2.7.2.3	K_{bPG}		3×10^{-3} [88]
		K_{ADP}		0.8 [88]
		K_{3PG}		1.5 [63]
		K_{ATP}		1.1 [63]
		K_{eq}		4×10^3 [89]
		V_{fPGK}	24.42	
PGM	5.4.2.1	K_{m3PG}	1.18 ± 0.36	1.1[63, 88]
		K_{m2PG}	—	0.08 [88]
		K_{eq}		0.2 [85]
		V_{fPGM}	0.26 ± 0.0022	
ENO	4.2.1.11	K_{m2PG}	0.033 ± 0.008	0.08 [63]
		K_{m3PG}	—	0.5 [88]
		K_{eq}		4 [85]
		V_{fENO}	0.08 ± 0.0038	
PK	2.7.1.40	K_{PEP}	0.25 ± 0.04	0.08 [63]
		K_{ADP}	0.08 ± 0.01	0.17 [63]
		K_{ATP}	0.58 ± 0.10	—
		K_{eq}		3.89×10^4 [85]
		V_{fPK}	4.3 ± 0.4	
PDC	4.1.1.1	K_{mPYR}	0.50 ±0.08	0.4 [90]
		K_{eq}		0.5 [85]
		V_{fPDC}	8.44 ±0.4	
ADH	1.1.1.1	K_{mACET}	0.744 ± 0.29	0.086 (ADH I) & 1.3 (ADH II) [91]
		K_{mNADH}	0.0455 ± 0.00012	0.027 (ADH I) & 0.012 (ADH II) [91]
		K_{mETOH}	39.29 ± 1.4	4.8 (ADH I) & 27 (ADH II) [91]
		K_{mNAD^+}	0.631 ± 0.0579	0.073 (ADH I) & 0.11 (ADH II) [91]
		K_{eq}		1.0×10^4 [85]
		V_{fADH}	2.07 ± 0.12	

All K_{m} values are in (mM), and V_f in (μmol.min^{-1}.mg^{-1})

[a] These enzyme reactions are fitted together. See Equation: (2.10)

Table 3.2: Summary of the kinetic model initial conditions.

Metabolite	Concentration (mM)	Reference
Glucose[a]	50	—
G6P	1.42	97
6PGL[b]	1.0	—
6PG	0.25	97
GAP	0.21	97
BPG	0.0007	97
3PG	2.36	97
2PG	0.24	97
PEP	0.17	97
PYR	2.5	87
ACET	3.72	97
Ethanol	0.5	18
ATP[a]	0.85	96
ADP [a]	0.73	96
NAD^+[a]	0.97	96
NADH[a]	0.24	96
$NADP^+$[a]	0.77	96
NADPH[a]	0.05	96
P_i[a]	0.5	98

[a] Fixed concentration in model.
[b] No literature values were available, the concentration was estimated in the same range as the substrates and products connected to this reaction.

and the kinetic parameters did not pin-point the problem. However the parameters for the model depend on the experimental work, and the likelihood of the problem residing with the experimental work was much greater.

To overcome this problem a second model was constructed.

Model B - using glucose uptake flux

Using the same rate equations as described in Section (3.4), and the experimentally determined glucose uptake flux (Figure 3.4 & Table 3.4) a new model was constructed. The parameters were all kept at the experimentally determined values excluding the maximal rates. Using published steady-state concentrations [97, 87, 96, 98], and the experimentally determined flux, the maximal rates were calculated by rearranging Equation (3.24) into Equation (3.25) which determines the V of the enzyme required to achieve the measured flux. This was done for each of the reactions.

$$J = V \cdot f(s) \tag{3.24}$$

$$V = \frac{J}{f(s)} \tag{3.25}$$

Model B is mathematically circular in that it will by definition accurately achieve the steady-state concentrations and flux. Furthermore glucose uptake flux cannot be used as a validation

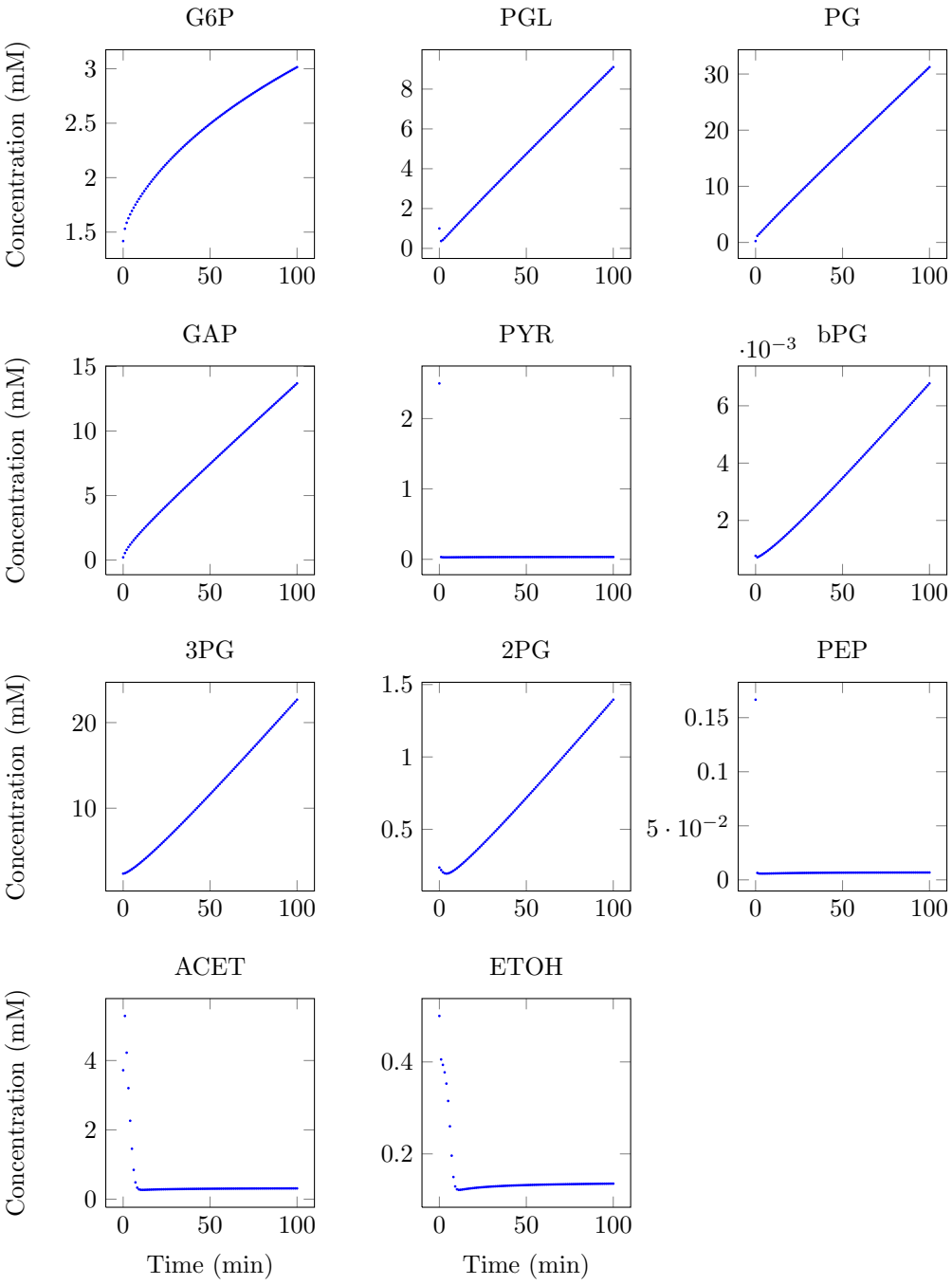

Figure 3.1: Time course simulation of Model A. Steady-states were not obtained, due to the continuous build-up of metabolites in glycolysis.

method for this model, because it is integrated into model construction. However, Model B can be used to identify possible errors in Model A because it shares the following characteristics with the initial model:

- The rate equations of Model B are the same.
- Binding affinity parameters (K_{m}) are the same.
- The model has the same set of ODEs.
- Conserved metabolite species (moieties) are identical.
- Starting metabolite concentrations are identical.

The only difference lies in the maximal rates for each reaction.

Discrepancies between Model A and Model B

Using the initial model (Model A), and comparing the maximal rates to those of Model B, shows that the reaction rates of GAPDH, PGM and ENO are much lower (Figure 3.2). The experimental characterisations of these enzymes were all done simultaneously using the same lysate, by coupled LDH assays. Firstly, we considered a decreased LDH activity in the coupled assays as a possible reason for lower V values obtained for these reactions. LDH from rabbit skeletal muscle is sensitive to pH changes. Between pH 6.2 and 6.5 the enzyme has a low turnover number, which decreases as the pH increases to 6.6. Activity substantially increases above pH 6.6, with a 70% increase in activity between pH 7.0 and 7.4. Furthermore at pH 5.0 - 6.8 LDH shows high substrate inhibition [99, 100].

Consider,

$$V = k_{cat}[E], \tag{3.26}$$

$$\therefore v \propto [E], \tag{3.27}$$

where k_{cat} gives a direct measure of the catalytic production of product under optimum conditions, and the above mentioned sensitivity of LDH to pH. Taking into consideration, that even at a 90% reduction in k_{cat} the assay protocol still contained a sufficient concentration of LDH, this excludes it as a cause of the above discrepancy.

Protein denaturation due to the extraction method was considered as a possible second reason. The characterisation of these enzymes are shown in Figures 2.7, 2.8 and 2.9 and Tables 2.5, 2.7 and 2.8. The K_{m} values for these enzymes all fall within the same range as the literature values. Furthermore the maximal rates are affected by the enzyme concentration, as shown by Equations 3.26 and 3.27. We therefore hypothesised that the decreased activity was due to possible protein denaturation.

We chose to correct the lower maximal rates by introduction of a correction factor (15) for the rate equation of GAPDH, PGM and ENO. This factor was calculated using the lowest ratio value of the rates of Model B, compared to Model A. Each of these reactions was increased by the same factor to produce Model C.

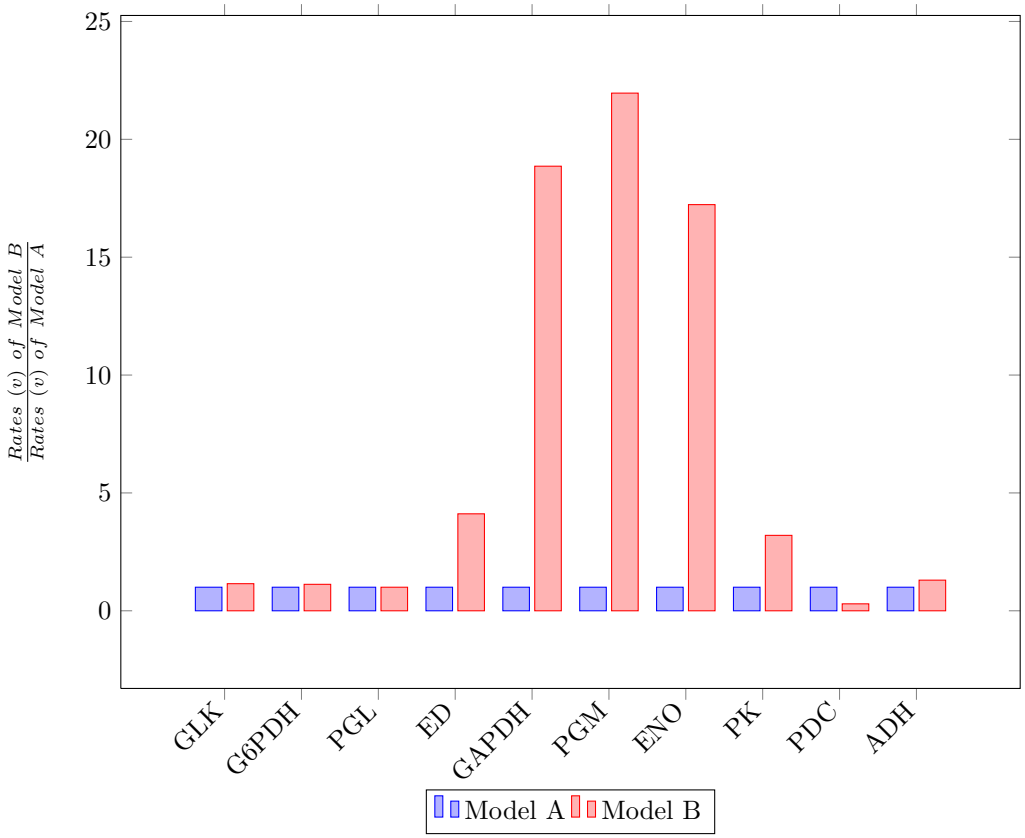

Figure 3.2: Initial rates at t = 0, of Model B scaled to Model A. GAPDH, PGM and ENO rates for Model A are significantly lower than the calculated rates of Model B.

Model C - steady-state capable

Model C is constructed from the Model A, and the kinetic rate equations for GAPDH, PGM and ENO adapted by the factor determined from a comparison between Model A and Model B. Including the correction factor into the model, and running a time simulation yielded a valid steady-state. The maximal rates of Model A, Model B, Model C and rates obtained from literature are shown in Table 3.3.

Model C was chosen as the final version, and used for model validation and analysis.

Model C can be summarised as follows:

- The rate equations of Model C are the same as Model A.
- Binding affinity parameters (K_{m}) are the experimentally determined values.
- The model has the same set of ODEs as Model A.
- Conserved metabolite species (moieties) are identical to Model A.
- Starting metabolite concentrations are identical to Model A.
- V are the same as in Model A, with exception of GAPDH, PGM and ENO, which were corrected by inclusion of a correction factor.

Table 3.3: Summary of maximal activities of glycolytic enzymes in Model A, Model B and Model C.

Enzyme	Model A	Model B	Model C	Literature
GLK	1.41	1.62	1.41	1.54 [53]
G6PDH	1.54	1.72	1.54	2.1 [53]
PGLS	6.27	6.7	6.27	—
ED	0.994	4.08	0.994	—
GAPDH	0.55	10.37	8.25	2.1 [53]
PGK[a]	24.42	24.42	24.42	2.8 [53]
PGM	0.26	5.71	3.9	14.3 [53]
ENO	0.08	1.37	1.2	—
PK	4.3	24.80	4.3	—
PDC	8.4	2.29	8.4	3.2 [53]
ADH	2.6	3.40	2.6	2.9 [53]

All enzyme activities expressed as (μmol.min^{-1}.mg^{-1})
[a] The reaction could not be characterised.

3.5 Model validation

This section will examine if the Model C can describe glycolytic flux and *in vivo* metabolite concentrations on the basis of enzyme kinetics alone. Following this validation we will be able to perform model analysis with MCA.

Glucose uptake flux

For the glucose uptake flux and to assess the ratios of fermentation products an *in vivo* ^{13}C NMR glucose uptake flux experiment was performed with a mixture of $\frac{1}{6}$D-glucose-1-^{13}C:$\frac{5}{6}$D-glucose-^{12}C. A blank (glucose excluded), was used to tune the spectrophotometer, by acquiring a lock signal and shimming the instrument. The reaction was initiated by removal of the tube and addition of glucose (50 mM), mixed by inverting several times, and re-inserting the tube to collect a time course spectra. The experimental protocol is described in Chapter 5. The results are shown in Figure 3.3 and Figure 3.4, and are within the same range as other literature values [10, 101]. The results of the model predicted glycolytic flux are compared to experimentally determined glycolytic flux, and are shown in Table 3.4. Furthermore, Table 3.3, shows the predicted flux using literature values for Model C. This was done to see if the model could obtain a steady-state, using literature values.

Table 3.4: Summary of experimental determined glycolytic flux and model predicted glycolytic flux for glucose and ethanol. Model C* is Model C, but uses literature values for maximal activities where available.

Flux	Model C (μmol.min^{-1}.mg^{-1})	Experimental (μmol.min^{-1}.mg^{-1})	Model C* (μmol.min^{-1}.mg^{-1})	Literature (μmol.min^{-1}.mg^{-1})
$J_{glucose}$	0.83	0.96	0.79	1.03 [53]
$J_{ethanol}$	1.66	1.92	1.57	2.05 [53]

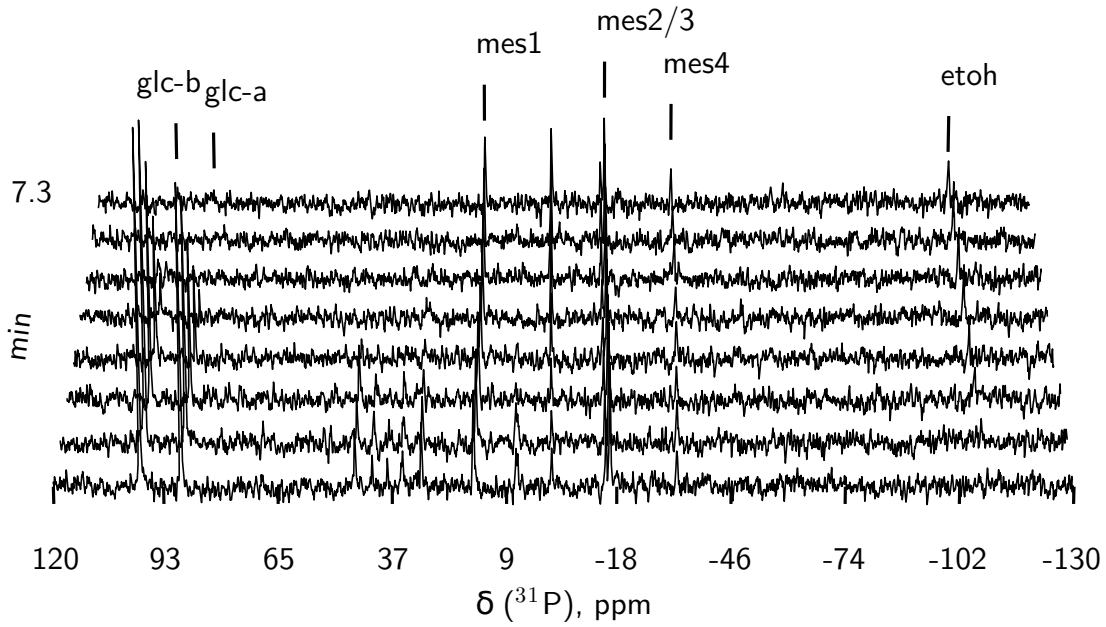

Figure 3.3: Time course of full 1-D NMR spectra to determine glucose uptake in *Z. mobilis*. ^{13}C NMR was performed at 30 °C on a 600 MHz Varian NMR operating at 150.87 MHZ to collect transients. An initial mixture of $\frac{1}{6}$D-glucose-1-^{13}C:$\frac{5}{6}$D-glucose-^{12}C (final concentration 50 mM) was used. MES-KOH buffer (40 mM) was used as an internal standard. The metabolites are assigned to peaks, determined from experimental standards, or literature values for chemical shifts.

Model predicted internal metabolite concentrations

Using Model C a time simulation was run until a steady-state was reached, to evaluate the internal metabolite concentration. Model predicted steady-state metabolite concentrations were compared to NMR data detailing *in vivo* internal metabolite accumulation [97], and for PYR and ethanol [87, 18] determined by enzymatic procedures and HPLC respectively. No literature value for internal steady state concentration was available for 6PGL. The results are shown in Table 3.5. The model predicted acetaldehyde concentration is three times higher than published values. This finding is further discussed in Chapter 4.

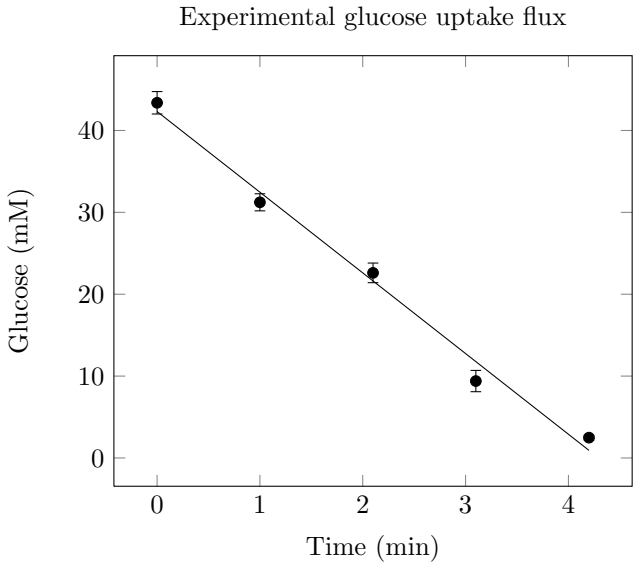

Figure 3.4: A ^{13}C glucose uptake assay. Log-phase cells were incubated with 50 mM ^{13}C glucose and the reaction monitored on a 600 MHz NMR spectrometer as shown in Figure 3.3. Concentration-time series were fitted to extract a rate approximation at each data point, where the slope of the linear regression = rate (11.484 mM/min). When normalised to protein concentration (determined using the Bradford assay), the glucose uptake flux was calculated as 0.957 μmol.min^{-1}.mg^{-1}. Error bars represent weighted mean, SEM (n=3).

Table 3.5: Comparison of steady-state metabolite concentrations obtained from model predictions, compared with literature values. * NAD$^+$/NADH and NADP$^+$/NADPH modelled as free variables (see p.41).

Metabolite	Model C (mM)	Model* (mM)	Literature (mM)	Reference
G6P	1.8958	13.25	1.4178	[97]
6PGL	1.2799	2.217	—	—
6PG	3.8000	1.558	0.2463	[97]
GAP	0.2272	0.153	0.2120	[97]
PYR	0.1235	0.107	2.5000	[87]
bPG	0.0008	0.0005	0.0008	[97]
3GP	2.3818	1.573	2.3600	[97]
2GP	0.1992	0.134	0.2365	[97]
PEP	0.1294	0.106	0.1666	[97]
ACET	12.8070	4.64	3.7200	[97]
ETOH	0.4341	0.387	0.5000	[18]

Model steady state fluxes were compared to our own NMR and literature data and model predicted metabolite concentrations were compared to literature internal metabolite concentrations. Model C was capable of reproducing glycolytic fluxes comparable to the experimentally determined glucose uptake flux and those reported earlier for *Z. mobilis* [10, 101]. Furthermore Model C was able to emulate published internal metabolite concentrations to a degree [97, 18, 87]. Eight of the eleven model predicted steady-state concentrations fall within the same range as literature values,

with acetaldehyde and 6PG being overestimated, and pyruvate being underestimated (further discussed in Chapter 4). Model C was chosen as a partially validated model because it can reproduce these observations.

NAD^+/NADH and $NADP^+$/NADPH free variables

Additional validation for Model C was done by un-fixing two of the moiety-conserved cycles in the model, making NAD^+/NADH and $NADP^+$/NADPH free variables. This reduced the number of fixed parameters in the model. This model could also obtain a steady-state, showing system robustness. Furthermore model predicted steady-state flux (J_glycolysis = J_G6PDH1 = 0.64 μmol.min^{-1}.mg^{-1}) with these co-factors as free variables, and concentrations (Table 3.5) were comparable to Model C, literature and experimentally determined values. The flux through G6PDH1 is the same as the flux through glycolysis since the conversion of glucose to ethanol has to be redox (NAD^+/NADH) balanced.

3.6 Model analysis

To evaluate steady-state behaviour it is important to quantify the role of each enzyme in the glycolytic pathway. MCA allows us a method to analyse sytem behaviour. MCA can be used in conjunction with ODE models to study the sensitivity of steady-state variables (fluxes and metabolite concentrations) to fluctuations in system parameters and local enzyme rates. The complete matrix of flux and concentration control coefficients is shown in Appendix B, however a visual representation is shown in Figure 3.5. Two sets of independent fluxes are present in the model, the first being J_glycolysis and J_G6PDH1 and the second being J_glycolysis and J_G6PDH2. Only one of these sets needs to be used to determine all the other fluxes as they are all dependent on this set (J_glycolysis = J_G6PDH1 + J_G6PDH2). Furthermore GLK shows large positive control on the concentration of acetaldehyde, and to a lesser extent on PGL and PG, and on the enzymes of lower glycolysis. ADH has the largest negative control on acetaldehyde as shown in Figure 3.5.

MCA performed by Rutkis *et al*, [22], showed that the ATP consuming reaction exerted a major control over glycolytic flux and revealed a negative flux control coefficient for the glucokinase reaction. This result resembles experimental observations with *E. coli*, which suggests that the majority of flux control ($> 75\%$) resides with the enzymes that hydrolyse ATP thus not inside but outside the glycolytic pathway [102]. However these reactions are not included in our model, and thus no comparison can be made in this regard. This is further discussed in Chapter 4.

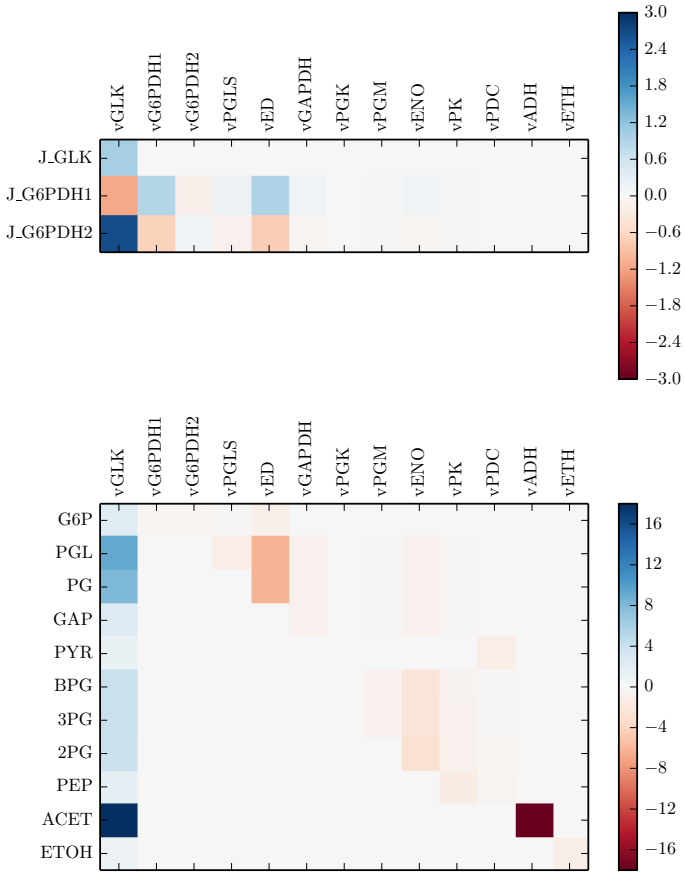

Figure 3.5: *Top*: Flux control coefficients for the reactions of Model C. Controlling reactions are indicated on the x-axis, dependent fluxes on the y-axis. Colorbars are normalised to represent identical scales, and for visual clarity are saturated over 3 and below -3. *Bottom*: Concentration control coefficients. Controlling reactions are indicated on the x-axis, dependent metabolite concentrations are indicated on the y-axis. Colorbars are normalised to represent identical scales, and for visual clarity are saturated over 18 and below -18.

Chapter 4

General Discussion

A general discussion is presented in which the findings of the research in this thesis are reviewed. A critique of this work is offered. Finally, future research directions are explored and the thesis concludes by reviewing the results in the light of the aims of this study.

4.1 Synopsis and discussion

The aim of this study was to construct and validate a detailed kinetic model of the Entner-Doudoroff glycolytic pathway in *Zymomonas mobilis*. *Z. mobilis* was cultured and the glycolytic enzymes were characterised kinetically from lysates. Kinetic parameters thus obtained were then used to construct a kinetic model, which was partially validated using experimentally measured glycolytic fluxes. The primary motivations of this study were manifold. First, this study is part of a larger project, with the aim to compare glycolytic regulation in several different micro-organisms, *Z. mobilis* [10], *E. coli* [11], *S. cerevisiae* [12] and *L. lactis* [13]. The kinetic model for *Z. mobilis* was required as a component of this larger project. The scarcity of published kinetic models of the Entner-Doudoroff glycolytic pathway in *Z. mobilis* was a second justification at the start of this project; one other kinetic model for glycolysis in *Z. mobilis* was available (by Altintas *et al*, [21]).

Indeed, the need for kinetic models of glycolysis was confirmed by the later puplication of a second kinetic model of glycolysis, by Rutkis *et al* [22], also based on literature kinetic parameters and metabolomics data. In many instances, assay conditions for literature obtained enzyme-kinetic parameters were set-up to yield the maximum activity of each enzyme. In this study the number of literature-based obtained parameters was minimised by kinetically characterising as many of the enzymes of the ED-pathway as possible. Chapter 2 presented the kinetic characterisation of these enzymes. It was shown than GLK is subject to product inhibition, with GLK insensitive to low concentrations of G6P, and GLK sensitive to low concentrations of ADP with an experimentally determined $K_{\mathrm{m}} \approx 1.75$ (Table 2.1). Furthermore much of the flux and concentration control resided with this reaction as shown in Figure 3.5, where the rate of GLK plays a role in the control of all the flux values of the model.

The characterisation of G6PDH was in agreement with literature and shows that the affinity for $NADP^+$ is greater compared to NAD^+ [48, 53]. Additionally we have shown that $NADP^+$ displays binding cooperativity on G6PDH, and that G6PDH is weakly inhibited by ATP. However we were not able to determine the K_{m} for PEP (Table 2.5).

The three enzymatic reactions following on G6PDH, catalysed by PGLS, EDD and EDA respec-

tively (Table 2.3 & Table 2.5), were characterised using ^{31}P NMR. NMR technology is an attractive method for systems biology, because NMR can be non-invasive to yield *in vivo* data, and because NMR technology is ideal for simultaneously observing numerous metabolites [103, 104]. Intermediate and enzymes for these reactions were not commercially available to perform 96-well plate assays, this was a useful alternative, allowing us to characterise these enzymes, without the need for all the intermediates. Furthermore the characterisation data allowed us to include the kinetic parameters of theses enzymes into the model, which would otherwise have been impossible.

The enzymes of the lower half of glycolysis (GAPDH, PGM and ENO) were also characterised and the results are shown in Tables 2.5, 2.7 and 2.8. The exception was PGK, which could not be characterised and the parameters were obtained from literature. Although the K_{m} values for the experimentally characterised enzymes agreed with literature values, we only realised during model construction (Chapter 3), that the maximal activities of these enzymes were much lower than expected.

The last part of Chapter 2 shows the experimental characterisation of PK, PDC and ADH. *Z. mobilis* possesses two well characterised isozymes of ADH, ZADH-1 and ZADH-2, however for this study these isozymes were characterised as one and represented the combined behaviour in the model.

The parameters obtained from experimental work were used to populate the rate equations for the model. The first part of Chapter 3 gives on overview of constructing a model as a set of ODEs. A summary of the model description is given by combining the rate equations, parameter values and initial conditions of the model. In the second part, the model is evaluated. The initial model (Model A) was not able to obtain a steady-state. In order to identify the problem, a secondary model was constructed using the experimentally determined glucose uptake flux and published metabolic steady-state concentrations, and calculating the expected rate of each reaction to achieve these concentrations (Model B).

Model B was created as a way to evaluate Model A, by comparing the rates of Model A, to Model B. The comparison revealed a complication in the lower half of glycolysis, in that the low rates of GAPDH, PGM and ENO were not able to quantify the degree to which each of these reactions consume their substrates.

Model C was created by correcting the maximal rates with the determined factor applied to each reaction, and the model was able to reach steady-state. Furthermore the model was able to predict steady-state metabolite concentrations and flux to a degree of certainty, as shown in Tables 3.4 and 3.5. Snoep *et al*, [53], showed that almost half of the control for glycolysis appears to reside with GLK when GLK was overexpressed, which is in agreement with our results. Furthermore by using literature V values in our model (Table 3.3) we showed that the predicted steady-state flux was similar to literature and experimentally determined values. Likewise when we reduced the number of fixed parameters by making NAD^+/NADH and $NADP^+$/NADPH free variables the predicted steady-state flux was also similar. The correlation between model predicted steady-state concentrations and published steady-state concentrations, and model predicted flux and experimentally determined flux, allowed for partial model validation.

The partially validated Model C was used for model analysis. In the final part of Chapter 3, the model is analysed by performing MCA to determine flux and concentration control coefficients. The results of the analysis are shown in Figure 3.5 which is a visual representation of flux and concentration control coefficients summarised in Appendix B, Table 1 and 2. MCA shows that GLK has the most positive control over the concentrations of metabolites.

4.2 Comparison to published kinetic models

A comparison has to be drawn between the model presented in this work and the published models to serve as a way validate and identify possible shortcoming in this model.

Firstly, a comparison was made with regards to the overall metabolic pathway of the three different models. The model presented in this work is a kinetic model of glycolysis of the ED-pathway in *Z. mobilis* and excludes the transport reactions and reactions related to ATP metabolism which are in included in Rutkis *et al*, [22]. Altintas *et al*, [21] also did not include these reactions, however this model is based on a genetically engineered *Z. mobilis* strain, and includes enzymatic reactions for the pentose phosphate pathway, which neither of the two aforementioned models contain. In our model we set the fixed glucose concentration at 50 mM, this assumes that the glucose transporter is in equilibrium. At low concentrations of glucose the transporter has some control. However at concentrations above 2.5 mM this is not evident. Glucose intracellular concentration quickly reaches a plateau closely equal to external concentration and in our model internal glucose is fixed. The glucose transporter has a K_{m} of 5 mM [105], and to ensure saturation we fixed the concentration in our model at 50 mM [105]. If the concentration of glucose is set at 5 mM, no difference is observed in steady-state flux or concentrations.

Secondly, the parameters of the two published models are obtained from the literature and in many instances, the assay conditions for these parameters were set-up to yield the maximum activity of each enzyme, determined under non-standardised conditions. A key difference between this study and the other kinetic models [21, 22] is that the kinetic parameters for those models have not been experimentally determined for the enzymes using the same strain and experimental conditions. Using standardised experimental conditions is essential [83, 84]. In our model the number of literature-based obtained parameters is minimised by kinetically characterising as many of the enzymes of the ED-pathway as possible, under standard conditions. Optimal conditions for each reaction would not represent the cellular environment under which these reactions occur in *Z. mobilis* [83, 84]. Furthermore the parameter sets might not take all variables into account, as some kinetic parameters which were not included in the literature are either omitted or estimated. ED-pathway reaction parameters used in this study are compared to the published models and summarised in Table 4.1.

Thirdly, individual model outputs such as steady-state concentrations and flux from the three models (summarised in Table 4.2) are also compared. The model by Altintas *et al*, [21], greatly underestimates the steady-state concentrations, however this model does include the pentose phosphate pathway, furthermore independent steady-state concentrations for the engineered strain must be determined to validate the model determined steady-state concentrations. Rutkis *et al*, [22], achieves steady-state concentrations well within the range of published values, but this is not surprising considering that the maximum velocities of all reactions in this model were optimized according to experimentally obtained steady-state intermediate concentrations.

The Model C in this work predicted the acetaldehyde concentration to be three times higher, and pyruvate concentrations lower than published values. It has been shown that if the PDC gene derived from *Z. mobilis* is expressed in transgenic tobacco, during the first 2-4 h of anoxia, acetaldehyde accumulates 10- to 35-fold higher than in wild-type, however under normoxic conditions no accumulation of acetaldehyde and ethanol could be measured [106]. Furthermore Stanley *et al.* [92] showed that acetaldehyde could accumulate in the cell to semi-saturating concentrations. However the reaction that produces acetaldehyde and uses pyruvate, is the only reaction

Table 4.1: Summary of the kinetic parameters either excluded or assumed for the three models.

Altintas *et al*, [21]		
Enzyme	**Parameter**	**Notes**
GLK	K_{ADP}	Excluded
G6PDH	K_{NADH}	Excluded
	K_{NADPH}	Excluded
PGLS	K_{PG}	Excluded
EDA	K_{PYR}	Excluded
	K_{GAP}	Excluded
GAPDH	K_{GAP}	Assumed
	K_{NAD^+}	Assumed
	K_{bPG}	Assumed
	K_{NADH}	Assumed
PGK	K_{bPG}	Assumed
	K_{ADP}	Assumed
PDC	K_{ACET}	Excluded
Rutkis *et al*, [22]		
GLK	K_{G6P}	Assumed
	K_{ADP}	Assumed
G6PDH	K_{PGL}	Assumed
	K_{NADH}	Assumed
	K_{NADP^+}	Excluded
	K_{NADPH}	Excluded
PGLS	K_{PG}	Assumed
EDA	K_{PYR}	Assumed
	K_{GAP}	Assumed
PDC	K_{ACET}	Excluded
This work		
G6PDH	K_{PGL}	Assumed
	K_{NADH}	Assumed
	K_{NADP^+}	Assumed
PDC	K_{ACET}	Excluded

Table 4.2: Summary of the steady-state concentrations and flux for the three models.

Metabolite	**Altintas *et al*, (mM) [21]**	**Rutkis *et al*, (mM) [22]**	***This work* (mM)**	**Literature (mM)**
G6P	0.0021	1.82	1.89	1.42 [97]
6PGL	0.0002	0.24	1.28	—
6PG	0.0004	0.26	3.80	0.25 [97]
GAP	0.12	0.35	0.23	0.21[97]
PYR	0.0058	0.94	0.12	2.50 [87]
bPG	0.0500	0.004	0.0008	0.0008 [97]
3GP	0.001	2.78	2.38	2.36 [97]
2GP	0.0021	0.023	0.19	0.24 [97]
PEP	0.0002	0.067	0.13	0.17 [97]
ACET	0.0636	—	12.81	3.72 [97]
ETOH	87.3182	—	0.43	0.50 [18]
Flux	(μmol.min^{-1}.mg^{-1})			
$J_{glucose}$	—	0.98	0.83	1.03 [53]
$J_{ethanol}$	—	—	1.66	2.05 [53]

that has an irreversible rate equation in our model; thus the accumulation of acetaldehyde and fast disappearance of pyruvate could be a possible model artefact. It has been shown that irreversible steps in kinetic models can have a large effect on downstream metabolites in a pathway, because it is product insensitive [107, 108]. The model predicted acetaldehyde concentration of this study and the model presented by Rutkis *et al*, [22], could not be compared, as the Rutkis model does not report its concentration. Both the Rutkis *et al*, model [22], and the one presented in this work were able to reach a steady-state flux, close to experimentally determined values. Their model could achieve 89 % of the experimentally determined flux, and our model 86 %.

Finally, the results of model analysis Altintas *et al*, [21], used simulations to predict how varying the different enzyme concentrations will affect intracellular metabolite concentrations for pentose phosphate pathway and ethanol production, however no statements were made about control and regulation. MCA performed by Rutkis *et al*, [22], suggests that the majority of flux control resides with the enzymes that hydrolyse ATP, thus not inside but outside the glycolytic pathway [102]. However these reactions are not included in our model, and thus no direct comparison can be made in this regard.

4.3 Critique

A number of pertinent questions remain with regard to the methodologies and outcomes of this study. Firstly, which parameters are better, those obtained from the literature or those determined experimentally? Models are often constructed from quantitative data obtained experimentally, which is better than estimating or guessing parameter values, but they may still contain experimental error. Furthermore, care should be taken to standardise the conditions under which characterisation is done [83, 84]. A great effort was made during this study to ensure that the conditions were standardised.

Secondly, if parameters cannot be determined should literature values be used? Some of the kinetic parameters for enzyme reactions could not be determined (e.g. the K_{m} of PEP in G6PDH), or for this model PGK could not be characterised. Literature obtained parameters are introduced into the model for completeness sake, however these are not necessarily determined under the same experimental set up, as the other assays. Including a literature obtained parameter is better than to exclude it all together from the model. When kinetic data for an enzyme from a certain organism are unavailable, data from a closely related species can often be substituted [108]. All enzyme-catalysed reactions are in principle reversible, and this has to be captured in kinetic models. Furthermore it has been shown that the effect of irreversible steps in kinetic models can have a large effect if downstream metabolites in a pathway cannot "communicate" with upstream enzymes [107, 108]. Literature obtained parameters can be used to overcome this problem, in that the rate equations can be written to be reversible.

Thirdly, how can the experimental set up be improved? Introduction of a milder, more predictable extraction technique, should be considered. Furthermore, extractions prepared from a single batch should preferably be used. For this study, fresh extractions were prepared for every set of enzymes being characterised, which could introduce experimental errors as was shown with GAPDH, PGM and ENO, where a possible over-extraction denatured the proteins, which could have had an influence on the maximal activity. The enzyme catalysed reactions of these three enzymes produced maximal activities that did not allow the model to reach a steady-state, and we hypothesised that this might have been introduced by the sonication procedure. Sonication

has several variables which need to be taken into account with each extraction, these include the relationship between sample volume and probe size, probe tip depth (if the tip is not submerged enough the sample will foam or bubble, and if the tip is too deep it will not circulate the sample effectively), vessel shape and size (if the vessel is too wide it will not mix effectively and some sample will remain untreated at the periphery), amplitude and temperature control.

An finally, is the model correct? A simple response to this question is that no models are ever "strictly speaking" correct or true as all models are a "work of fiction" [109, 11]. However we seek to bring the models assumptions close to reality which can be done by embracing the details of its components and interactions. As with the case with the model presented here, it excludes system behaviour not captured in this model. However this model allows as to study some "system" behaviour, even if to a much lesser degree.

4.4 Further research

The model lacks some key parameters that could not be determined during this study, and should be considered for incorporation into future work. These include: characterisation of PGK, K_{PEP} for G6PDH, K_{6PGL} for PGLS, K_{BPG} and K_{NADH} for GAPDH, K_{2PG} for PGM, K_{PEP} for ENO and K_{iNADH} and K_{iNAD^+} for ADH. Additionally the characterisation of GAPDH, PGM and ENO should be redone, to validate the assumptions made with the correction factor. Furthermore PDC has to be characterised so that the rate equation for this reaction is reversible. Additionally the inclusion of transport reactions and reactions related to ATP metabolism should also be considered for inclusion in the model. Furthermore this detailed model should be used to simulate the flux experiments from Scopes *et al*, [87], as a method for model validation. For additional validation the model should include a protein burden component, to simulate the high expression experiments as shown by Snoep *et al.* [110]. This detailed kinetic model has potential for application in *Z. mobilis* metabolic engineering (Bio-fuel production), and by making the ED-pathway model available in public databases, it can serve as a basis for the development of models for other micro-organisms possessing this type of glycolytic pathway. Small scale fermentations to test model predictions could also be a starting point for further development, and model expansion.

4.5 Conclusion

The aim of this study was to construct and partially validate a detailed kinetic model of the Entner-Doudoroff glycolytic pathway in *Zymomonas mobilis*. The micro-organism was cultured and the glycolytic enzymes were then characterised from lysates. We were able to kinetically characterise most of the enzymes of the ED-pathway. Kinetic parameters obtained were then used to construct a kinetic model. Additionally we have shown that the model describes the steady-state fluxes well and in addition gives similar metabolite concentrations when compared to published values. Furthermore, assumptions made during model construction (the correction factor introduced for GADPH, PGM and ENO), allowed us to produce a model that can obtain steady-state. Having constructed and partially validated a model, we were able to analyse the model as a whole with MCA, to identify control and regulation in the pathway, which for this model predominantly resided with the GLK reaction.

Z. mobilis has potential as a bio-ethanol producing bacterium. A kinetic model of metabolism can be a powerful tool, providing the ability to identify key regulatory points and to suggest focus

areas for metabolic redesign. This model is a good starting point, as it can be expanded to include the connected metabolic pathways of genetically engineered strains of *Z. mobilis*. On a broader perspective, many other bacteria use the ED-pathway, and this model may act as a template for inclusion in their respective kinetic models.

This work also illustrates the value of an integrated experimental-theoretical approach, and using computational systems biology to unravel complex biological networks.

Chapter 5

Methods and Experimental Procedures

The aim of the project was to construct a kinetic model of the Entner-Doudoroff pathway for anaerobic fermentation of glycolysis in *Z. mobilis*. As such, *Z. mobilis* had to be cultured, cell lysates obtained and the glycolytic enzymes kinetically characterised from lysates. Additionally, glycolytic fluxes had to be determined to provide validation data. This chapter outlines the methods and experimental procedures used for this study.

5.1 Culturing of *Zymomonas mobilis*

Wild type *Z. mobilis* (CP4) [44], freezer stock was prepared by growing overnight cultures in liquid media (composition described in this section) and adding to 40% sterile glycerol for storage at $-80\,^{\circ}\mathrm{C}$.

A swipe of prepared freezer stock was used for growth on agar plates at $30\,^{\circ}\mathrm{C}$. In order to prevent caramelisation of glucose it was sterilised separately from the growth media (autoclaving at $121\,^{\circ}\mathrm{C}$ for 15 minutes). Agar plate growth media contained the following per 1L: 1 g KH_2PO_4, 1 g $(NH_4)_2SO_4$, 0.5 g $MgSO_4.7H_20$, 20 g glucose, 10 g yeast extract, 15 g agar [44].

Single colonies from agar plates where used to inoculate liquid media. 250ml shaker flasks were used, with the necks pluged with cotton wool, and coved with aluminium foil. Anaerobic growth conditions were obtained by bubbling nitrogen-gas through the liquid media.

Cell were grown in an orbital shaker at 120 rpm at $30\,^{\circ}\mathrm{C}$, OD was measured spectrophotometrically at 550nm. Pre-cultures were grown until $OD_{600} \approx 0.5$-1. Pre-cultures where used to inoculate 200ml liquid media and grown until OD ≈ 4 (approximately mid-exponential growth phase), before being harvested. Liquid growth media contained the following per 1L: 1 g KH_2PO_4, 1 g $(NH_4)_2SO_4$, 0.5 g $MgSO_4.7H_20$, 100 g glucose, 10 g yeast extract and pH 7.0. In order to prevent caramelisation of glucose it was sterilised separately from the growth media (autoclaving at $121\,^{\circ}\mathrm{C}$ for 15 minutes) [87].

Whole cells were harvested and prepared for sonication by centrifuging (4332 $\times$ g, 15 min at $4\,^{\circ}\mathrm{C}$), and re-suspending the pellet in buffer (20 mM MES-KOH, pH 6.5, 2 mM $MgCl_2$ and 10 mM β-mercapthoethanol), and repeating so as to include wash steps.

5.2 Sonication optimisation

Washed and resuspended cells in a 50 mL centrifuge tube (total volume 20ml, $OD_{600} \approx 20$) were placed in an ice slurry and sonicated using a micro-tip at 138 kPa for 30 s intervals with

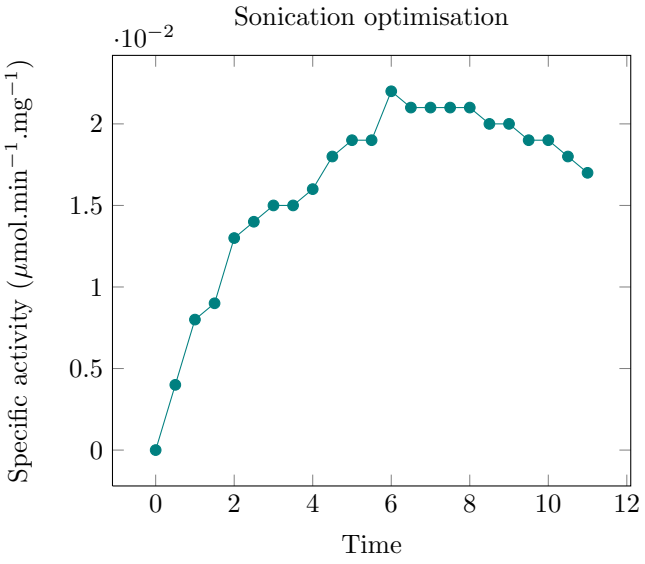

Figure 5.1: The sonication optimisation of *Z. mobilis*. A G6PDH/NAD$^+$ enzyme assay was performed on lysate samples taken every 30 s

30 s breaks (to prevent overheating from sonication) for a total sonication time of 7 min. The optimal sonication time was determined by performing a G6PDH/NAD$^+$ enzyme assay using a series of extractions for various time points. The optimal, steady specific activity (2.1 $\times$ 10^{-2} μmol.min^{-1}.mg^{-1}) was reached after 7 min sonication time (Figure 5.1).

5.3 Preparation of cell free extracts

Cell free extracts were obtained by following the above sonication procedure. After 7 min total sonication time, aliquots of the sonicated cell suspension were centrifuged (3823 $\times$ g, 20 min at 4 °C), and the supernatant drawn off for experimental enzyme characterisation.

5.4 Protein determination

Total protein of cell free lysates was determined using the Bradford method. Standards of 0.2 mg/ml, 0.4 mg/ml, 0.6 mg/ml, 0.8 mg/ml and 1.0 mg/ml BSA, were prepared, and a standard BSA calibration curve drawn. The procedure was adapted for 96-well plates, where 5 μl of standard or sample was added to 195 μl Bradford reagent, and absorbance read at 595nm after 15 min incubation time [111, 112].

5.5 Dry weight determination

A cellulose acetate filter (Osmonics, 0.22 μm), was dried for 4 min in a microwave (330 Watt), and cooled for 10 min in silica gel containing dessicator, before weighing. Cells were vacuum filtered with continuous rinsing. The cell containing filter was microwaved for 8 min (330 Watt), and cooled in dessicator for 10 min before weighing to determine dry weight [113].

5.6 NMR spectroscopy

A standard enzyme assay performed with NMR consisted of the following: for a 5 mm glass tube, 50 mM Triethyl phosphate (TEP), 100 μl D_2O, 100 μl substrate, 100 μl cell lysate, filled to 1 ml final volume with MES-KOH buffer (20 mM, pH 6.5). TEP was added as an internal NMR standard due to its metabolic inertness [114].

A blank (cell lysate excluded), was used to tune the spectrophotometer, by acquiring a lock signal and shimming the instrument. The reaction was started by removal of the tube and addition of cell lysate, mixed by inverting several times, and re-inserting the tube. With stable lock signal acquired data acquisition was started. ^{31}P NMR was performed on a 300 MHz Varian NMR operating at 121.33 MHz at 30 °C, with probe spinning at 10 Hz, pulse angle 90°, repetition time 1.5 s (1.0 s acquisition, 0.5 s relaxation) to collect 64 - 128 transients.

Proton decoupling (Waltz-16), including Nuclear Overhauser effect (NOE) for signal enhancement, was performed for acquisition.

For complete details on determining enzyme kinetics with Nuclear Magnetic Resonance Spectroscopy, refer to [82].

5.7 Glucose uptake flux

For determination of steady-state flux, a ^{13}C NMR experiment was performed on a 600 MHz Varian NMR operating at 150.87 MHZ. Cells were cultured and harvested as per Section 5.1, at mid-log phase. Cells were washed and re-suspended in MES-KOH buffer (40 mM, pH 6.5). The assay mixture consisted of 2.3 ml cells at $OD_{600} \approx 200$, 0.3 ml of a mixture of $\frac{1}{6}$D-glucose-1-^{13}C:$\frac{5}{6}$D-glucose-^{12}C (final concentration 50 mM), and 0.3 ml D_2O, in a 10 ml NMR glass tube. The ^{13}C NMR was performed at 30 °C, repetition time 0.6 s (0.1 s acquisition, 0.5 s relaxation), and pulse angle of 90°, in addition with proton decoupling to collect 100 transients per FID (1 min). A blank (glucose excluded), was used to tune the spectrophotometer, by acquiring a lock signal and shimming the instrument. The reaction was started by removal of the tube and addition of glucose, mixed by inverting several times, and re-inserting the tube. Spectra were corrected for incomplete relaxation, by adjusting integrals according to a fully relaxed spectrum obtained from non reacting standards (TEP) (15 s relaxation time). The non reacting standard is an inert substance that does not take part in any of the reactions, so the concentration remains constant, because it is constant, we can use it to calculate all the other concentrations, and changes in the integral of TEP signal peak will be due to non-metabolic effects, such as a deterioration of the NMR signal over time. Thus normalising the other peaks by the standard automatically corrects for these effects in the other metabolites and quantities them simultaneously.

Time series were fitted with splines to extract uptake rates (using the `SciPy.interpolate` module [115]). Peaks were normalised to buffer concentration (as an internal standard) for quantification and rates were normalised to protein concentration obtained by performing a Bradford assay on sonicated cells.

5.8 Reagents

All intermediates, enzymes and reagents were obtained from Sigma (Steinheim, Germany), except in the case of KH_2PO_4, D-glucose and D_2O obtained from Merck (Darmstadt, Germany & Modderfontein, South Africa), and D-glucose-1-^{13}C obtained form Cambridge Isotopes Laboratory inc (Tewksbury, MA).

5.9 Enzyme Characterisation

All assays where performed at 30 °C, in a buffer with the following composition (20 mM MES-KOH, pH 6.5, 2 mM $MgCl_2$ and 10 mM β-mercapthoethanol). In assays where ATP/ADP is present, $MgCl_2$ (4 mM) was used, the high magnesium concentration was used to ensure that ATP was predominantly in the active MgATP form. The maximal activities obtained where scaled to their respective V. This was done to eliminate day-to-day variations in extraction efficiency, and to counter variation in protein expression levels between batches. The maximal rates of the glycolytic enzymes were all determined from a homogenate of cell lysates.

Glucokinase *Forward reaction:* Glucose phosphorylation reaction rate was obtained by coupling glucokinase to G6PDH/NAD^+ and measuring NADH accumulation at 340 nm. Glucose was added to wells containing cell lysate, assay buffer, ATP (1 mM), NAD^+ (1 mM) and G6PDH (5 U/ml). Similarly ATP added to wells with the same composition with a fixed glucose concentration (1 mM).

Inhibition reaction: GK inhibition by G6P were assayed using saturating concentrations of glucose (1 mM) and ATP (1 mM), and coupling the reaction to LDH (5 U/ml) and NADH (0.48 mM), via PK (5 U/ml) and PEP (1 mM). Correspondingly inhibition by ADP was assayed using saturating concentrations of glucose and ATP, coupled to G6PDH (5 U/ml) and NAD^+ (1 mM). Protocols where adapted from [87, 48].

Fructokinase *Forward reaction:* Fructose phosphorylation reaction rate was obtained by coupling fructokinase to G6PDH (5U/ml) and NAD^+ (1 mM), in the presence of excess PGI (5 U/ml) and measuring NADH accumulation at 340 nm. Fructose was added to wells containing cell lysate, assay buffer, ATP (1 mM). Similarly ATP was added to wells with the same composition with a fixed fructose concentration (1 mM).
Inhibition reaction: FRK inhibition by ADP was assayed using saturating concentrations of fructose and ATP, and coupling the reaction to G6PDH (5 U/ml) and NAD^+ (1 mM), via PGI (5 U/ml). However inhibition by glucose could not be measured by coupling the reaction to G6PDH/NAD^+ due to production of G6P, by GK in the assay mixture. Protocols were adapted from [87, 48].

Phosphoglucose isomerase *Forward reaction:* The rate of F6P isomeration was obtained by coupling the reaction to G6PDH (5 U/ml) and NAD^+ (1 mM).
Reverse reaction: The reverse rate could not be measured by linking the reaction to FRK, presumably since it is not very reversible.
Inhibition reaction: PGI inhibition by 6PG was assayed using saturating concentrations of F6P (1

mM), and linking the reaction to G6PDH (5U/ml) and NAD^+ (1 mM). Protocols were adapted from [48].

Glucose-6-Phosphate Dehydrogenase *Forward reaction:* The conversion rate of G6P and NAD^+ was determined my measuring the amount of G6P and NAD^+/$NADP^+$ utilised with time in each reaction respectively. Lysate was added to wells, one substrate concentration was varied, while keeping the other constant. G6PDH was assayed with regards to substrate G6P (0-4.5 mM), using saturating concentrations of NAD^+ (1 mM), and NADP (1 mM) respectably. NAD^+ (0-5 mM) as substrate was assayed using saturating concentrations the G6P (1.5 mM), and similarly NADP (0-1 mM) as substrate using saturating concentrations of G6P (1.5 mM).

Inhibition reaction: G6PDH inhibition by ATP was assayed using saturating concentrations of G6P and NAD^+/NADH, and varying the concentrations of ATP (0-35 mM).

G6PDH inhibition by PEP was assayed using saturating concentrations of G6P (1.5 mM) and NAD^+/NADH, and varying the concentration of PEP (0-60 mM), however it delivered non-reproducible kinetics.

Inhibition by 6-PGL could not be determined as this intermediate is not commercially available. Protocols were adapted from [87, 63, 48].

6-Phosphogluconolactonase, 6-Phosphogluconate Dehydratase, 2-Keto-3-Deoxy-6--Phosphogluconate Aldolase The intermediates KDPG and 6PGL are not commercially available, nor the enzymes EDA and EDD. This precluded us from performing a coupled enzyme assay. As a consequence it were decided to characterise these enzymes using NMR spectroscopy (described in Section 5.6), starting with 6PG as an intermediate. The enzyme assay consisted of the following: for a 5 mm glass tube, 50 μl TEP (50 mM), 100 μl D_2O, 100 μl 6PG (10 mM) 100 cell lysate 650 μl MES-KOH buffer (pH 6.5), final volume 1 ml.

Glyceraldehyde-3-Phosphate Dehydrogenase *Forward reaction:* The conversion rate of GAP and NAD^+ was determined my measuring the amount of GAP and NAD^+ utilised with time in each reaction respectively. Lysate was added to wells, one substrate concentration was varied, while keeping the other constant. Substrate concentrations GAP (0-4.5 mM) was varied, using saturating concentrations of NAD^+/NADP (1 mM) respectively. NAD^+ (0-5 mM) as substrate was assayed using saturating concentrations the GAP (1.5 mM), and similarly NADH (0-1 mM) was assayed as substrate using saturating concentrations of GAP (1.5 mM). Protocols were adapted from [58].

3-Phosphoglycerate Kinase *Forward reaction:* The forward dephosphorylation could not be measured since the substrate for this reaction bPG, is chemically unstable. Consequently parameters values obtained from literature were used in the rate equations for the model.

Phospoglycerate Mutase *Forward reaction:* The forward conversion of 2PG to 3PG, was linked to the oxidation of NADH (0.48 mM) by LDH, via PK (10 U/ml), ADP (1 mM) and enolase (5 U/ml). Substrate concentrations were varied between (0-2.0 mM). Protocols were adapted from [63].

Enolase *Forward reaction:* The rate of conversion of 2PG (0-2.0 mM) to PEP was measured by coupling the assay to LDH (5 U/ml) and NADH (0.48 mM), and excess PK (10 U/ml) and ADP (1 mM). Protocols were adapted from [63].

Pyruvate Kinase *Forward reaction:* The rate of PEP and ADP utilisation was linked to LDH (5 U/ml) and NADH (0.48 mM), using a varying concentration of PEP (0-2 mM) and ADP (0-2.1 mM) respectively.
Inhibition reaction: The inhibition of PK by ATP were assayed under saturating concentrations of PEP(1 mM) and ADP(1 mM), and varying concentrations of ATP (0-25 mM), and coupled to LDH (5 U/ml) and NADH (0.48 mM). ATP was found to completely inhibit PK at high concentrations. Protocols were adapted from [63].

Pyruvate Decarboxylase *Forward reaction:* The rate for this reaction was assayed by coupling to ADH (10 U/ml) in the presence of thiamine pyrophosphate (0.2 mM) and NADH (0.48 mM) to remove product, with varying concentrations of pyruvate (0-5 mM). Protocols were adapted from [116, 72].

Alcohol Dehyrogenase *Forward reaction:* The conversion rate of acetaldehyde and NADH, to ethanol and NAD^+, was obtained by measuring the decrease in NADH concentration. Acetaldehyde was added to wells containing cell lysate, assay buffer and NADH (0.48 mM). Similarly NADH was added to wells with the same composition with a fixed acetaldehyde concentration (2 mM).
Reverse reaction: The ADH rate was determined by measuring the increase in NADH concentration, for the reaction of ethanol and NAD^+ to acetaldehyde and NADH. Ethanol was added to wells containing cell lysate, assay buffer, NAD^+ (1 mM). Similarly NAD^+ was added to wells with the same composition with a fixed ethanol concentration (25 mM). Protocols were adapted from [91].

5.10 Fitting of data

Fitting of NMR data

Assays are prepared according to Section (5.6). An appropriate NMR nucleus is selected and time course data acquired as the enzymatic reaction(s) progress towards equilibrium. The time course data is captured as an array of Free Induction Decays (FIDs). This data is processed, and quantified with an internal standard, to yield a progress curve of concentration over time. The array of spectra is quantified by deconvolution or box-integration. Progress curves are spline fitted, to interpolate the concentration and rate of change. Appropriate rate curves for each of the metabolites are selected and globally fitted to a kinetic rate equation to obtain kinetic parameters for that equation. All fitting procedures were performed by using a custom genetic algorithm [82], to obtain a general solution. Levenberg-Marquardt least-squares algorithm was employed to obtain root estimates of the fit. The Levenberg-Marquardt least-squares algorithm was employed as in the `SciPy.optimize.leastsq` module [11, 82].

Fitting of 96-well plate data

Assays are prepared according to Section (5.9). The initial reaction rates were determined over a minimum period of 30 sec for each different substrate/product concentration by using the linear slope ($R^2 > 0.90$) and the extinction coefficient for NADH (6.22 $mM^{-1} \cdot cm^{-1}$). Plotting the initial rates (normalised to protein concentration) versus corresponding substrate concentration, a non-linear curve was typically obtained. Non-linear regression of these data, using the using appropriate rate equations, yielded K_m and V constants. The `SciPy.optimize` library was used for non-linear regression of data, for weighted fits. Weights ware added as reciprocals of the standard deviation squared.

5.11 Methods for model construction

Using the parameter values determined for each enzyme and standard kinetic equations, a kinetic model was constructed using the `PySCeS 0.8.0` software package developed by our group [117], and available for download from `http://pysces.sourceforge.net`. `PySCeS` is written in the Python programming language. Python is a widely used general-purpose object orientated programming language (object-oriented programming is an approach to designing modular, reusable software systems), with a design philosophy that emphasizes code readability, and functionality. `SciPy` is a Python package of algorithms and mathematical tools. The `SciPy.optimize` library was used for non-linear regression of data, using appropriate rate equations [115].

In instances, where parameters could not be determined experimentally or obtained from literature, they were estimated. The model consists of a set of ordinary differential equations (ODE's), which describe the change in metabolite concentration over time as a function of enzyme rates. The rate of each each enzyme is described using rate equations. Other parameters for model construction (starting concentration, starting conditions and the model as a set of ODEs) are summarised in Chapter 3. Furthermore model validation data are also listed as steady-state concentration and glucose uptake flux.

Appendix A

Summary of the rate equations for the model

$$v_{GLK} = V_{fGLK} \cdot \left(1 - \frac{\frac{G6P \cdot ADP}{Glucose \cdot ATP}}{K_{eq}}\right) \cdot \frac{\frac{Glucose}{K_{glucose}} \cdot \frac{ATP}{K_{ATP}}}{\left(1 + \frac{Glucose}{K_{glucose}} + \frac{G6P}{K_{G6P}}\right)\left(1 + \frac{ATP}{K_{ATP}} + \frac{ADP}{K_{ADP}}\right)}$$

$$v_{G6PDH} = V_{fG6PDH} \cdot \left(1 - \frac{\frac{6PGL \cdot NADPH}{G6P \cdot NADP}}{K_{eq}}\right) \cdot \frac{\frac{G6P}{K_{G6P}} \cdot \frac{NAD}{K_{NAD}}}{\left(\left[\frac{1 + \frac{PEP}{K_{PEP}}}{1 + \alpha \cdot \frac{PEP}{K_{PEP}}}\right] + \frac{G6P}{K_{G6P}} + \frac{6PGL}{K_{6PGL}}\right)\left(\left[\frac{1 + \frac{PEP}{K_{PEP}}}{1 + \alpha \cdot \frac{PEP}{K_{PEP}}}\right] + \frac{NAD}{K_{NAD}} + \frac{NADH}{K_{NADH}} + \frac{ATP}{K_{ATP}}\right)}$$

$$v_{G6PDH} = V_{fG6PDH} \cdot \left(1 - \frac{\frac{6PGL \cdot NADPH}{G6P \cdot NADP}}{K_{eq}}\right) \cdot \frac{\left(\frac{G6P}{K_{G6P}} \cdot \frac{NADP}{K_{NADP}}\right)^{h-1}}{\left(\left[\frac{1 + \left(\frac{PEP}{K_{PEP}}\right)^{h}}{1 + \alpha^{2h} \cdot \left(\frac{PEP}{K_{PEP}}\right)^{h}}\right] + \left(\frac{G6P}{K_{G6P}} + \frac{6PGL}{K_{6PGL}}\right)^{h}\right)\left(\left[\frac{1 + \left(\frac{PEP}{K_{PEP}}\right)^{h}}{1 + \alpha^{2h} \cdot \left(\frac{PEP}{K_{PEP}}\right)^{h}}\right] + \left(\frac{NADP}{K_{NADP}} + \frac{NADPH}{K_{NADH}} + \frac{ATP}{K_{ATP}}\right)^{h}\right)}$$

$$v_{PGLS} = V_{fPGLS} \cdot \left(1 - \frac{\frac{6PG}{6PGL}}{K_{eq}}\right) \cdot \frac{\frac{6PGL}{K_{6PGL}}}{\left(1 + \frac{6PGL}{K_{6PGL}} + \frac{6PG}{K_{6PG}}\right)}$$

$$v_{ED} = V_{fED} \cdot \left(1 - \frac{\frac{GAP \cdot PYR}{6PG}}{K_{eq1} \cdot K_{eq2}}\right) \cdot \frac{\frac{6PG}{K_{6PG}}}{\left(1 + \frac{GAP}{K_{GAP}} + \frac{PYR}{K_{PYR}}\right) + \left(\frac{6PG}{K_{6PG}} + \left(\frac{6PG}{K_{6PG}} \cdot \frac{PYR}{K_{PYR}}\right)\right)}$$

$$v_{GAPDH} = V_{fGAPDH} \cdot \left(1 - \frac{\frac{bPG \cdot NADH}{GAP \cdot NAD}}{K_{eq}}\right) \cdot \frac{\frac{GAP}{K_{GAP}} \cdot \frac{NAD}{K_{NAD}}}{\left(1 + \frac{GAP}{K_{GAP}} + \frac{bPG}{K_{bPG}}\right)\left(1 + \frac{NAD}{K_{NAD}} + \frac{NADH}{K_{NADH}}\right)}$$

$$v_{PGK} = V_{fPGK} \cdot \left(1 - \frac{\frac{3PG \cdot ATP}{bPG \cdot ADP}}{K_{eq}}\right) \cdot \frac{\frac{3PG}{K_{3PG}} \cdot \frac{ADP}{K_{ADP}}}{\left(1 + \frac{bPG}{K_{bPG}} + \frac{3PG}{K_{3PG}}\right)\left(1 + \frac{ADP}{K_{ADP}} + \frac{ATP}{K_{ATP}}\right)}$$

$$v_{PGM} = V_{fPGM} \cdot \left(1 - \frac{\frac{PEP}{2PG}}{K_{eq}}\right) \cdot \frac{\frac{3PG}{K_{3PG}}}{\left(1 + \frac{3PG}{K_{3PG}} + \frac{2PG}{K_{2PG}}\right)}$$

$$v_{ENO} = V_{fENO} \cdot \left(1 - \frac{\frac{PEP}{2PG}}{K_{eq}}\right) \cdot \frac{\frac{2PG}{K_{2PG}}}{\left(1 + \frac{PEP}{K_{PEP}} + \frac{2PG}{K_{2PG}}\right)}$$

$$v_{PK} = V_{fPK} \cdot \left(1 - \frac{\frac{Pyruvate \cdot ATP}{PEP \cdot ADP}}{K_{eq}}\right) \cdot \frac{\frac{PEP}{K_{PEP}} \cdot \frac{ADP}{K_{ADP}}}{\left(1 + \frac{PEP}{K_{PEP}} + \frac{Pyruvate}{K_{Pyruvate}}\right)\left(1 + \frac{ADP}{K_{ADP}} + \frac{ATP}{K_{ATP}}\right)}$$

$$v_{PDC} = V_{fPDC} \cdot \frac{\frac{Pyruvate}{K_{pyruvate}}}{1 + \frac{Pyruvate}{K_{Pyruvate}}}$$

$$v_{ADH} = V_{fADH} \cdot \left(1 - \frac{\frac{Ethanol \cdot NAD}{ACET \cdot NADH}}{K_{eq}}\right) \cdot \frac{\frac{ACET}{K_{ACET}} \cdot \frac{NADH}{K_{NADH}}}{\left(1 + \frac{ACET}{K_{ACET}} + \frac{Ethanol}{K_{Ethanol}}\right)\left(1 + \frac{NADH}{K_{NADH}} + \frac{NAD}{K_{NAD}}\right)}$$

Appendix B

Complete set of flux and concentration control coefficients

Table 1: Complete set of flux control coefficients for the model of *Z. mobilis* glycolysis. Only G6PDH1 and G6PDH2 are shown explicitly, the flux in the rest of glycolysis is stoichiometrically coupled and has thus been summarised as $J_$glycolysis. The coefficients were determined with `PySCeS`.

	$J_$G6PDH2	$J_$G6PDH1	$J_$glycolysis
vPDC	-0.010979	0.013987	0.000015
vGLK	2.671579	-1.130046	0.997599
vENO	-0.086182	0.10982	0.000124
vPGM	-0.026986	0.034387	0.000039
vPGK	-0.003573	0.004552	0.000005
vGAPDH	-0.087831	0.111921	0.000126
vED	-0.732867	0.933878	0.001055
vPGL	-0.137509	0.175225	0.000198
vPK	-0.028127	0.035834	0.000037
vG6PDH1	-0.68583	0.872498	0.000353
vADH	0	0	0
vETH	0	0	0
vG6PDH2	0.128304	-0.162057	0.000449

Table 2: Complete set of concentration control coefficients for the model of *Z. mobilis* glycolysis. The coefficients were determined with PySCeS.

	PYR	PGL	G6P	GAP	PG	bPG	3PG	2PG	PEP	ACET	ETOH
vPDC	-1.246877	-0.085456	-0.01358	-0.086516	-0.086022	-0.243468	-0.250098	-0.288893	-0.461656	0.000263	0.000015
vGLK	1.243901	9.202613	2.236568	2.26952	8.115896	4.047998	4.060535	3.83794	1.78335	17.988809	0.997599
vENO	0.000155	-0.714132	-0.115592	-0.816947	-0.718862	-2.298963	-2.36157	-2.727882	0.000222	0.002238	0.000124
vPGM	0.000048	-0.22361	-0.036195	-0.255804	-0.225092	-0.719856	-0.739459	0.000149	0.000069	0.000701	0.000039
vPGK	0.000006	-0.029603	-0.004792	-0.033865	-0.029799	-0.095299	0.000021	0.00002	0.000009	0.000093	0.000005
vGAPDH	0.000158	-0.727792	-0.117804	-0.832575	-0.732613	0.000513	0.000515	0.000487	0.000226	0.00228	0.000126
vED	0.001316	-6.072755	-0.982963	0.002401	-6.112982	0.004282	0.004295	0.00406	0.001886	0.019028	0.001055
vPGL	0.000247	-1.13944	-0.184435	0.00045	0.001611	0.000803	0.000806	0.000762	0.000354	0.00357	0.000198
vPK	0.000046	-0.21722	-0.034435	-0.248487	-0.218658	-0.699264	-0.718307	-0.829726	-1.325894	0.000667	0.000037
vG6PDH1	0.00044	0.003256	-0.328829	0.000803	0.002872	0.001432	0.001437	0.001358	0.000631	0.006365	0.000353
vADH	0	0	0	0	0	0	0	0	0	-18.020935	0
vETH	0	0	0	0	0	0	0	0	0	-0.011169	-1
vG6PDH2	0.000559	0.004139	-0.417945	0.001021	0.00365	0.001821	0.001826	0.001726	0.000802	0.00809	0.000449

Bibliography

[1] U. Sauer, M. Heinemann, and N. Zamboni. Genetics. getting closer to the whole picture. *Science*, 316(5824):550–551, Apr 2007.

[2] A Cornish-Bowden, M. L. Crdenas, Letelier J., J. Soto-Andrade, and F. Guez Abarza. Understanding the parts in terms of the whole. *Biol Cell*, 96(9):713–717, Dec 2004.

[3] A. Cornish-Bowden and M. L. Crdenas. Systems biology may work when we learn to understand the parts in terms of the whole. *Biochem Soc Trans*, 33(Pt 3):516–519, Jun 2005.

[4] H. Kitano. Systems biology: a brief overview. *Science*, 295:1662–1664, 2002.

[5] J.H.S Hofmeyr. Metabolic control analysis in a nutshell. In *Proc. ICSB*, pages 291–300, 2000.

[6] H. Kacser and J. A. Burns. The control of flux. *Biochem Soc Trans*, 23(2):341–366, May 1995.

[7] R. Heinrich and S. Schuster. *The Regulation of Cellular Systems*. Springer, 1996.

[8] M. Salter, R. G. Knowles, and C. I. Pogson. Metabolic control. *Essays Biochem*, 28:1–12, 1994.

[9] J.H.S Hofmeyr and A. Cornish-Bowden. Regulating the cellular economy of supply and demand. *FEBS Lett*, 476:47–51, 2000.

[10] C Crous. Supply-demand analysis of anaerobic free-energy metabolism in *Zymomonas mobilis*. Thesis MSc (Biochemistry), Stellenbosch University, 2011.

[11] J. J. Eicher. Understanding glycolysis in *Escherichia coli* : a systems approach using nuclear magnetic resonance spectroscopy. Thesis PhD (Biochemistry), Stellenbosch University. Faculty of Science. Dept. of Biochemistry., 2013.

[12] J. A. Smith. Experimental supply demand analysis of yeast fermentative free energy metabolism : an in vivo and in situ investigation. Thesis MSc (Biochemistry), University of Stellenbosch. Faculty of Science. Dept. of Biochemistry., 2010.

[13] S. Jordaan. Supply-demand analysis of energy metabolism in *Lactococcus lactis* under anaerobic conditions. Thesis MSc (Biochemistry), Stellenbosch University. Faculty of Science. Dept. of Biochemistry., 2011.

[14] M. Cocaign-Bousquet, S. Even, N. D. Lindley, and P. Loubire. Anaerobic sugar catabolism in *Lactococcus lactis*: genetic regulation and enzyme control over pathway flux. *Appl Microbiol Biotechnol*, 60(1-2):24–32, Oct 2002.

[15] C. Siebold, K. Flkiger, R. Beutler, and B. Erni. Carbohydrate transporters of the bacterial phosphoenolpyruvate: sugar phosphotransferase system (pts). FEBS *Letters*, 504(3):104 – 111, 2001. Structure, Dynamics and Function of Proteins in Biological Membranes.

[16] P. W. Postma, J. W. Lengeler, and G. R. Jacobson. Phosphoenolpyruvate:carbohydrate phosphotransferase systems of bacteria. *Microbiol Rev*, 57(3):543–594, Sep 1993.

[17] N. D. Meadow, D. K. Fox, and S. Roseman. The bacterial phosphoenol-pyruvate: glycose phosphotransferase system. *Annu. Rev. Biochem.*, 59(1):497–542, 1990.

[18] S. M. Schoberth, B. E. Chapman, P. W. Kuchel, R. M. Wittig, J. Grotendorst, P. Jansen, and A. A. DeGraff. Ethanol transport in *Zymomonas mobilis* measured by using in vivo nuclear magnetic resonance spin transfer. *J Bacteriol*, 178(6):1756–1761, Mar 1996.

[19] T. Conway. The Entner - Doudoroff pathway: history, physiology and molecular biology. *FEMS Microbiol. Rev*, 103:1–28, 1992.

[20] N. Entner and M. Doudoroff. Glucose and gluconic acid oxidation of *Pseudomonas saccharophila*. *J Biol Chem*, 196(2):853–862, May 1952.

[21] M. M. Altintas, C. K. Eddy, M. Zhang, J. D. McMillan, and D.S Kompala. Kinetic modeling to optimize pentose fermentation in *Zymomonas mobilis*. *Biotechnol Bioeng*, 94(2):273–295, Jun 2006.

[22] R. Rutkis, U. Kalnenieks, E. Stalidzans, and D. A. Fell. Kinetic modelling of the *Zymomonas mobilis* Entner-Doudoroff pathway: insights into control and functionality. *Microbiology*, 159(Pt 12):2674–2689, Dec 2013.

[23] N. Entner and M. Doudoroff. Glucose and gluconic acid oxidation of *Pseudomonas saccharophila*. *J Biol Chem*, 196(2):853–862, May 1952.

[24] A. H. Romano and T. Conway. Evolution of carbohydrate metabolic pathways. *Res Microbiol*, 147(6-7):448–455.

[25] N. Peekhaus and T. Conway. What's for dinner?: Entner-Doudoroff metabolism in *Escherichia coli*. *J Bacteriol*, 180(14):3495–3502, Jul 1998.

[26] T. G. Lessie and PV Phibbs, Jr. Alternative pathways of carbohydrate utilization in *pseudomonads*. *Annu Rev Microbiol*, 38:359–388, 1984.

[27] N. J. Palleroni. The *Pseudomonas* story. *Environ Microbiol*, 12(6):1377–1383, Jun 2010.

[28] P. W. Hager, M. W. Calfee, and P. V. Phibbs. The *Pseudomonas aeruginosa* devb/sol homolog, pgl, is a member of the hex regulon and encodes 6-phosphogluconolactonase. *J Bacteriol*, 182(14):3934–3941, Jul 2000.

[29] A. Daddaoua, T. Krell, and J. Ramos. Regulation of glucose metabolism in *Pseudomonas*: the phosphorylative branch and Entner-Doudoroff enzymes are regulated by a repressor containing a sugar isomerase domain. *J Biol Chem*, 284(32):21360–21368, Aug 2009.

[30] C. H. Verhees, S.W. M. Kengen, J. E. Tuininga, G. J. Schut, M. W. W. Adams, W. M. De Vos, and J. Van Der Oost. The unique features of glycolytic pathways in archaea. *Biochem J*, 375(Pt 2):231–246, Oct 2003.

[31] M. De Rosa, A. Gambacorta, B. Nicolaus, P. Giardina, E. Poerio, and V. Buonocore. Glucose metabolism in the extreme thermoacidophilic archaebacterium *Sulfolobus solfataricus*. *Biochem J*, 224(2):407–414, Dec 1984.

[32] P. Giardina, M. G. de Biasi, M. de Rosa, A. Gambacorta, and V. Buonocore. Glucose dehydrogenase from the thermoacidophilic archaebacterium *Sulfolobus solfataricus*. *Biochem J*, 239(3):517–522, Nov 1986.

[33] B. Siebers and P. Schnheit. Unusual pathways and enzymes of central carbohydrate metabolism in archaea. *Curr Opin Microbiol*, 8(6):695–705, Dec 2005.

[34] T. Ohshima, R. Kawakami, Y. Kanai, S. Goda, and H. Sakuraba. Gene expression and characterization of 2-keto-3-deoxygluconate kinase, a key enzyme in the modified Entner-Doudoroff pathway of the aerobic and acidophilic hyperthermophile *Sulfolobus tokodaii*. *Protein Expr Purif*, 54(1):73–78, Jul 2007.

[35] N. J. Sweeney, D. C. Laux, and P. S. Cohen. *Escherichia coli* F-18 and *E. coli* k-12 eda mutants do not colonize the streptomycin-treated mouse large intestine. *Infect Immun*, 64(9):3504–3511, Sep 1996.

[36] R. C. Eisenberg and W. J. Dobrogosz. Gluconate metabolism in *Escherichia coli*. *J Bacteriol*, 93(3):941–949, Mar 1967.

[37] J. M. Pouyssgur, P. Faik, and H. L. Kornberg. Utilization of gluconate by *Escherichia coli*. uptake of D-gluconate by a mutant impaired in gluconate kinase activity and by membrane vesicles derived therefrom. *Biochem J*, 140(2):193–203, May 1974.

[38] S. Tong, A. Porco, T. Isturiz, and T. Conway. Cloning and molecular genetic characterization of the *Escherichia coli* gntR, gntK, and gntU genes of Gnti, the main system for gluconate metabolism. *J Bacteriol*, 178(11):3260–3269, Jun 1996.

[39] A. Porco, N. Peekhaus, C. Bausch, S. Tong, T. Isturiz, and T. Conway. Molecular genetic characterization of the *Escherichia coli* gntT gene of Gnti, the main system for gluconate metabolism. *J Bacteriol*, 179(5):1584–1590, Mar 1997.

[40] S. E. Egan, R. Fliege, S. Tong, A. Shibata, R. E . Wolf, and T. Conway. Molecular characterization of the Entner-Doudoroff pathway in *Escherichia coli*: sequence analysis and localization of promoters for the edd-eda operon. *J Bacteriol*, 174(14):4638–4646, Jul 1992.

[41] T. Patra, H. Koley, T. Ramamurthy, A. C. Ghose, and R. K. Nandy. The Entner-Doudoroff pathway is obligatory for gluconate utilization and contributes to the pathogenicity of *Vibrio cholerae*. *J Bacteriol*, 194(13):3377–3385, Jul 2012.

[42] D. C. White, S. D. Sutton, and D. B. Ringelberg. The genus *Sphingomonas*: physiology and ecology. *Curr Opin Biotechnol*, 7(3):301–306, Jun 1996.

[43] J. S Seo, H. Chong, H. S. Park, K. O. Yoon, C. Jung, J. J. Kim, J. H. Hong, H. Kim, J. H. Kim, J.l. Kil, C. J. Park, H. M. Oh, J. S. Lee, S. J. Jin, H. W. Um, H. J. Lee, S. J. Oh, J. Y. Kim, H. L. Kang, S. Y. Lee, K. J. Lee, and H. S. Kang. The genome sequence of the ethanologenic bacterium *Zymomonas mobilis* ZM4. *Nat Biotechnol*, 23(1):63–68, Jan 2005.

[44] J. Swings and J. De Ley. The biology of *Zymomonas*. *Bacteriol Rev*, 41:1–46, 1977.

[45] J. C. Baratti and J. D. Bu'lock. *Zymomonas mobilis*: a bacterium for ethanol production. *Biotechnol Adv*, 4(1):95–115, 1986.

[46] W. O. Barnell, K. C. Yi, and T. Conway. Sequence and genetic organization of a *Zymomonas mobilis* gene cluster that encodes several enzymes of glucose metabolism. *J Bacteriol*, 172(12):7227–7240, Dec 1990.

[47] J. P. Mejia, M. E. Burnett, H. An, W. O. Barnell, K. F. Keshav, T. Conway, and L. O. Ingram. Coordination of expression of *Zymomonas mobilis* glycolytic and fermentative enzymes: a simple hypothesis based on mRNA stability. *J Bacteriol*, 174(20):6438–6443, Oct 1992.

[48] R. K. Scopes, V. Testolin, A. Stoter, K. Griffiths-Smith, and E. M. Algar. Simultaneous purification and characterization of glucokinase, fructokinase and glucose-6-phosphate dehydrogenase from *Zymomonas mobilis*. *Biochem J*, 228(3):627–634, Jun 1985.

[49] B. Zembrzuski, P. Chilco, X. L. Liu, J. Liu, T. Conway, and R. Scopes. Cloning, sequencing, and expression of the *Zymomonas mobilis* fructokinase gene and structural comparison of the enzyme with other hexose kinases. *J Bacteriol*, 174(11):3455–3460, Jun 1992.

[50] H. W. Doelle. Kinetic characteristics and regulatory mechanisms of glucokinase and fructokinase from *Zymomonas mobilis*. *Appl. Microbiol. Biotechnol*, 14:241–246, 1982.

[51] T. L. Hesman, W. O. Barnell, and T. Conway. Cloning, characterization, and nucleotide sequence analysis of a *Zymomonas mobilis* phosphoglucose isomerase gene that is subject to carbon source-dependent regulation. *J Bacteriol*, 173(10):3215–3223, May 1991.

[52] G. A. Sprenger. Carbohydrate metabolism in *Zymomonas mobilis*: a catabolic highway with some scenic routes. *FEMS Microbiol. Lett*, 145:301–307, 1996.

[53] J. L. Snoep, N. Arfman, L. P. Yomano, H. V. Westerhoff, T. Conway, and L. O. Ingram. Control of glycolytic flux in *Zymomonas mobilis* by glucose 6-phosphate dehydrogenase activity. *Biotechnol. Bioeng*, 51:190–197, 1996.

[54] R.K. Scopes. 6-phosphogluconolactonase from *Zymomonas mobilis*: An enzyme of high catalytic efficiency. *FEBS letters*, 193(2):185–188, 1985.

[55] R. K. Scopes and K. Griffiths-Smith. Use of differential dye-ligand chromatography with affinity elution for enzyme purification: 6-phosphogluconate dehydratase from *Zymomonas mobilis*. *Anal Biochem*, 136(2):530–534, Feb 1984.

[56] H. P. Meloche and W. A. Wood. The mechanism of 6-phosphogluconic dehydrase. *J Biol Chem*, 239:3505–3510, Oct 1964.

[57] A. R. Rendina, J. D. Hermes, and W. W. Cleland. Use of multiple isotope effects to study the mechanism of 6-phosphogluconate dehydrogenase. *Biochemistry*, 23(25):6257–6262, Dec 1984.

[58] T. Conway, G. W. Sewell, and L. O. Ingram. Glyceraldehyde-3-phosphate dehydrogenase gene from *Zymomonas mobilis*: cloning, sequencing, and identification of promoter region. *J Bacteriol*, 169(12):5653–5662, Dec 1987.

[59] H. C. Aldrich, L. McDowell, M. F. Barbosa, L. P. Yomano, R. K. Scopes, and L. O. Ingram. Immunocytochemical localization of glycolytic and fermentative enzymes in *Zymomonas mobilis*. *J Bacteriol*, 174(13):4504–4508, Jul 1992.

[60] T. Conway and L. O. Ingram. Phosphoglycerate kinase gene from *Zymomonas mobilis*: cloning, sequencing, and localization within the gap operon. *J Bacteriol*, 170(4):1926–1933, Apr 1988.

[61] C. Q. Hu and J. M. Sturtevant. Thermodynamic study of yeast phosphoglycerate kinase. *Biochemistry*, 26(1):178–182, Jan 1987.

[62] T. M. Thomas and R. K. Scopes. The effects of temperature on the kinetics and stability of mesophilic and thermophilic 3-phosphoglycerate kinases. *Biochem J*, 330 (Pt 3):1087–1095, Mar 1998.

[63] A. Pawluk, R. K. Scopes, and K. Griffiths-Smith. Isolation and properties of the glycolytic enzymes from *Zymomonas mobilis*. The five enzymes from glyceraldehyde-3-phosphate dehydrogenase through to pyruvate kinase. *Biochem J*, 238(1):275–281, Aug 1986.

[64] L. P. Yomano, R. K. Scopes, and L. O. Ingram. Cloning, sequencing, and expression of the *Zymomonas mobilis* phosphoglycerate mutase gene (pgm) in *Escherichia coli*. *J Bacteriol*, 175(13):3926–3933, Jul 1993.

[65] M. E. Burnett, J. Liu, and T. Conway. Molecular characterization of the *Zymomonas mobilis* enolase (eno) gene. *J Bacteriol*, 174(20):6548–6553, Oct 1992.

[66] P. Steiner, M. Fussenegger, J. E. Bailey, and U. Sauer. Cloning and expression of the *Zymomonas mobilis* pyruvate kinase gene in *Escherichia coli*. *Gene*, 220(1-2):31–38, Oct 1998.

[67] A. Mattevi, M. Bolognesi, and G. Valentini. The allosteric regulation of pyruvate kinase. *FEBS Lett*, 389(1):15–19, Jun 1996.

[68] S. Gao, J. Bao, X. Gu, X. Xin, C. Chen, and D. Ryu. Substrate promiscuity of pyruvate kinase on various deoxynucleoside diphosphates for synthesis of deoxynucleoside triphosphates. *Enzyme Microb. Technol.*, 43:455–459, 2008.

[69] A. D. Neale, R. K. Scopes, R. E. Wettenhall, and N. J. Hoogenraad. Pyruvate decarboxylase of *Zymomonas mobilis*: isolation, properties, and genetic expression in *Escherichia coli*. *J Bacteriol*, 169(3):1024–1028, Mar 1987.

[70] R. J. Diefenbach and R. G. Duggleby. Pyruvate decarboxylase from *Zymomonas mobilis*. structure and re-activation of apoenzyme by the cofactors thiamin diphosphate and magnesium ion. *Biochem J*, 276 (Pt 2):439–445, Jun 1991.

[71] B. C. Farrenkopf and F. Jordan. Resolution of brewer's yeast pyruvate decarboxylase into multiple isoforms with similar subunit structure and activity using high-performance liquid chromatography. *Protein Expr Purif*, 3(2):101–107, Apr 1992.

[72] J. Rivoal, B. Ricard, and A. Pradet. Purification and partial characterization of pyruvate decarboxylase from *Oryza sativa L. Eur J Biochem*, 194(3):791–797, Dec 1990.

[73] J. M. Candy and R. G. Duggleby. Structure and properties of pyruvate decarboxylase and site-directed mutagenesis of the *Zymomonas mobilis* enzyme. *Biochim Biophys Acta*, 1385(2):323–338, Jun 1998.

[74] P. J. O'Mullan, S. E. Buchholz, T. Chase, and D. E. Eveleigh. Roles of alcohol dehydrogenases of *Zymomonas mobilis* (ZADH): characterization of a ZADH-2-negative mutant. *Appl. Microbiol. Biotechnol.*, 43(4):675–678, 1995.

[75] C. Wills, P. Kratofil, D. Londo, and T. Martin. Characterization of the two alcohol dehydrogenases of *Zymomonas mobilis*. *Arch. Biochem. Biophys*, 210(2):775–785, 1981.

[76] A. D. Neale, R. K. Scopes, J. M. Kelly, and R. E. Wettenhall. The two alcohol dehydrogenases of *Zymomonas mobilis*. purification by differential dye ligand chromatography, molecular characterisation and physiological roles. *Eur J Biochem*, 154(1):119–124, Jan 1986.

[77] F. J. Bruggeman and H. V. Westerhoff. The nature of systems biology. *TRENDS in Microbiol*, 15(1):45–50, 2007.

[78] J.H.S Hofmeyr and A Cornish-Bowden. The reversible Hill equation: how to incorporate cooperative enzymes into metabolic models. *CABIOS*, 13(4):377–385, 1997.

[79] K. A. Johnson and R. S. Goody. The original Michaelis constant: translation of the 1913 Michaelis–Menten paper. *Biochemistry*, 50(39):8264–8269, 2011.

[80] Symbolism and terminology in enzyme kinetics recommendations 1981. *Eur. J. Biochem*, 128(2-3):281–291, 1982.

[81] Athel Cornish-Bowden. *Fundamentals of enzyme kinetics*. Wiley. com, 2013.

[82] J.J. Eicher, J. L. Snoep, and J. M. Rohwer. Determining enzyme kinetics for systems biology with nuclear magnetic resonance spectroscopy. *Metabolites*, 2(4):818–843, 2012.

[83] K. van Eunen, J. Bouwman, P. Daran-Lapujade, J. Postmus, A. B. Canelas, F. I. C. Mensonides, I. Orij, R.and Tuzun, J. van den Brink, G. J. Smits, W. M. van Gulik, S. Brul, J. J. Heijnen, J. H. de Winde, M.J.T. de Mattos, C. Kettner, J. Nielsen, H. V. Westerhoff, and B. M. Bakker. Measuring enzyme activities under standardized in vivo-like conditions for systems biology. *FEBS J*, 277(3):749–760, Feb 2010.

[84] R. N. Tipton, K. F.and Armstrong, B. M. Bakker, A. Bairoch, A. Cornish-Bowden, P. J. Halling, J. H. Hofmeyr, T. S. Leyh, C. Kettner, F. M. Raushel, J. Rohwer, D. Schomburg, and C. Steinbeck. Standards for reporting enzyme data: The *STRENDA* consortium: What it aims to do and why it should be helpful. *Perspectives in Science*, 1:131 – 137, 2014.

[85] R. A. Alberty. *Thermodynamic of biochemical reactions*. Wiley-Interscience, 2003.

[86] R. K. Scopes. Allosteric control of *Zymomonas mobilis* glucose-6-phosphate dehydrogenase by phosphoenolpyruvate. *Biochem J*, 326 (Pt 3):731–735, Sep 1997.

[87] E. M. Algar and R. K. Scopes. Studies on cell-free metabolism: Ethanol production by extracts of *Zymomonas mobilis*. *J. Biotechnol.*, 2:275–287, 1985.

[88] B. Teusink, J. Passarge, C. A. Reijenga, E. Esgalhado, C. C. van der Weijden, M. Schepper, M. C. Walsh, B. M. Bakker, K. van Dam, H. V. Westerhoff, and J. L. Snoep. Can yeast glycolysis be understood in terms of in vitro kinetics of the constituent enzymes? Testing biochemistry. *Eur J Biochem*, 267(17):5313–5329, Sep 2000.

[89] N. W. Cornell, M. Leadbetter, and R. L. Veech. Effects of free magnesium concentration and ionic strength on equilibrium constants for the glyceraldehyde phosphate dehydrogenase and phosphoglycerate kinase reactions. *J Biol Chem*, 254(14):6522–6527, Jul 1979.

[90] S. Bringer-Meyer, K-L Schimz, and H. Sahm. Pyruvate decarboxylase from *Zymomonas mobilis*. isolation and partial characterization. *Arch. Microbiol*, 146(2):105–110, 1986.

[91] S. Kinoshita, T. Kakizono, K. Kadota, K. Das, and H. Taguchi. Purification of two alcohol dehydrogenases from *Zymomonas mobilis* and their properties. *Appl. Microbiol. Biotechnol*, 22(4):249–254, 1985.

[92] G.A. Stanley, T.J. Hobley, and N.B. Pamment. Effect of acetaldehyde on *Saccharomyces cerevisiae* and *Zymomonas mobilis* subjected to environmental shocks. *Biotechnol. Bioeng.*, 53(1):71–78, 1997.

[93] R. Heinrich and S. Schuster. The modelling of metabolic systems. structure, control and optimality. *Biosystems*, 47(1):61–77, 1998.

[94] R. Heinrich and T.A. Rapoport. A linear steady-state treatment of enzymatic chains. *Eur. J. Biochem*, 42(1):89–95, 1974.

[95] H. Kacser. Recent developments beyond metabolic control analysis. *Biochem Soc Trans*, 23(2):387–391, May 1995.

[96] Y.A. Osman, T. Conway, S.J. Bonetti, and L.O. Ingram. Glycolytic flux in *Zymomonas mobilis*: enzyme and metabolite levels during batch fermentation. *J. Bacteriol.*, 169(8):3726–3736, 1987.

[97] K. D. Barrow, J. G. Collins, R. S. Norton, P. L Rogers, and G. M. Smith. 31P nuclear magnetic resonance studies of the fermentation of glucose to ethanol by *Zymomonas mobilis*. *Journal of biological chemistry*, 259(9):5711–5716, 1984.

[98] A. A. De Graaf, K. Striegel, R. M. Wittig, B. Laufer, G. Schmitz, W. Wiechert, G. A. Sprenger, and H. Sahm. Metabolic state of *Zymomonas mobilis* in glucose-, fructose-, and xylose-fed continuous cultures as analysed by 13C- and 31P-NMR spectroscopy. *Arch Microbiol*, 171(6):371–385, 1999.

[99] P. J. Fritz. Rabbit lactate dehydrogenase isozymes: effect of pH on activity. *Science*, 156(3771):82–83, Apr 1967.

[100] D. De Arriaga, J. Soler, and E. Cadenas. Influence of pH on the allosteric properties of lactate dehydrogenase activity of *Phycomyces blakesleeanus*. *Biochem J*, 203(2):393–400, May 1982.

[101] P. L. Rogers, Y. J. Jeon, K. J. Lee, and H. G Lawford. *Zymomonas mobilis* for fuel ethanol and higher value products. *Adv Biochem Eng Biotechnol*, 108:263–288, 2007.

[102] B. J. Koebmann, H. V. Westerhoff, J. L. Snoep, and P. R. Nilsson, D.and Jensen. The glycolytic flux in *Escherichia coli* is controlled by the demand for ATP. *J Bacteriol*, 184(14):3909–3916, Jul 2002.

[103] F. Exnowitz, B. Meyer, and T. Hackl. NMR for direct determination of Km and Vmax of enzyme reactions based on the Lambert W function-analysis of progress curves. *Biochimica et Biophysica Acta (BBA) - Proteins and Proteomics*, 1824(3):443 – 449, 2012.

[104] S. Meier, P. R. Jensen, and J. O. Duus. Real-time detection of central carbon metabolism in living *Escherichia coli* and its response to perturbations. *FEBS Lett*, 585(19):3133–3138, Oct 2011.

[105] A. A. Dimarco and A. H. Romano. D-glucose transport system of *Zymomonas mobilis*. *Appl Environ Microbiol*, 49(1):151–157, Jan 1985.

[106] M. Bucher, R. Brndle, and C. Kuhlemeier. Ethanolic fermentation in transgenic tobacco expressing *Zymomonas mobilis* pyruvate decarboxylase. *EMBO J*, 13(12):2755–2763, Jun 1994.

[107] A. Cornish-Bowden and M. L. Crdenas. Information transfer in metabolic pathways. effects of irreversible steps in computer models. *Eur J Biochem*, 268(24):6616–6624, Dec 2001.

[108] J.M. Rohwer. Kinetic modelling of plant metabolic pathways. *J Exp Bot*, 63(6):2275–2292, Mar 2012.

[109] N. Cartwright. *How the laws of physics lie.* Cambridge Univ Press., 1983.

[110] J. L. Snoep, L. P. Yomano, H. V. Westerhoff, and L. O. Ingram. Protein burden in zymomonas mobilis: negative flux and growth control due to overproduction of glycolytic enzymes. *Microbiology*, 141(9):2329–2337, 1995.

[111] M. M. Bradford. A rapid and sensitive method for the quantitation of microgram quantities of protein utilizing the principle of protein-dye binding. *Anal Biochem*, 72:248–254, May 1976.

[112] C. M. Stoscheck. Quantitation of protein. *Methods Enzymol*, 182:50–68, 1990.

[113] G. Bratbak and I. Dundas. Bacterial dry matter content and biomass estimations. *Appl. Environ. Microbiol*, 48(4):755–757, 1984.

[114] J. Strohhäcker, A. A. de Graaf, S. M. Schoberth, R. M. Wittig, and H. Sahm. 31P nuclear magnetic resonance studies of ethanol inhibition in *Zymomonas mobilis*. *Arch. Microbiol*, 159(5):484–490, 1993.

[115] E. Jones, T. Oliplant, P. Peterson, et al. SciPy: Open source scientific tools for Python, 2001–.

[116] G. Miczka, J. Vernau, M. R. Kula, B. Hofmann, and D. Schomburg. Purification and primary structure of pyruvate decarboxylase from *Zymomonas mobilis*. *Biotechnol Appl Biochem*, 15(2):192–206, Apr 1992.

[117] B. G. Olivier, J. M. Rohwer, and J. H. S. Hofmeyr. Modelling cellular systems with pysces. *Bioinformatics*, 21(4):560–561, 2005.